nuSTORM at CERN

Feasibility Study

C.C. Ahdida[1], R. Appleby[2], W. Bartmann[1], J. Bauche[1], M. Calviani[1], J. Gall[1], S. Gilardoni[1], B. Goddard[1], C. Hessler[1], P. Huber[3], I. Efthymiopoulos[1], J.B. Lagrange[4], M. Lamont[1], K. Long[5,4], J.A. Osborne[1], J. Pasternak[5,4], F.J.P. Soler[6], S. Tygier[1], F.M. Velotti[1]

[1] *CERN, Esplanade des Particules 1, 1217 Meyrin, Switzerland*

[2] *School of Physics & Astronomy, University of Manchester, Oxford Road, Manchester, M13 9PL, UK*

[3] *Virginia Polytechnic Institute and State University, 925 Prices Fork Road, Blacksburg, VA 24061, USA*

[4] *STFC, Rutherford Appleton Laboratory, Harwell Campus, Didcot, OX11 0QX*

[5] *Imperial College London, Exhibition Road, London, SWZ 2AZ, UK*

[6] *School of Physics and Astronomy, University of Glasgow, Glasgow, G12 8QQ, UK*

The nuSTORM collaboration is presented in the addendum.

Abstract

nuSTORM ("Neutrinos from Stored Muons") is a short-baseline neutrino project based on a low-energy muon decay ring. The scientific objectives of nuSTORM are: to make detailed and precise measurements of neutrino-nucleus interactions not only as a service to the long- and short-baseline neutrino oscillation programmes but also as a means of studying the nucleus using a weak probe and seeking evidence for non-standard interactions; and to take forward the search for light sterile neutrinos should the results of the Short Baseline Neutrino (SBN) programme at FNAL indicate that such a programme is required. The feasibility of implementing nuSTORM at CERN has been studied by the nuSTORM group as part of the CERN Physics Beyond Colliders study. An outline of the proposed siting of nuSTORM at CERN is presented. The SPS would provide the primary beam and offers a credible location for fast extraction towards a suitable green field site where a target complex and decay ring could be located. The decay ring would provide the ability to store muon beams with a central momentum from 1 GeV/c to 6 GeV/c.

CERN-PBC-REPORT-2019-003
October 30, 2020

Contents

1 Introduction **3**

2 Motivation **5**
2.1 Neutrino-nucleus scattering 5
2.2 Sterile neutrino search 7
2.3 Technology test-bed 7

3 Experimental programme **10**
3.1 Sterile neutrino search 10
3.2 Neutrino cross-section measurements 13

4 Accelerator facility **18**
4.1 Pion-production target and pion capture 18
4.2 Storage ring design, simulation of performance 19

5 Implementation at CERN **25**
5.1 Overview 25
5.2 Preamble 26
5.3 Primary Proton Beam 26
5.4 Extraction and transfer 27
5.5 Experimental hall 29
5.6 Civil engineering and infrastructure considerations 31

6 Radiation protection and safety **44**
6.1 Radiation protection and radiation safety 44
6.2 Safety 48
6.3 Non-Ionising Radiation 57

7 Construction costs **58**
7.1 Project Costs FNAL 59

8 Next steps **60**

1 Introduction

Overview

nuSTORM, the 'Neutrinos from Stored Muons' facility, has been designed to provide intense beams composed of equal fluxes of electron- and muon-neutrinos for which the energy spectrum is known precisely from the decay of muons confined within a storage ring. It will be possible to store muon beams with central momentum from 1 GeV/c to 6 GeV/c with a momentum acceptance of 16%. The nuSTORM facility will have the capability to:

- Serve a definitive neutrino-nucleus scattering programme with uniquely well-characterised $\overset{(-)}{\nu}_e$ and $\overset{(-)}{\nu}_\mu$ beams;
- Allow searches for light sterile neutrinos with the exquisite sensitivity necessary to go beyond the reach of the FNAL Short Baseline Neutrino programme; and
- Provide the technology test-bed required for the development muon beams capable of serving as the basis for multi-TeV lepton-antilepton (muon) collider.

nuSTORM is based on a low-energy muon decay ring (see figure 1). Pions, produced in the bombardment of a target, are captured in a magnetic channel. The magnetic channel is designed to deliver a pion beam with central momentum p_π and momentum spread $\sim \pm 10\% p_\pi$ to the muon decay ring. The pion beam is injected into the production straight of the decay ring. Roughly half of the pions decay as the beam passes through the production straight. At the end of the straight, the return arc selects a muon beam of central momentum $p_\mu < p_\pi$ and momentum spread $\sim \pm 16\% p_\mu$ that then circulates. Undecayed pions and muons outside the momentum acceptance of the ring are directed to a beam dump. The intense flux of muons emerging from the dump may serve a test facility dedicated to the development of the technologies required to deliver high-brightness muon beams [1, 2].

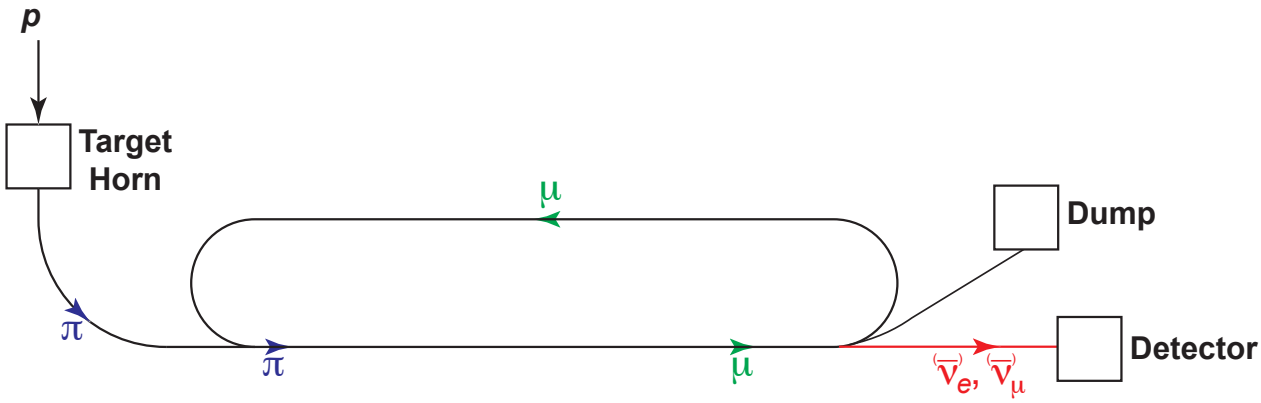

Figure 1: Schematic of the nuSTORM neutrino-beam facility.

At low neutrino energy ($\lesssim 2$ GeV), $\overset{(-)}{\nu}_{e,\mu} A$ scattering is dominated by the quasi-elastic (QE) and 1-$\pi(\Delta)$ processes. At higher energies, $E_\nu \gtrsim 2$ GeV, poorly-known multi-pion resonance-production as well as shallow- and deep-inelastic scattering processes play an increasingly important role. The nuSTORM facility must be capable of delivering neutrino beams that cover this poorly known region with energies that span from the QE-dominated regime to the kinematic regime where deep-inelastic-scattering dominates ($E_\nu \gtrsim 3$ GeV). To span this range requires that nuSTORM be capable of storing muon beams with a central momentum, p_μ, in the range $1 \lesssim p_\mu \lesssim 6$ GeV/c [3].

A detector placed on the axis of the production straight will receive a bright flash of muon neutrinos from pion decay followed by a series of pulses of muon and electron neutrinos from subsequent turns of the muon

beam. Appropriate instrumentation in the decay ring and production straight will be capable of determining the integrated neutrino flux with a precision of $\lesssim 1\%$. The flavour composition of the neutrino beam from muon decay is known and the neutrino-energy spectrum can be calculated precisely using the Michel parameters and the optics of the muon decay ring. The pion and muon momenta (p_π and p_μ) can be optimised to measure $\overset{(-)}{\nu}_e A$ and $\overset{(-)}{\nu}_\mu A$ interactions with per-cent-level precision over the neutrino-energy range $0.2 \lesssim E_\nu \lesssim 6\,\text{GeV}$ and to search for light sterile neutrinos with exquisite sensitivity.

nuSTORM as a stepping stone to high-brightness muon beams for particle physics

In 1961 the first true neutrino beam was created at CERN using the Van der Meer horn to focus pions produced in the bombardment of a solid target by protons extracted from the PS. Such horn-focused beams have been used at CERN, ANL, BNL, FNAL, IHEP, KEK, and J-PARC, first to establish the quark-parton model and the Standard Model, and then to study neutrino oscillations and to search for new phenomena such as the existence of sterile neutrinos.

The Deep Underground Neutrino Experiment (DUNE) [4–8] in the US and the Tokai-to-Hyper-Kamiokande (Hyper-K) [9–12] experiment in Japan will use horn-focused pion beams produced using proton-beam powers in excess of 1 MW to search for the violation of CP invariance in the neutrino sector. The high-flux beams illuminating the large DUNE and Hyper-K detectors will allow very large data sets to be accumulated. Projections of the rate at which data will be collected indicate that the statistical error will be reduced to the percent level by 2028–30. To optimise the discovery potential requires that the systematic uncertainties be reduced to the percent level on a comparable timescale. The systematic uncertainties are dominated by the lack of a micro-physical understanding of neutrino–nucleus interactions and, in particular, the $\overset{(-)}{\nu}_e A$ cross-sections. At nuSTORM, the flavour composition of the neutrino beam is known and its energy spectrum may be determined precisely using the storage-ring instrumentation. The precise knowledge of the neutrino flux combined with advanced detector techniques that are currently being developed will allow nuSTORM to provide the measurements necessary to maximise the sensitivity of the next generation of long-baseline experiments.

The exploitation of time-varying electromagnetic fields to accelerate charged particles to high energy was pioneered in the 1930s. Synchrotrons have been used to explore the energy frontier since 1959 when CERN's proton synchrotron began operation. The discovery of the Higgs boson and the search for new particles and forces at the LHC rests on this tradition. To take the direct search for new phenomena into new energy domains requires a collider capable of producing collisions between fundamental constituents of matter with centre-of-mass energies in excess of a few TeV. The fundamental nature of leptons makes a lepton-antilepton collider the ideal candidate to serve this programme. The large muon mass, 207 times that of the electron, suppresses synchrotron radiation by a factor of 10^9 compared with electron beams of the same energy. Rings can therefore be used to accelerate muon beams efficiently and bring them into collision repeatedly, serving several experiments simultaneously.

nuSTORM would be the first neutrino-beam facility to be based on a stored muon beam and will provide a test-bed for the development of the technologies required for a multi-TeV muon collider and/or a neutrino factory. It will also serve the nuclear physics community by providing a unique 100% polarised probe of flavour-dependent collective effects in nuclei. CERN is uniquely well-placed to implement nuSTORM; its proton infrastructure is well matched to the nuSTORM requirements and the scientific and technology-development outcomes of nuSTORM are an excellent match to CERN's mission. It is conceivable that the implementation of nuSTORM at CERN will help drive a step-change in capability comparable to that produced by Van der Meer's focusing horn and John Adam's proton synchrotron, paving the way for the deployment of a new technique for the study of the nature of matter and the forces that bind it.

2 Motivation

2.1 Neutrino-nucleus scattering

2.1.1 Impact on searches for leptonic CP-invariance violation

The search for CP-invariance violation (CPiV) in present and planned long-baseline neutrino-oscillation experiments is based on the measurement of the rate of $\overset{(-)}{\nu}_e$ appearance in $\overset{(-)}{\nu}_\mu$ beams. The phenomenological description of the effect relies on the assumption of three neutrino-mass eigenstates that mix to produce the three neutrino flavours [13–16]. CPiV arises in this framework if the value of a phase parameter, δ, is such that $\sin\delta \neq 0$.

The oscillation probability is a function of the source-detector distance (the baseline) and the neutrino energy. Neutrino interactions that occur as the neutrino beam passes through the earth introduce a "matter effect" that causes the oscillation probability of neutrinos to differ from that of anti-neutrinos. This introduces an "apparent" CPiV effect that depends on the neutrino mass hierarchy. The discovery of CPiV in neutrino oscillations requires that the "true" CPiV that depends on δ be distinguished from the apparent CPiV that arises from neutrino interactions with the earth.

The projected sensitivity to CPiV of the DUNE experiment is plotted as a function of exposure in figure 2 [17]. The significance is evaluated assuming the normal hierachy and plotted for the case when $\delta_{\rm CP} = -\pi/2$ and when the range of values over which CPiV can be determined is extended to 50% and 75% of all possible values of $\delta_{\rm CP}$. The width of the bands show the impact of applying an external constraint on θ_{13}. If $\delta_{\rm CP} = -\pi/2$, CPiV can be established at 5σ significance with an exposure of ~ 336 kt MW years. This will be achieved after approximately seven years of running with the planned staging to reach a total detector mass of 40 kt and a proton beam-power of 2.4 MW [17]. After approximately ten years (624 kt MW years), CPiV can be established at 5σ significance over 50% of all values of $\delta_{\rm CP}$. After 10 years of running, 3σ sensitivity to CPiV is achieved over 75% of values of $\delta_{\rm CP}$.

The projected sensitivity of the Hyper-K experiment is also shown in figure 2 [10, 18]. The result assumes a single detector with a fiducial volume of 187 kt and a proton beam-power of 1.3 MW at 30 GeV. The fraction of all value12s of $\delta_{\rm CP}$ at which CPiV can be excluded at 5σ and 3σ confidence level is plotted as a function of running time. The statistical reach of the Hyper-K experiment is compared to the reach when systematic uncertainties are taken into account. The systematic uncertainties assumed by the Hyper-K collaboration are dominated by the $\overset{(-)}{\nu}_e$ cross section uncertainties [18, 19]. The impact of reducing the systematic uncertainty related to the $\overset{(-)}{\nu}_e$ cross sections is significant. For example, the running time required to reach 5σ sensitivity over 50% of all values of $\delta_{\rm CP}$ is reduced by a factor of ≈ 1.8 when the uncertainty on the $\overset{(-)}{\nu}_e$ cross sections is reduced from 3.2% to 2%.

The theoretical description of the structure of the nucleus is considerably less accurate than the detailed and precise understanding of the structure of the nucleon. As a consequence, it is now widely recognised that the ultimate sensitivity of studies of neutrino oscillations will be determined by the degree to which the systematic uncertainty arising from the modelling of neutrino-nucleus interactions can be reduced. The reduction of this systematic uncertainty will rest on a significant effort to develop accurate simulations of neutrino-nucleus interactions based on detailed and precise measurements. Neutrino interaction measurements supplement electron- and photon-scattering studies of hadronic physics by including the axial-vector interactions. Neutrino-nucleus scattering studies are therefore extremely important.

Neutrino-nucleus scattering is usually performed with a neutrino of unknown energy interacting in a detector made of heavy nuclei. Typically the final-state lepton is the charged partner of the incoming neutrino. The exchanged W (or Z) boson interacts with a bound nucleon that is moving with Fermi momentum within

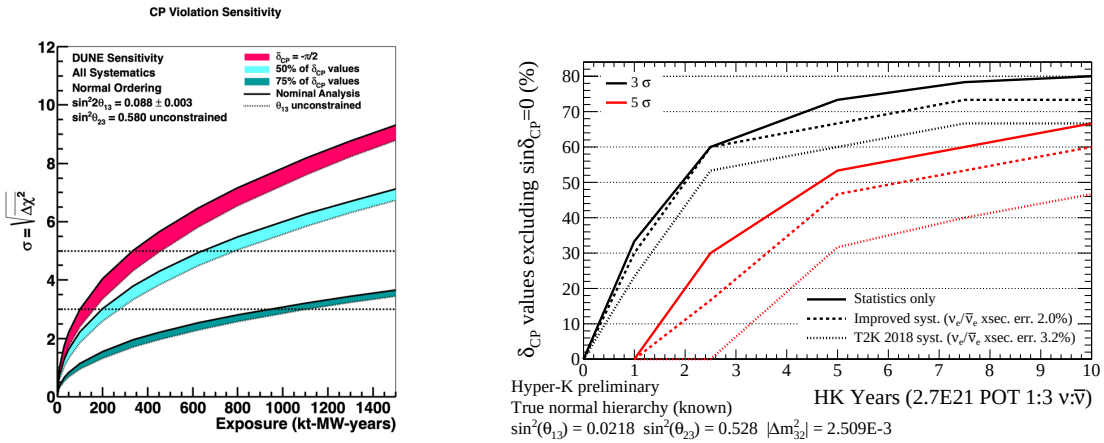

Figure 2: Left panel: Expected sensitivity of the DUNE experiment to CP-invariance violation plotted as a function of exposure in kt MW years assuming $\delta_{\rm CP} = -\pi/2$ (red band) and for 50% (light blue band) and 75% (turquoise band) of all possible values of $\delta_{\rm CP}$. The width of the band shows the impact of applying an external constraint on θ_{13}. The figure is taken from [17]. Right panel: Expected sensitivity of the Hyper-K experiment to CPiV [18]. The fraction of all values of the CPiV phase, δ ($= \delta_{\rm CP}$), for which $\delta = \delta_{\rm CP} = 0, \pi$ can be excluded at 3σ (black) or 5σ (red) is plotted as a function of running time. The solid lines show the statistical sensitivity while the dotted lines assume the systematic uncertainties of 3.2% on the $\overset{(-)}{\nu}_e$ cross sections assumed by T2K in 2018 [19]. The impact of reducing the $\overset{(-)}{\nu}_e$ cross section uncertainties to 2% is shown by the dashed lines.

the nucleus, producing an outgoing nucleon and, if the neutrino energy is high enough, additional hadrons, mostly pions. In a subset of scatters, the exchanged boson interacts with a pair of correlated nucleons. In such cases a second nucleon is released in the initial interaction: these 'two-particle-two-hole' events are fascinating from the perspective of nuclear physics and of quantitative importance in the extraction of neutrino-oscillation parameters. Such nuclear effects in the initial interaction, including the Fermi momentum of the bound nucleon and the existence of correlated multi-nucleon ensembles, affect the kinematic distributions of both the outgoing lepton and hadronic shower.

The final state lepton escapes the nucleus, however the hadronic shower initiated in the hard interaction undergoes significant further nuclear interactions as it propagates through the dense nuclear matter within the nucleus. These final state interactions (FSI) can change the energy, angle and even the charge state of the hadrons that were originally produced; the pions having a reasonable probability of being totally absorbed within the nucleus and not emerging into the detector.

Measurement of the scattered lepton and the final-state hadrons can only be used to provide an estimate the true event kinematics since the incident neutrino energy is not known a priori and the hadrons initially produced are subject to FSI. A neutrino-oscillation experiment exploits the initial neutrino-energy spectrum and information about final state particles to extract oscillation parameters. For this process to result in unbiased estimates of neutrino-oscillation parameters requires the analysis to unfold the effect of the energy-dependent neutrino flux and the energy-dependent neutrino-nucleon cross section. Crucially, the evaluation of the neutrino-nucleon cross sections must include precise and accurate calculations of significant energy-dependent nuclear effects.

Practically, information about the energy dependence of all exclusive cross sections as well as nuclear effects is combined into a nuclear model. This model, along with the best estimate of the spectrum of incoming neutrino energies, then enters the Monte Carlo predictions of target-nucleus response and the topology of final states. Thus, the nuclear model is a critical component of oscillation analyses.

The use of a near detector, although extremely useful, does not reduce the oscillation analysis to a simple

rescaling. Differences, both geometric and oscillation-induced, between near and far fluxes as well as differing near- and far-detector capabilities, such as particle detection efficiencies, make the precise modelling of neutrino-nucleus interactions a necessary and critical element of the analysis. A large and growing body of work over the past several years highlights how mis-modelling of the nucleus could lead to unacceptably large systematic uncertainties or, worse, biased measurements in current and future oscillation experiments [20–29]. The study of CP-invariance violation at DUNE and Hyper-K will require as-yet-un-achieved percent-level control over the appearance signals, implying that the understanding of the nuclear model has to be critically examined and refined to deliver predictions of the requisite precision.

Neutrino-nucleus interactions are the least well understood component of a detector's response to neutrinos. Understanding the subtleties of the nuclear model can only be performed accurately if highly accurate neutrino-nucleus interaction data is available to test the predictive power of the nuclear model. Therefore, the challenges facing the community are:

- The development of significantly improved nuclear models that include:
  1. A unified model of nuclear structure that gives the initial kinematics and the dynamics of nucleons bound in the nucleus;
  2. An improved understanding of the role played by nucleon-nucleon correlations in interactions and their implementation in Monte Carlo generators without double counting; and
  3. Improved models of final state interactions.

  These improved models must be incorporated in the nuclear neutrino-event generators.
- The quantitative validation of the improved nuclear models and the generators that employ them against both accelerator-based precision neutrino-nucleus interaction measurements and, via a collaborative particle- and nuclear-physics effort, electron-nucleus interaction measurements.

To meet these challenges requires high-precision neutrino-interaction experiments to extend the current GeV-scale neutrino-scattering programme. The future programme should include consideration of a hydrogen- or deuterium-scattering experiment to supplement the currently poorly known (anti)neutrino-nucleon cross sections and the exploitation of muon-based neutrino beams to provide extremely accurate knowledge of the neutrino flux and an intense electron-neutrino beam.

The proposed nuSTORM facility at CERN, providing extremely well-known fluxes of both $\overset{(-)}{\nu}_{\mu}$ and $\overset{(-)}{\nu}_{e}$ neutrino beams, is by far the best way to provide the necessary constraint on the nuclear models so essential to the success of neutrino oscillation experiments.

2.2 Sterile neutrino search

A detailed sterile neutrino analysis was presented in [30]. The analysis considered the sensitivity of a ν_μ appearance experiment at nuSTORM to the presence of sterile neutrinos in a model in which a fourth, sterile, neutrino is allowed to mix with the three Standard Model neutrinos. By evaluating the sensitivity in the parameter space of the mass-squared splitting and the sine of the mixing angle, the sensitivity of nuSTORM was shown to be such that the region of parameter space presently allowed at the 99% confidence could be excluded with a significance of 10σ.

2.3 Technology test-bed

Muon beams of high brightness have been proposed as the source of neutrinos at a neutrino factory and as the means to deliver multi-TeV lepton-antilepton collisions at a muon collider. In most of these proposals the muon beam is derived from pion decay as is proposed here for nuSTORM. An alternative approach, in which

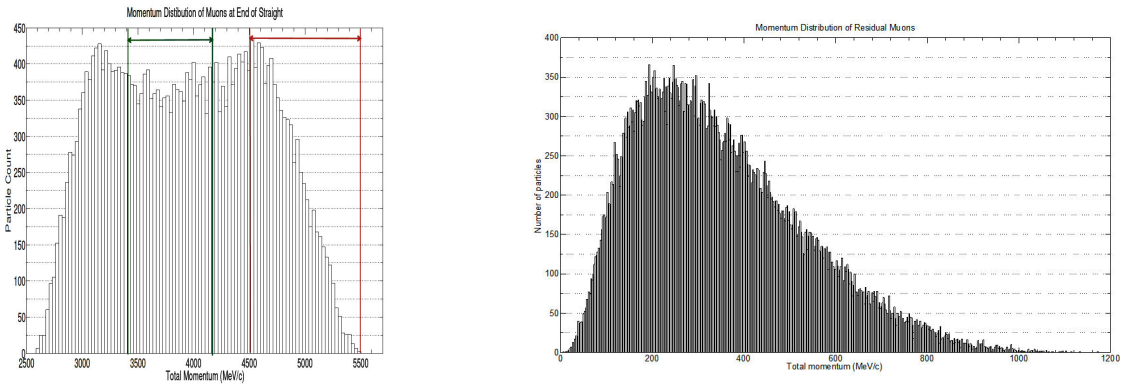

Figure 3: Left panel: momentum distribution of muons after the first straight. Right panel: muon momentum distribution after the degrader.

muons are produced with an energy of 22 GeV in the annihilation of 45 GeV positrons with electrons at rest has recently been proposed. The rest mass of the muon, 207 times that of the electron, suppresses the rate of synchrotron radiation and beamsstrahlung making it possible to conceive of lepton-antilepton collisions at centre of mass energies in excess of 5 TeV with an energy spread of a few percent.

The implementation of nuSTORM at CERN will allow many of the challenges associated with the muon storage ring in such facilities to be addressed. These challenges include the following.

- The complete implementation of a muon storage ring of large acceptance including the injection and extraction sections; and
- The design and implementation of instrumentation by which to determine the muon-beam energy and flux to 1% or better. A novel polarimeter system will be required to determine the stored-muon energy and the energy spread.

The development of these techniques will be invaluable in the future development of high-brightness muon beams for particle physics.

Of particular importance is the opportunity nuSTORM provides for the study of ionization cooling. Muon ionization cooling improves the stored-muon flux at a neutrino factory by a factor ~ 2. Proton-driven muon-collider schemes require a substantial reduction in the phase-space occupied by the muon beam at production in all 6 phase-space dimensions. The Muon Ionisation Cooling Experiment (MICE) [31] has demonstrated ionization cooling in the 4-dimensional transverse phase space [32]. To prove the feasibility of a muon collider therefore requires a follow-on demonstration of ionization cooling in the full six-dimensional (6D) phase space.

MICE was a "single-particle" experiment; the four-momenta of single muons were measured before and after the cooling cell. The properties of beams entering and leaving the cooling cell were then reconstructed from ensembles of single-muon events. A 6D cooling experiment could be done in the same fashion, but doing the experiment with a high-intensity pulsed muon beam is preferred. nuSTORM is uniquely capable of providing an appropriate low-energy muon beam with the characteristics required to mount a definitive experiment to demonstrated 6D-cooling.

Figure 1 shows a schematic of the decay ring. Pions are injected at one end of the production straight. As noted above, only $\sim 50\%$ of the pions decay in the production straight. Since the arcs are set for the central muon momentum lower than the momentum of the injected pion beam, pions remaining at the end of the straight will not be transported through the arc. The pion-beam power that reaches the end of the production straight has been estimated to be ~ 5 kW making it necessary to dump the undecayed pion beam into an appropriate absorber.

The same optics that are used for injection can be used to extract the pions at the end of the straight and transport them to an absorber. If the absorber is 'redefined' to be a 'degrader' capable of stopping the pions but allowing muons above a certain energy to pass, then a low-energy muon beam appropriate for a 6D muon cooling experiment can be produced. The left panel of figure 3 shows the momentum distribution for the first pass of muons at the end of the decay-ring straight for an injected pion-beam energy of 5 GeV. The green band indicates the momentum acceptance of the decay ring. The red band covers the same momentum band as the input pions, these muons will be extracted along with the remaining pions. If the degrader is sized appropriately, a muon beam of the desired momentum for a 6D cooling experiment will emerge downstream of the degrader. The right panel of figure 3 shows the momentum distribution of the muons that exit the degrader. It has been estimated that approximately 10^{10} muons-per-spill will emerge from the degrader in the momentum band of interest for a 6D cooling experiment (100–300 MeV/c).

3 Experimental programme

The experimental programme of nuSTORM was described in detail in the Letter of Intent and Proposal to FNAL [1, 2] and in the Expression of Interest to CERN [33].

The precise knowledge of the neutrino flux at nuSTORM must be matched by a high-precision detector capable of delivering neutrino measurements with 1–2% precision. A number of near detector concepts have been studied in the context of Neutrino Factory and DUNE studies. For example, the HiResMν detector [34], gaseous argon or liquid argon detectors inside a magnetic field would meet the requirements.

A number of studies have been carried out to ascertain the performance of nuSTORM to be able to deliver the physics programme in sterile neutrinos (Sub-section 3.1) and for cross-section measurements (Sub-section 3.2).

3.1 Sterile neutrino search

The capabilities of the nuSTORM facility to search for sterile neutrinos was demonstrated in reference [30]. In this study, the central momentum of the muons was assumed to be 3.8 GeV/c with a momentum acceptance of $\approx \pm 10\%$. It was assumed that $\approx 2 \times 10^{18}$ useful μ^+ decays in the production straight pointing towards the far detector site are generated by nuSTORM from a total of 10^{21} protons on target (POT) over a total of five years [1, 33]. The uncertainty in the neutrino flux is expected to be less than 0.5%.

The neutrinos from the decay $\mu^+ \to e^+ + \bar{\nu}_\mu + \nu_e$ in the straight are measured in a near detector. The evidence for sterile neutrinos is searched for in the far detector by observing either the appearance of ν_μ from the $\nu_e \to \nu_\mu$ transition or the disappearance of $\bar{\nu}_\mu$ from $\bar{\nu}_\mu \to \bar{\nu}_e$ oscillations, mediated via sterile neutrinos. The probability for the appearance of a $\nu_e \to \nu_\mu$ transition is given by

$$P_{e\mu} = \sin^2 2\theta_{e\mu} \sin^2 \left(\frac{\Delta m^2 L}{4E} \right), \tag{1}$$

where $\theta_{e\mu}$ is the effective mixing angle, and Δm^2 is the effective mass difference, independent of the sterile neutrino model. In the (3+1) sterile neutrino model [35] consistent with the LSND anomaly, then $\sin^2 2\theta_{e\mu} \equiv 4|U_{\mu 4}|^2|U_{e4}|^2$, where $U_{\epsilon n}$ is an element of the enlarged PMNS mixing matrix with sterile neutrinos. The disappearance probability of $\bar{\nu}_\mu$ is given by

$$P_{\mu\mu} = 1 - \sin^2 2\theta_{\mu\mu} \sin^2 \left(\frac{\Delta m^2 L}{4E} \right), \tag{2}$$

where $\sin^2 2\theta_{\mu\mu} \equiv 4|U_{\mu 4}|^2 \left(1 - |U_{\mu 4}|^2\right)$ in the (3+1) model.

For 10^{21} POT, with $\approx 2 \times 10^{18} \mu^+$ decays and assuming the (3+1) sterile neutrino model, the rates of neutrinos expected are shown in Table 1. The ν_μ appearance experiment is conducted by observing μ^- in the detector and identifying the charge of the muon compared to the very large μ^+ background, which has to be rejected at the 10^{-4} level. The $\bar{\nu}_\mu$ disappearance experiment relies on measuring a spectral distortion in the μ^+ spectrum in the detector. Therefore, the sensitivity to oscillations depends on the ability of the detector to distinguish the charge of the leptons and to measure accurately the momentum of the muons produced in the neutrino charged current (CC) interactions.

Direct measurement of the cross-section and flux of both electron and muon neutrinos is performed at a near detector, 50 m from the end of the decay straight. The number of ν_e and $\bar{\nu}_\mu$ CC events (per 100 ton fiducial mass) is 4.0×10^6 and 2.1×10^6, respectively, for a 10^{21} POT exposure. It is also possible to select μ^- in the storage ring. The antineutrino oscillations will have a lower yield due to the smaller antineutrino cross section (1.8×10^6 $\bar{\nu}_e$ and 4.6×10^6 ν_μ CC events would be observed in the near detector in this case).

Table 1: Expected rates for neutrino oscillation channels observed at a 1.3 kt detector, 2 km away from a muon storage ring with an exposure of 10^{21} POT. The significance of the measurement is defined as $\sigma_{osc.} = (N_{osc.} - N_{null})/\sqrt{N_{osc.} + N_{null}}$.

Channel	Oscillation	$N_{osc.}$	N_{null}	$\sigma_{osc.}$
ν_μ Appearance	$\nu_e \to \nu_\mu$ CC	332	0	18.2
$\bar{\nu}_\mu$ Disappearance	$\bar{\nu}_\mu \to \bar{\nu}_\mu$ CC	122322	128433	-12.2
ν_e Disappearance	$\nu_e \to \nu_e$ CC	216657	230766	-21.1
NC Disappearance	$\bar{\nu}_\mu \to \bar{\nu}_\mu$ NC	47679	50073	-7.7
NC Disappearance	$\nu_e \to \nu_e$ NC	73941	78805	-12.4

A 1.3 kt magnetized iron-scintillator calorimeter was proposed as the detector for the short-baseline oscillation physics programme at nuSTORM, as it has excellent charge selection and detection characteristics for muons. This 6 m diameter detector, called Super Bind, is to be constructed of modules of 1.5 cm thick steel plates, and two layers of scintillator bars to yield 3D space points at each measurement plane. The overall length of this detector is 13 m. Each scintillator bar has a cross-section of 2.0×0.75 cm^2 to be read out using silicon photo-multipliers. For a schematic of this detector, see Fig. 4. The magnetic field is generated by a 240 kA-turns current carried by 8 turns of a super-conducting transmission line. This provides a toroidal magnetic field between 1.9 and 2.6 Tesla within the steel.

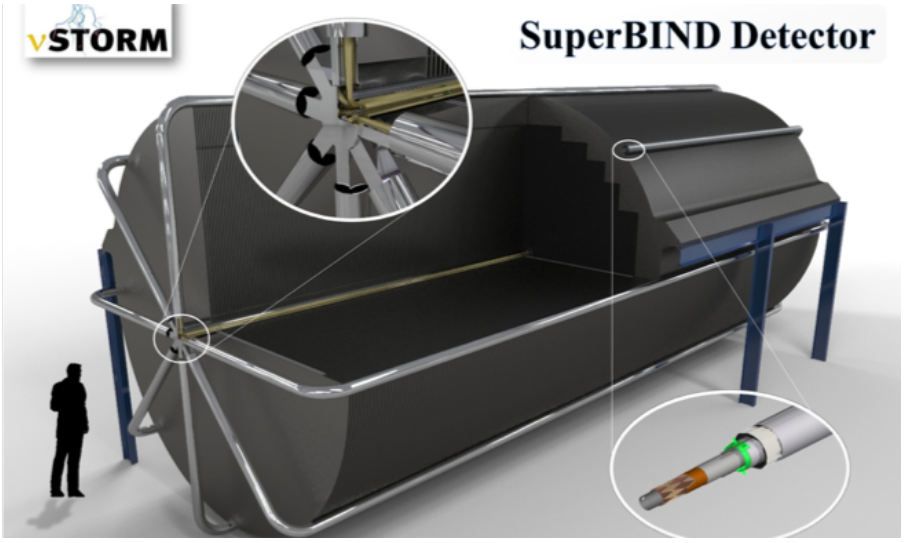

Figure 4: Prospective iron-scintillator Super Bind neutrino detector (6 m in diameter and 13 m in length).

A detailed simulation of the iron-scintillator far detector was developed, using the GENIE [36] neutrino event generator and simulating the neutrino interactions in the detector using GEANT4 [37]. A simple digitization to cluster hits and to replicate the effects of resolution and attenuation within the scintillator bars was also developed. Tracks were reconstructed by applying a Kalman fitter algorithm [38] to determine the momentum and charge of tracks.

A series of pre-selection cuts were applied first. These consisted of finding one or more tracks in the event, successfully fitting the longest track, and imposing a maximum momentum cut of $p_\mu < 4$ GeV/c, applying a fiducial cut of 1 m before the end of the detector and imposing that 60% of the hits are associated to the longest track. Further quality cuts on the charge over momentum ratio (q/p) were also imposed: the normalised error $\sigma_{q/p}/(q/p) < 10.0$ and the ratio of the initial curvature over the fitted curvature satisfies

$(q_{init}/p_{init}) \times (p/q) > 0$.

A multi-variate analysis based on the TMVA [39] subset of the ROOT [40] analysis package was used to distinguish signal events from background with a high degree of purity. A boosted decision tree (BDT) algorithm, in which five track variables (shown in Table 2) are used to discriminate between muons from ν_μ CC interactions and all other types of interactions, was used to carry out the appearance analysis. The method reduces these five track variables to one classifier variable, between 0 and 1, to distinguish between ν_μ CC events, the experimental signal, and $\bar{\nu}_\mu$ NC events, representing the experimental backgrounds. An optimal signal significance, quantified as $S/\sqrt{S+B}$, where S is the number of signal events and B is the number of background events, is achieved for the trained multivariate analysis (MVA) when the classifier has a value greater than 0.86. This yields an integrated signal efficiency of 0.17 and a background efficiency of 4×10^{-5}. A cuts-based analysis [1,41], based on the number of hits in a trajectory and the track quality, yielded a smaller physics sensitivity (signal efficiency of 0.16 and background efficiency of 5×10^{-5}).

Table 2: Variables used in the definition of the classifier for the multi-variate analysis of events in the detector simulation.

Variable	Description
Track Quality	$\sigma_{q/p}/(q/p)$, the normalized error in the track curvature.
Hits in Trajectory	The number of sci. planes in track.
Curvature Ratio	$(q_{init}/p_{range}) \times (p_{fit}/q_{fit})$: ratio of the initial estimate and Kalman fit momentum.
Mean Energy Deposition	$\sum_{i=0}^{N} \Delta E_i/N$ for planes in track.
Variation in Energy	$\sum_{i=0}^{N/2} \Delta E_i / \sum_{j=N/2}^{N} \Delta E_j$, where the energy deposited per hit $\Delta E_i < \Delta E_{i+1}$.

For the disappearance analysis, a different optimization was required, since background rejection was less demanding. An optimization using a χ^2-statistic between neutrino spectra, given the (3+1) sterile neutrino hypothesis and the standard neutrino hypothesis, concluded that a neural network (MLPBNN) algorithm [39] that retains classifier values greater than 0.94 outperformed the BDT algorithm. The efficiency curves for the optimized analysis are shown in Fig. 6.

The detector response for each class of event shown in Figs. 5 and 6 is extracted from the detector simulation as a "migration" matrix of the probability of a neutrino generated in the i^{th} energy bin being reconstructed in the j^{th} energy bin. The migration matrices are input into a simulation of the oscillation experiment using the GLoBES software package [42] with modifications to simulate non-standard interactions [35] and accelerator effects, such as the integration of muon decays from positions throughout the decay straight [41, 43]. The GLoBES simulations assume an experiment with a 1.3 kt far detector at a distance of 2 km from the end of the storage ring, with $1.6{\times}10^{18}$ useful muon decays. The total appearance signal is 73 events, with a combined background of 6 events, assuming $\Delta m^2_{14} = 0.89$ eV^2 and $\theta_{14} = 0.15$ rad.

The sensitivity of a ν_μ appearance experiment to the presence of sterile neutrinos in a (3+1) model as a function of Δm^2_{14} and $\sin^2 2\theta_{e\mu}$ is shown in Fig. 7. The neutrino cross-section uncertainties can be reduced by direct measurements conducted with the beams produced by nuSTORM in both the ν_μ and ν_e channels. The sum of these systematic uncertainties yields a total 1% uncertainty to the total normalization of the signal

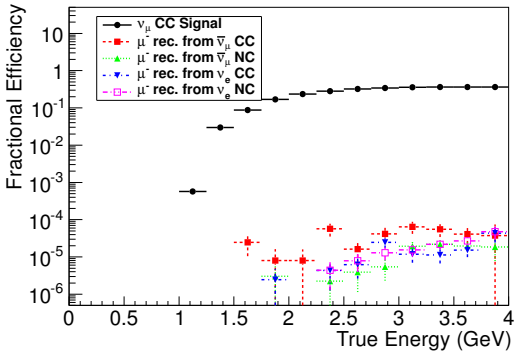

Figure 5: Efficiencies of signals and backgrounds for ν_μ appearance for an iron-scintillator neutrino detector optimized for the region of interest for nuSTORM. The appearance analysis used a BDT algorithm to determine the efficiencies.

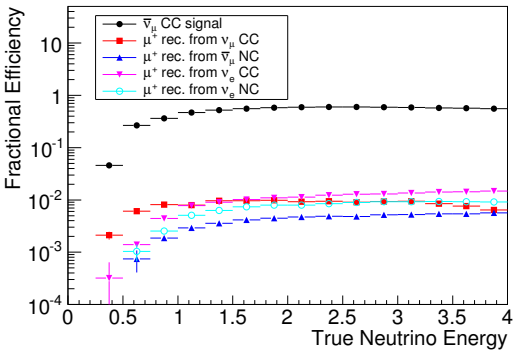

Figure 6: Efficiencies of signals and backgrounds for $\bar{\nu}_\mu$ disappearance for an iron-scintillator neutrino detector optimized for the region of interest for nuSTORM. The disappearance analysis used a neural network (MLPBNN) algorithm to determine the efficiencies.

and a 10% uncertainty to the background. However, In the absence of these measurements, we take an upper limit on the systematic uncertainties from existing experiments, such as MINOS [44]. For an upper bound to the sensitivity of the appearance experiment using a boosted decision tree, we assume conservative systematic uncertainties of 5% in the signal and 50% in the background. This is compared to the 99% confidence contours from fits generated by Kopp *et. al.* [35] to the combination of LSND, MiniBooNE, and the reactor and gallium disappearance experiments (Evidence), and to all available appearance data (Appearance) and to the 99% C.L. contour from the long-baseline ICARUS experiment [45].

The appearance experiment is still sensitive to the presence of a sterile neutrino consistent with the existing evidence at the 10σ level, as shown in Fig. 7. Cosmic ray backgrounds were also considered through the application of the CRY software package [46]. With the application of self-vetoing cuts on the fiducial volume to a skin depth of 30 cm, the cosmic ray background is reduced to less than 1 event per year.

A simultaneous and statistically independent $\bar{\nu}_\mu$ disappearance measurement will be conducted with the same experimental setup. Sensitivity contours as a function of Δm^2_{14} and $\sin^2 2\theta_{\mu\mu}$ are shown in Fig. 8. A near detector is essential to extrapolate the expected neutrino flux at the far detector [47, 48]. It is assumed that the systematic uncertainties used in the appearance measurement are the same as those for the disappearance measurement, which includes a 200 ton iron scintillator near detector. The $\bar{\nu}_\mu$ disappearance measurement is far more sensitive to systematic uncertainties and shows improvement in the 99% C.L. bounds over the current fits as in Fig. 8. An optimization of a ν_e disappearance experiment at a similar muon storage ring facility with idealized detector systems was carried out, demonstrating the near-far extrapolation [49], but the realistic assessment of this channel has not been carried out.

3.2 Neutrino cross-section measurements

Figures 9 and 10 show the expected charged-current quasi-elastic (CCQE) cross-section performance, plotted as a function of neutrino energy E_ν, in a detector, such as HiResMν, exposed to the nuSTORM beam. The figure shows the precision with which the cross-section would be measured if the systematic uncertainties estimated for the HiResMν detector are combined with the 1% flux uncertainty from nuSTORM (green); the detector systematics dominate over the 1% flux uncertainty. A compilation of measurements of the CCQE cross-sections

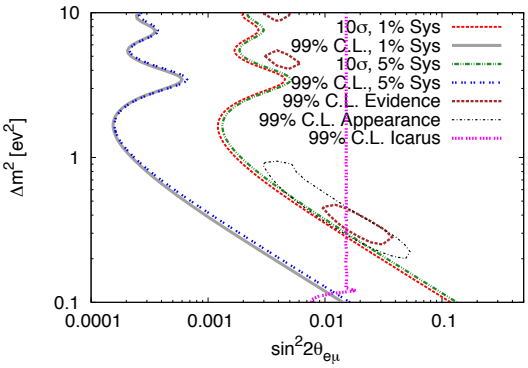

Figure 7: Sensitivity to the presence of sterile neutrinos assuming a (3+1) model with anticipated and inflated systematics, compared to 99% confidence contours from fits generated by Kopp *et. al.* [35] and limits set by ICARUS [45].

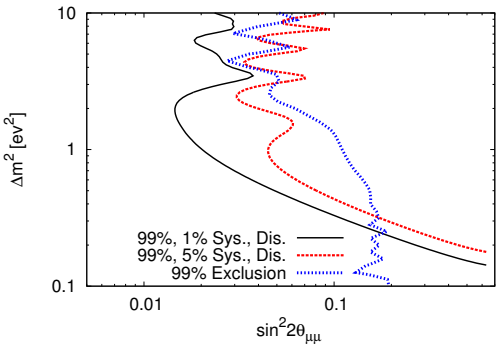

Figure 8: Sensitivity of nuSTORM to ν_μ disappearance oscillations assuming a (3+1) neutrino model. Contours are generated from a χ^2 statistic assuming both the anticipated and inflated systematic uncertainties compared to the exclusion contour produced from the fit of $\sin^2 2\theta_{\mu\mu}$ and Δm^2 to the existing disappearance data [35].

for muon-neutrino beams (there is limited or no data available for electron-neutrino and electron-anti-neutrino beams) is also shown. nuSTORM has the potential to improve the systematic uncertainty on muon-neutrino (muon-anti-neutrino) CCQE cross-section measurements by a factor of $\sim$ 5–6 and would provide unique contributions for electron-neutrino and electron-anti-neutrino CCQE measurements.

Recently, an analysis was performed to extract ν_μ charged-current (CC) scattering events simulated with the GENIE neutrino interaction generator [36] in a totally-active scintillator detector, with muon reconstruction in a magnetised-iron detector [50]. Events were generated for incident neutrino energies uniformly distributed between 0.5 GeV and 3 GeV, reweighted to the nuSTORM flux (Figure 11) and scaled to the number of interactions expected for an exposure of 10^{21} POT on a 10 ton fiducial mass at a distance of 50 m from the end of the production straight.

The study included a multi-variate-analysis event selection and particle identification to separate muons from pions. The muon charge identification efficiency for fully reconstructed muons from ν_μ and $\bar{\nu}_\mu$ CC interactions is shown in Figure 12. The multi-variate analysis was also based on the TMVA [39] package. The main variables used in the selection are the following:

- Maximum distance between hits in an event;
- Angle of the track compared to the z-axis that defines the length of the detector;
- Number of total hits in the event;
- Number of planes hit; and
- Average number of hits per plane.

The Multi-layer Perceptron Bayesian Neural Network (MLPBNN) algorithm was chosen as the best performing model and its response can be seen in Figure 13, showing a clear distinction between ν_μ CC signal and background from $\bar{\nu}_e$ CC and Neutral Current (NC) events. The optimised figure of merit was chosen to be $S/\sqrt{S+B}$. The optimal cut value is achieved with an event classifier of 0.50. Applying the TMVA algorithm to a mixed sample of ν_μ and $\bar{\nu}_e$ in the correct proportions gives an 84% efficiency for the signal events while only accepting 7.6% of the background.

The event rates expected for 10^{21} POT estimated for a 10 ton detector at a distance of 50 m from the end of the straight of the nuSTORM storage ring before applying the TMVA selection are shown in Figure 14 and

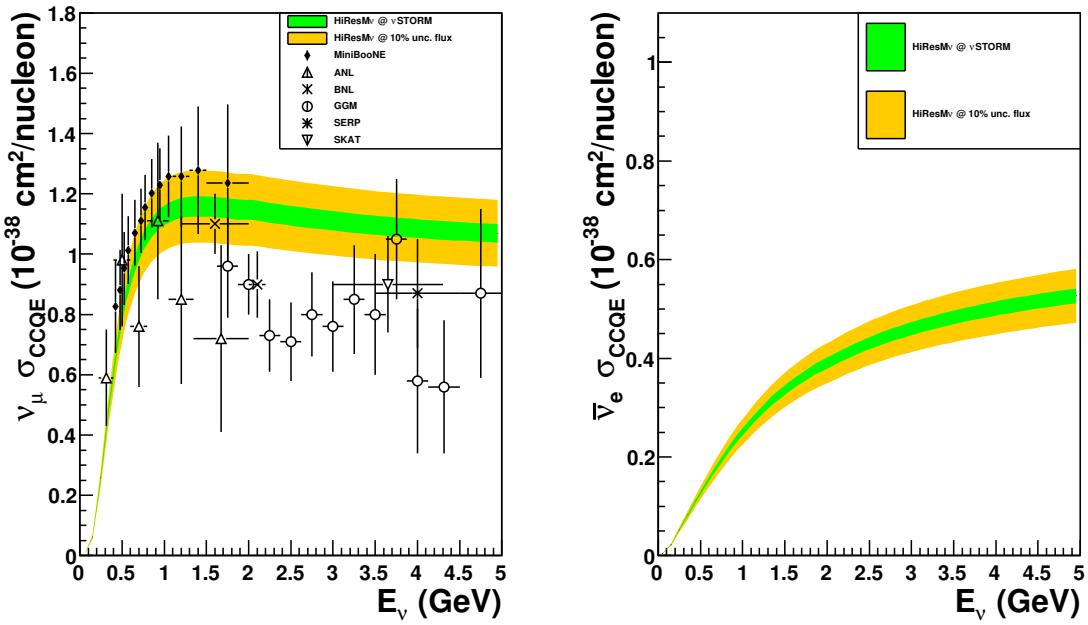

Figure 9: The ν_μ (left) and $\bar{\nu}_e$ (right) CCQE cross-section plotted as a function of incident neutrino energy (E_ν). The total uncertainty from nuSTORM is shown by the width of the coloured bands: the green (yellow) band shows 1% (10%) neutrino-flux uncertainty combined with the detector uncertainty [1, 2]. A compilation of measurements for ν_μ beams is also shown; there is limited or no data available for $\bar{\nu}_e$ beams.

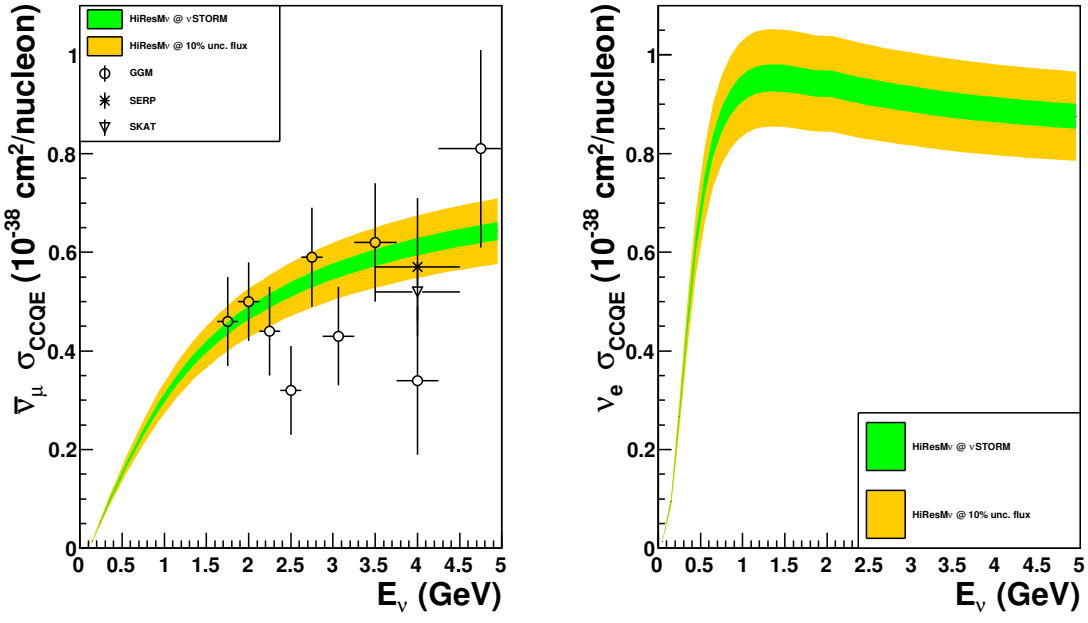

Figure 10: The $\bar{\nu}_\mu$ (left) and ν_e (right) CCQE cross-section plotted as a function of incident neutrino energy (E_ν). The total uncertainty from nuSTORM is shown by the width of the coloured bands: the green (yellow) band shows 1% (10%) neutrino-flux uncertainty combined with the detector uncertainty [1, 2]. A compilation of measurements for $\bar{\nu}_\mu$ beams is also shown; there is limited data available for ν_e beams.

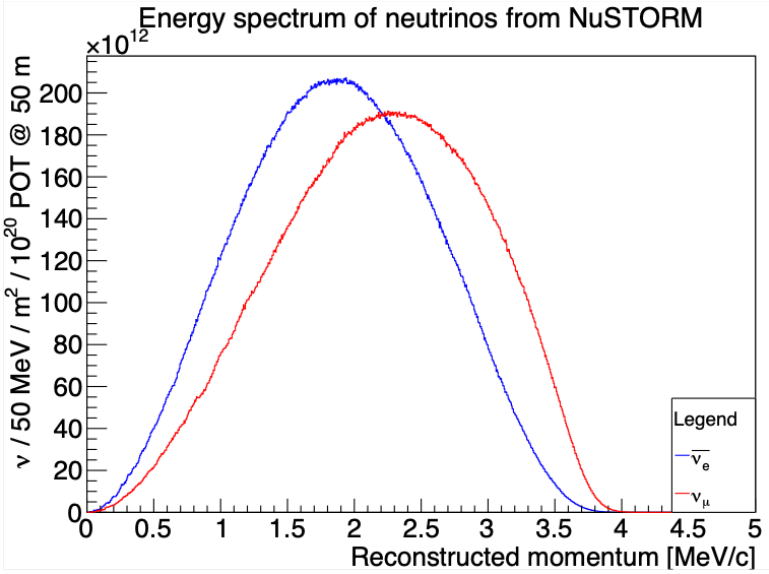

Figure 11: Energy spectrum of ν_μ and $\bar{\nu}_e$ produced at nuSTORM and recorded at 50 m from the storage ring [50].

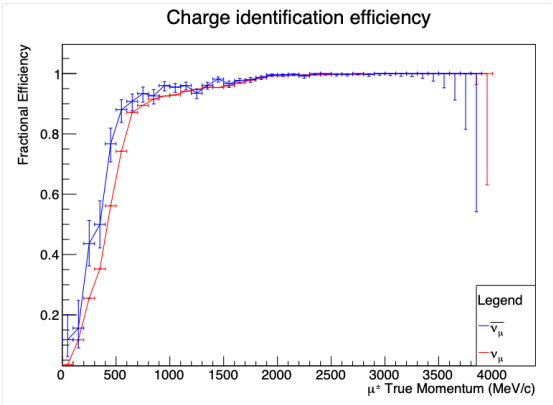

Figure 12: Muon charge reconstruction efficiency in a totally active scintillator detector with a muon spectrometer [50].

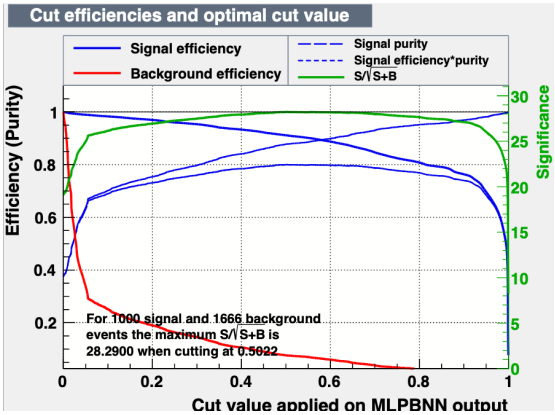

Figure 13: Cut efficiency plots and optimisation from the TMVA package, applying a MLPBNN algorithm to distinguish ν_μ CC events from $\bar{\nu}_e$ and neutral current (NC) background.

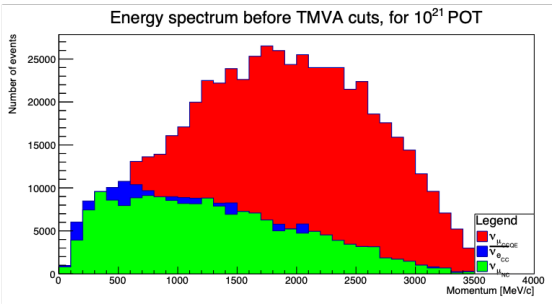

Figure 14: Energy spectrum of $\bar{\nu}_e$ CC, ν_μ CC and ν_μ NC events recorded from 10^{21} POT in a 10 ton detector at 50 m, before passing through the TMVA algorithm [50].

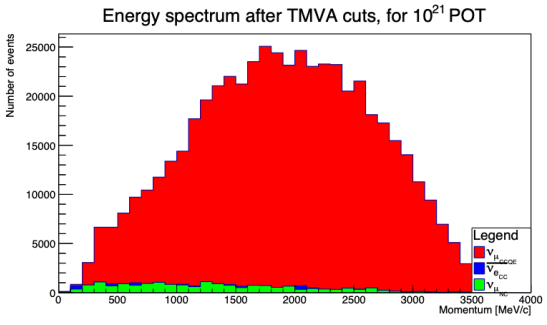

Figure 15: Energy spectrum of $\bar{\nu}_e$ CC, ν_μ CC and ν_μ NC events recorded from 10^{21} POT in a 10 ton detector at 50 m, after the MLPBNN algorithm of TMVA to distinguish ν_μ CC events from $\bar{\nu}_e$ CC and neutral current (NC) background [50].

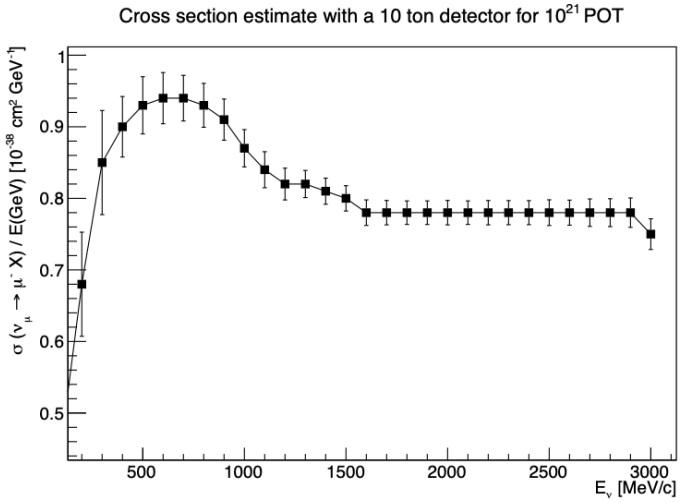

Figure 16: Inclusive ν_μ CC cross section for a 10 ton totally active scintillator detector for 10^{21} POT at a distance of 50 m from the end of the nuSTORM storage ring [50].

after the MLPBNN algorithm are shown in Figure 15. The number of events expected are 6.1×10^5 ν_μ CC events, 2.5×10^5 $\bar{\nu}_e$ CC events, 2.1×10^5 ν_μ NC events and 1.0×10^5 $\bar{\nu}_e$ NC events in a 10 ton detector for 10^{21} POT.

The ν_μ CC cross section is derived from the subtraction of the total background from the signal, and dividing by the neutrino flux and the total number of nucleons in the detector. The estimated uncertainty is given by the quadratic sum of the errors for the signal and the total background. An expected quasi-elastic ν_μ CC cross-section measurement, based on the μ^+ decay rates, is shown in Figure 16. The uncertainties include statistical, detector systematic (2–3%) uncertainties and the 1% nuSTORM flux uncertainty, which makes a relatively small contribution to the overall uncertainty, leaving the detector systematic as the dominant source of uncertainty.

4 Accelerator facility

4.1 Pion-production target and pion capture

The basic structure of the pion-production and capture scheme developed at FNAL has been adopted. Protons extracted from the SPS at 100 GeV are focused on a solid (low-Z) target placed inside a focusing horn. A pair of quadrupoles collect the particles focused by the horn. The beam is then passed through a short transfer line composed of dipoles, collimators and quadrupoles to reduce the radiation load on the downstream transfer line. It is proposed that the target and initial focusing section is contained in an inert helium atmosphere to reduce activation and corrosion of beam-line equipment by limiting the presence of ozone and nitrogen oxides. The target-and-collection system will be installed underground in a cavern with a shaft giving access to a surface building. The shaft and surface building will be offset with respect to the incoming proton beam direction, the target, and the out-going pion beam.

The FNAL proposal used a water-cooled graphite target, based on that successfully used on the NuMI beam. In a CERN implementation, the vast experience accumulated with the operation of the CNGS neutrino beam line would be exploited. In this case, a radiation-cooled graphite target heats the vessel in which it is embedded. The vessel is cooled using a forced flow of air. Alternative schemes studied for the CENF Project [51] in 2014 used a graphite target cooled by the forced convection of helium or other inert gas; such a solution is similar to that used in the T2K neutrino beam-line. The key issues to be addressed in a future detailed design of the target and capture system are radiation safety and the containment for transport of a beam with a momentum spread of $\sim \pm 10\%$. These requirements have led to the consideration of the scheme successfully used in the PS complex to produce anti-protons for physics in the Anti-proton Decelerator (AD). In the AD, pulses of the 26 GeV/c PS proton beam are delivered at an intensity of 1.5×10^{13} protons-per-pulse (ppp) in 4 bunches over a period of 450 ns. The beam is focused to a spot of size $0.5 \times 1\,\mathrm{mm}^2$ at the iridium target. Focusing is provided by an air-cooled magnetic horn, pulsed at 400 kA. The beam is captured using a quadrupole beam line that includes a pair of dipoles to provide a 'dog leg' that reduces the proton contamination in the beam downstream of the target (see figure 17). Any of the proton beam that has not interacted in the target is transported to a dump.

The nuSTORM Target Complex (TC) design could be based on the extensive work done for the CENF and LAGUNA-LBNO projects (see figure 18). In this design, the target, horn and various target-related systems would be moved vertically in the target hall on specially designed supporting structures, which would also provide the fine alignment for the beam equipment. Shielding blocks would fit in the vertical space in an optimised manner to minimise radiation streaming to the surface. Annexed underground areas would house all related services required for the operation of the infrastructure, including cooling and ventilation units and powering systems for the horns.

As in the FNAL design, pion-capture is provided by a magnetic horn. CERN has built horns for the CNGS beam line as well as for antiproton focusing. A genetic algorithm was used to optimise the horn design for the LAGUNA-LBNO proposal; this design is still employed in the LBNF project. In addition, horns for the anti-proton machine have operated for many years and are still operated today. Recently, a newly optimised horn was redesigned and built to serve experiments on the AD. A horn test bench has been built and it is currently in operation, pulsing up to 450 kA. Experience gained from the construction, test and operation of the AD horn has been used in the estimation of the cost of the pion-capture system.

4.1.1 Pion transfer line and proton absorber

The design of the pion transfer line was based on the initial FNAL design, with changes based on the projected radiation hazards and improved injection scheme. The results from the radiation protection study of the CENF

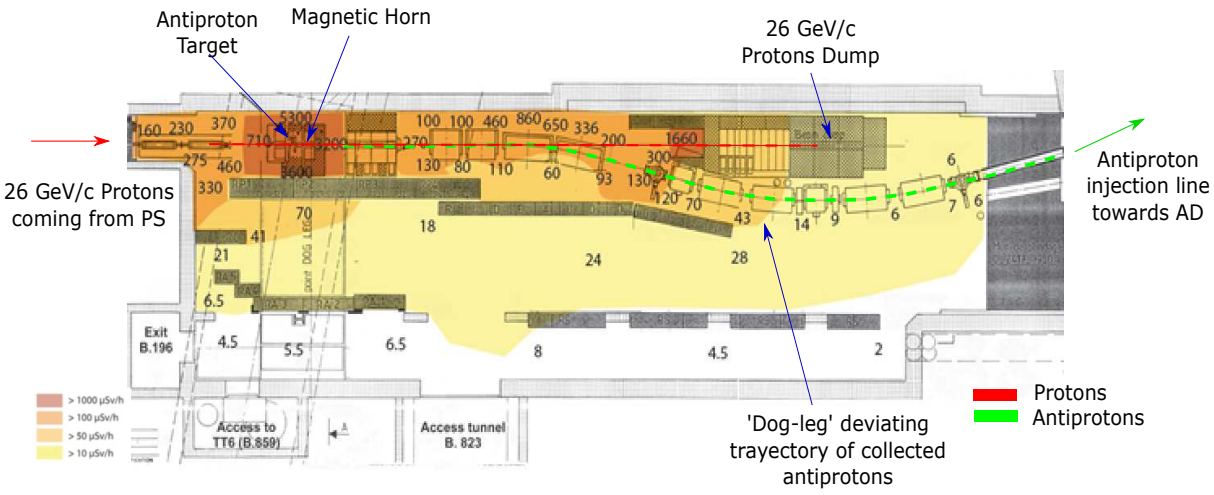

Figure 17: Schematic of the AD Target Area, showing the injection line from the PS, the target, the magnetic horn, the 'dog-leg' and the injection line towards AD. The radiation dose rate present in various areas is indicated by the coloured shading. Figure adapted from [52].

target implied that it is preferential to move sensitive equipment a minimum of 5 m off axis from the primary proton beam. This ensures that both prompt and residual dose rates are kept to a minimum in the main cavern. Moreover the length of the capture section contained within the primary target vessel should be kept to a minimum to ensure that the prompt radiation dose is well contained and as few elements as possible are liable for activation.

A modular construction was chosen allowing for a greater degree of flexibility during the design phase utilising simple quadrupole FODO cells and achromatic dipole bends. An initial capture section will be present inside the initial containment vessel, followed by the proton absorber. The design of the proton absorber could be based on the current SPS internal dump (TIDVG4) that was installed in 2017. Alternatively, the new LIU-SPS internal dump (TIDVG5) could be adapted to cope with the power requirements imposed by nuSTORM. The length of the initial capture section was shortened from the FNAL design in order to reduce the volume of the containment vessel and decrease the number of elements kept within it. A series of collimators will be used in addition to the bending sections to reduce the load on the downstream beam lines.

The first achromatic bending section is used to divert particles within the desired momentum range away from the proton absorber towards the ring. This is key to reduce the radiation dose to downstream elements and provide a momentum selection for the transmitted pion beam. A quadrupole FODO lattice is used to transport the beam to a second achromatic bending section followed by beta-function matching and injection into the ring. The length of this section was chosen to ensure the radiation contamination within the arc sections of the ring is minimized, whilst being short enough to ensure that pions of low momentum can be successfully transported. The beta-function matching section is not fully defined as the length and number of elements depends on the matching parameters for injection. At present sufficient degrees of freedom exist in the current design to allow for a wide range of matching parameters to be considered.

4.2 Storage ring design, simulation of performance

The nuSTORM decay ring, shown schematically in figure 19 is a compact racetrack storage ring with a circumference of ~ 616 m that incorporates large aperture magnets. In order to incorporate the orbit combination section (OCS), used for the stochastic injection of the pion beam into the ring, a dispersion suppressor is needed

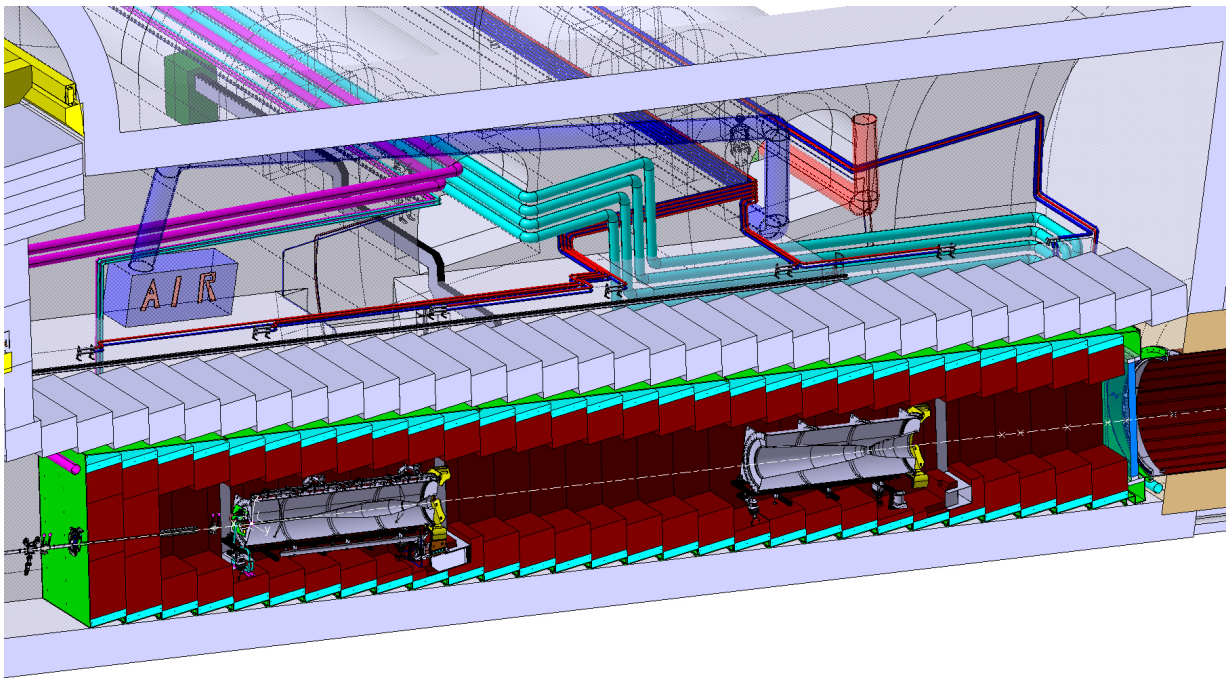

Figure 18: Cut view of the target chamber. Shielding elements (red iron blocks), cooling plates (blue aluminium plates) and elements as target, horn, reflector and its ancillaries and services are placed inside the helium vessel (in green). The helium vessel is surrounded by concrete blocks. Figure taken from [52].

adjacent to the OCS. In addition, in order to maximise the number of useful muon decays, strong bending magnets are needed in the arcs to minimize the arc length.

4.2.1 Storage ring design

Several designs for the nuSTORM storage ring have been already proposed. The first is the FODO solution [2, 53] with large-aperture conventional quadrupoles with alternating gradients in the long straight sections and with lattice based on separate function magnets in the arcs. It was optimised to store 3.8 GeV/c muons with a momentum acceptance of $\sim \pm 8\%$. The acceptance of this design is limited by the large chromaticity of the FODO ring. The second solution is based on the recent developments in Fixed Field Alternating gradient (FFA) accelerators [54]. The advantages of such a lattice are the large momentum acceptance of $\pm 16\%$ together with the possibility of a large transverse acceptance achieved through the choice of a ring tune far from dangerous resonances, thus increasing the momentum band of stored muons in the ring and reducing losses. However, the presence of non-zero dispersion after injection limits the efficiency of the muon beam accumulation in this design.

To serve the neutrino-scattering programme, the ring was redesigned to store muon beams with a momentum of between 1 GeV/c and 6 GeV/c with a momentum acceptance of up to $\pm 16\%$, thereby increasing the neutrino flux. To keep the momentum acceptance and transverse dynamic acceptance large, and simultaneously to maximise the muon accumulation efficiency, a hybrid concept was developed (figure 19). Conventional FODO optics, used in the production straight, are combined with FFA cells, for which the chromaticity is zero, in the arcs and in the return straight. This allows the revised lattice to achieve:

- Zero dispersion in the quadrupole injection/production straight;
- Zero chromaticity in the arcs and in the return straight, thereby limiting the overall chromaticity of the

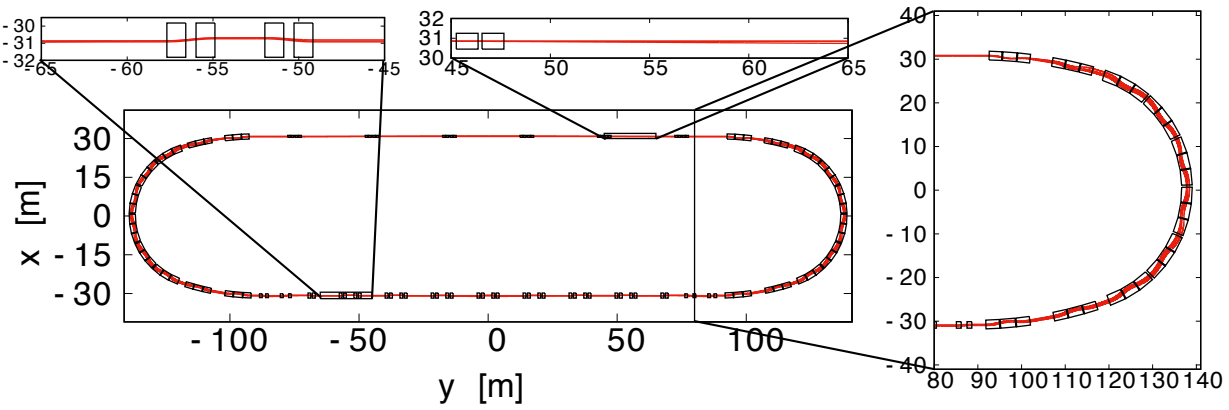

Figure 19: Schematic drawing of the revision of the muon storage ring. The beam circulates in an anti-clockwise direction. The production straight (at $z \sim 30$ m) is composed of large aperture quadrupoles that produce the large values of the betatron function required to minimise the divergence of the neutrino beam produced in muon decay. The lattices of the arcs and return straight are based on the Fixed-Field Alternating gradient (FFA) concept and allow a large dynamic aperture to be maintained.

ring; and thus

- Large overall transverse and momentum acceptance.

The arcs exploit superconducting combined-function magnets with magnetic fields of up to ~ 2.6 T. The return straight is based on combined-function room-temperature magnets. The production straight uses large-aperture room temperature quadrupoles. The vertical magnetic field around the ring for the maximum momentum (~ 6 GeV/c) muon closed orbit in the racetrack FFA ring is shown in figure 20. The mean betatron functions in both the production and return straights are kept large enough to minimise the contribution of betatron oscillations to the angular spread of the neutrino beam, such that both can be used to serve a neutrino-physics programme.

The arc cells have a high magnet-packing factor to minimise the arc length and are connected with the injection and return straights using specific matching sections. The matching section serving the injection straight matches dispersion to zero and allows a long straight for injection to be accommodated. Additional matching sections are between the arcs and the cells of the return straight. The Twiss parameters around the ring are shown in figure 21. Selected parameters of the hybrid design for the racetrack ring are summarised in table 3. The reference tunes of the machine (8.203, 5.159) are chosen such that they are not close to the dangerous resonances. The off-momentum tunes have been chosen to avoid integer and half-integer resonances (see figure 22). Further reduction of the chromaticity of the ring is possible by altering the nonlinear magnetic field distribution in the regular arc cells.

4.2.2 Storage ring performance

The performance of the hybrid FFA design for the storage ring was verified in tracking studies. In order to incorporate tracking through the combined-function magnets taking into account the fringe fields and large amplitude effects a code used for the full FFA machine developed previously was used [54]. It is a stepwise tracking code based on Runge-Kutta integration, using Enge-type fringe fields. The results of the multiturn tracking shows that the dynamical acceptance of the machine is about $1\,\pi$ mm rad in both transverse planes, which is what is required for the needs of the experimental programme, see figure 23. The studies to cross-check the results with the PyZgoubi code, as performed successfully before [54], are underway.

Total circumference	616 m
Length of one straight section	180 m
One straight section/circumference ratio	29%
Operational momentum range	1–6 GeV/c
Reference momentum	5.2 GeV/c
Reference tunes (Q_h, Q_V)	(8.203, 5.159)
Momentum acceptance	$\pm$16%
Number of cells in the ring:	
Straight quad cells	6
Arc first matching cells	4
Arc cells	12
Arc second matching cells	4
Straight matching FFA cells	1 (+1 mirror)
Straight FFA cells	8

Table 3: Selected parameters of the hybrid FFA storage ring.

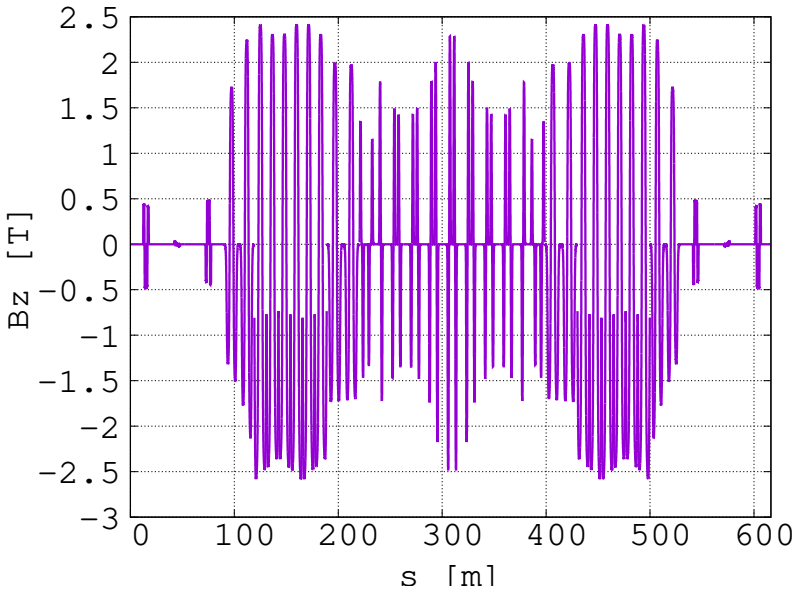

Figure 20: The vertical magnetic field for the maximum momentum ($\sim$ 6 GeV/c) muon closed orbit in the racetrack FFA ring.

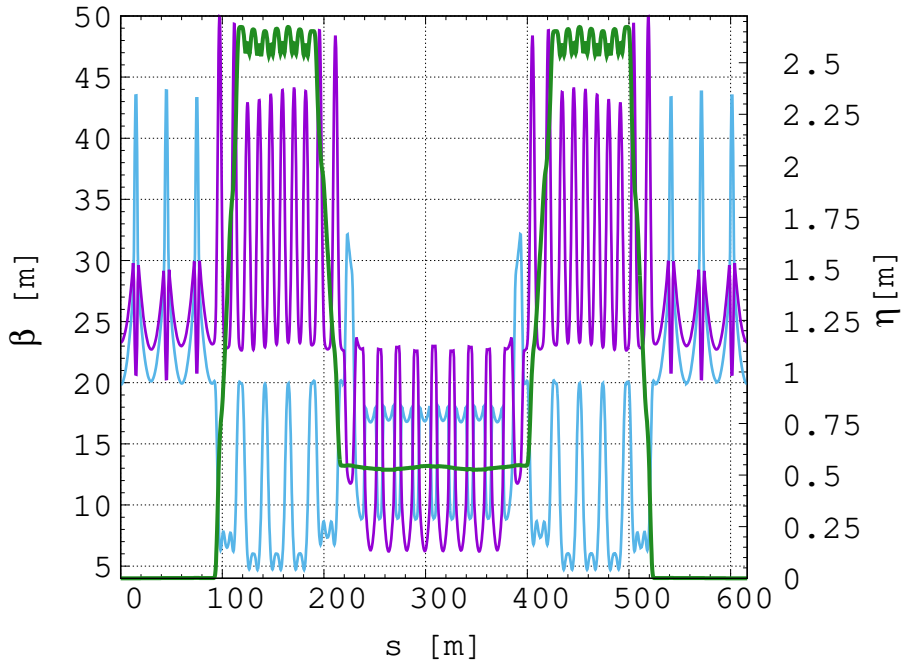

Figure 21: The vertical magnetic field (left-hand plot) for the maximum momentum (~ 6 GeV/c) muon closed orbit in the racetrack FFA ring. The betatron functions (horizontal-blue and vertical-purple) and dispersion (green) for reference momentum (5.2 GeV/c) muon closed orbit in the racetrack FFA ring.

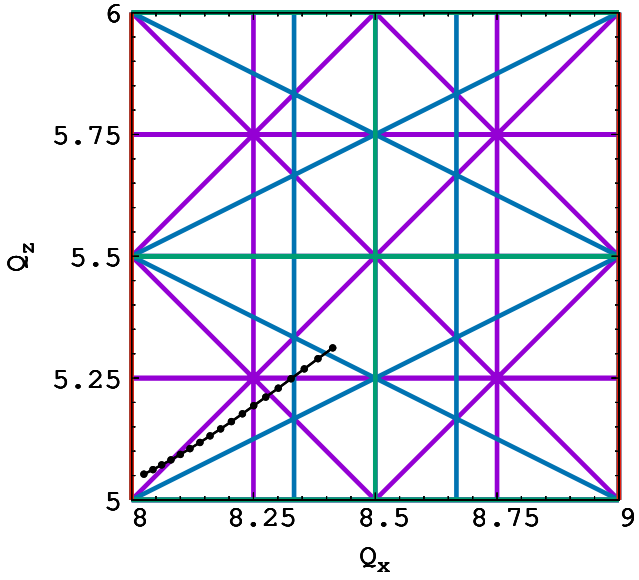

Figure 22: The machine tunes for the muon beam stored in the nuSTORM ring at the reference momentum of 5.2 GeV/c with the momentum spread of $\pm 16\%$.

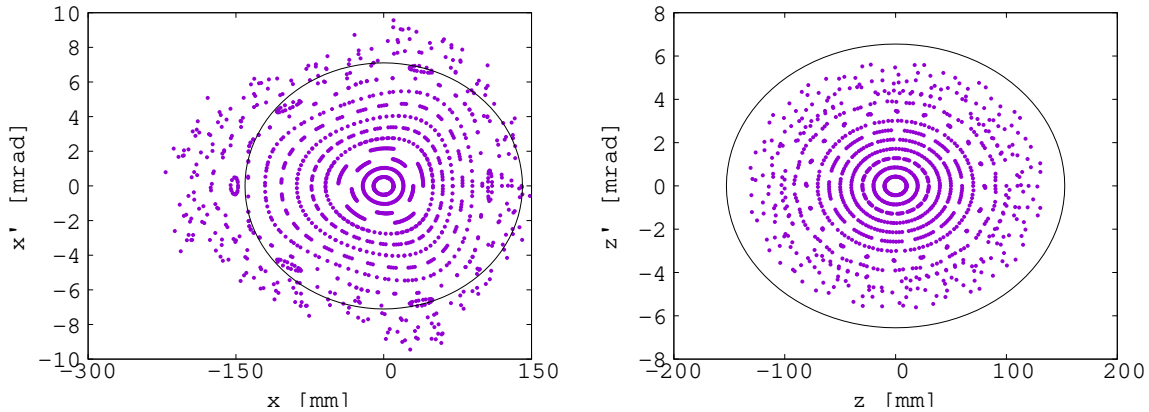

Figure 23: The horizontal (left-hand plot) and the vertical (right-hand plot) dynamical acceptance studies in the hybrid nuSTORM ring at the reference momentum of 5.2 GeV/c. Particles are tracked over 100 turns with different amplitudes in the plane of study including a small off-set from the closed orbit in the other plane. The black ellipse represents the acceptance of $1\,\pi$ mm rad.

5 Implementation at CERN

5.1 Overview

An overview of the proposed implementation of nuSTORM at CERN is shown in figure 24. Protons for nuSTORM will be extracted from the SPS at 100 GeV. The fast-extraction system will be installed in LSS6 where an existing extract system serves beam to the West Area. An upgrade to the present extraction kickers will be required to accommodate the two 10.5 μs long pulses. Beam will be transported through an existing transfer tunnel (TT60). Before TT60 enters the Meyrin site, the beam will be taken through a new transfer tunnel to the nuSTORM pion-production target. Approximately 165 kW will be delivered to the nuSTORM target in a cycle with a period of 3.6 s. The key parameters of the SPS beam required to deliver nuSTORM are summarised in table 4. Operational scenarios which will allow 10^{21} protons to be delivered to nuSTORM over the first five years of operation whilst serving other users of the SPS are under discussion.

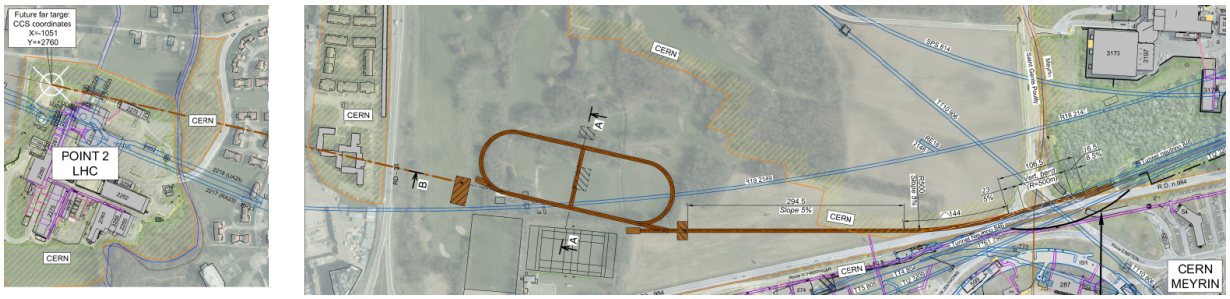

Figure 24: Overview of the implementation of nuSTORM at CERN. The nuSTORM ring and associated infrastructure is shown in the right panel. The possible location for a far detector is shown in the left panel.

Table 4: Key beam parameters foreseen for nuSTORM (based on the analysis of CENF.)

Momentum	100 GeV/c
Beam Intensity per cycle	4×10^{13}
Cycle length	3.6 s
Nominal proton beam power	156 kW
Maximum proton beam power	240 kW
Protons on target (PoT)/year	4×10^{19}
Total PoT in 5 year's data taking	2×10^{20}
Nominal / Maximum repetition rate	6/3.6 s
Max. normalized horizontal emittance (eh at 1 σ s)	8 mm.mrad
Max. normalized vertical emittance (ev at 1 σ)	5 mm.mrad
Number of extractions per cycle	2
Interval between extractions	50 ms
Duration per extraction	10.5 μs
Number of bunches per extraction	2100
Bunch length (4s)	2 ns
Bunch spacing	5 ns
Momentum spread (dp/p at 1s)	2×10^{-4}

Beam will be delivered onto a graphite target. Pions and other secondary hadrons will be collected using a pulsed electromagnetic horn. The beam emerging from the horn will be captured in a large-aperture quadrupole

channel which will bring the pion beam with momentum in the range 3 GeV to 8 GeV to the nuSTORM ring. Injection will be into the production straight of the storage ring. Muons from pion decay will be captured as the pions pass through the production straight. At the end of the production straigh undecayed pions and muons outside the momentum selected for storage will be directed to a dump. A near detector hall will be placed 50 m from the end of the production straight. The neutrino beam is dircted to LHC Point 2 where it may be possible to install a far detector to be used in the search for light sterile neutrinos.

5.2 Preamble

The SPS has demonstrated its ability to produce beams in the sub-MW range for neutrino experiments. For CNGS the fast extracted 400 GeV/c proton beam from the SPS operated at a maximum beam power of 510 kW in a 6 s cycle in which delivered two 10.5 μs bursts of 2.25×10^{13} protons each. During CNGS operation the SPS routinely delivered a daily-averaged power of 380 kW. Operation with a peak beam power of 405 kW was achieved over periods of a few hours.

In normal operation, the average beam power delivered was 300 kW. This was less than the maximum possible beam power due to:

- Intensity limitations due to beam loss in the PS during acceleration and extraction towards SPS;
- Intensity limitations at injection to the SPS to during acceleration due to the minimal-loss requirement in the delivery of high-intensity, large duty factor beams; and
- Competition for beam from the LHC, the Fixed Target Physics program and Machine Development.

The beam required by nuSTORM is similar to that used by CNGS albeit at the lower momentum of 100 GeV/c. A beam power of 156 kW has been considered for nuSTORM and corresponds to a total intensity of 4×10^{13} per cycle. clearly demonstrated during the CNGS era to be with the reach of the PS and SPS. Studies to understand the performance of the machines have been performed and will be briefly reported in the next sections. Bottlenecks and their mitigation to reach the high-intensity beam parameters required for nuSTORM will also be discussed.

5.3 Primary Proton Beam

The SPS will be set up to deliver beam in bunches separated by 5 ns. This is the 'standard' beam to used to serve the fixed-target experiments in CERN's North Area. The SPS will be filled using two injections from the PS. Beam will be extracted from the SPS in two spills, each spill will be 10.5 μs in length and separated by 50 ms. The beam structure and requirements at the target are shown in tables 4 and 5 respectively.

The maximum PS intensity that has been achieved at 14 GeV/c is approximately 3×10^{13} using a single PSB batch injection with a PS cycle time of 1.2 s. An intensity of approximately 4×10^{13} has been achieved using double PSB batch injection. The double-batch injection adds 1.2 s to the length of the PSB cycle, yielding a PS cycle time of 2.4 s. Without losses, therefore, the double-batch PS-injection scheme corresponds to a maximum intensity at 14 GeV/c of 6×10^{13} ppp (protons per pulse) with an injection plateau of 1.2 s. 8×10^{13} pp will be injected over 2.4 s.

These considerations imply that the maximum intensity that can be accelerated by the SPS is 7.6×10^{13} ppp in a 7.2 s cycle or 5.7×10^{13} ppp in a 6.0ṡ cycle. In deriving these intensities the optimistic assumption has been made that no more than 5% of the beam is lost. The intensity per cycle proposed for nuSTORM should therefore be comfortably within reach even taking into account the fact that relative beam loss increases with intensity and that the reliability of the accelerator reduces in high intensity operation.

The High Luminosity LHC (HL-LHC) also requires high total beam intensity. However the acceleration cycle for the LHC beams is longer by more than a factor 3. In this mode, therefore, the SPS will deliver a

Table 5: Proton-beam parameters at the entrance face of the nuSTORM pion-production target.

Minimum beam size (H and V, 1 σ RMS)	2.1	mm
Minimum beam size (H and V, 1 σ RMS)	1.5	mm
Maximum beam size (H and V, 1 σ RMS)	2.7	mm
Maximum beam divergence (H and V, 1 σ RMS)	1.0	mrad
Maximum dispersion (H and V)	n/a	m
Maximum dispersion angle (H and V)	n/a	mrad
Maximum position steering range (H and V)	$\pm$10	mm
Maximum angle steering range (H and V)	$\pm$0.5	mrad
Total delivery precision (jitter, drift) all sources (H and V, 1 σ RMS)	$\pm$0.1	mm
Position measurement precision (H and V, 1 σ RMS)	$\pm$0.05	mm
Minimum distance from last beam-line element to target face	10	m

beam power reduced by a factor of 3 compared to that which can be delivered in the CNGS mode. The main difference between the CNGS-type beam and the LHC-type beam accelerated in the SPS is related to the shorter PS cycle, which is only possible with beam injection at 14 GeV/c, and which results in transition crossing in the SPS. The CNGS-type beam fills the whole SPS ring while the LHC-type beam fills less than half. The two beam types therefore have different RF requirements. The CNGS-type beam has a smaller bunch spacing (5 ns) and lower bunch intensity. As a result these beams also require different beam control (LLRF) systems and suffer from different intensity effects (beam loading, instabilities, beam-induced heating).

Studies of the stability of the CNGS beam were performed in 2012 to verify the existing intensity limitations in light of the performance required by the proposed LAGUNA/LBNO. The RF voltage programme on the flat bottom was modified to see whether the beam quality could be improved and losses reduced. It was confirmed that the operational programme outlined above is practically optimum for an injected beam intensity of 3.6×10^{13}).

The LHC Injectors Upgrade (LIU) project [55], which is scheduled to be completed by 2020, will allow higher intensity CNGS-type beams to be considered.

5.4 Extraction and transfer

Various options for the fast extraction of the SPS beam were considered for nuSTORM. The development of the existing fast extraction channel in LSS6 that serves beam to the West Area was chosen as the delivery of the extracted proton beam to the nuSTORM target is relatively straight forward. At present this channel serves both the HiRadMat facility and the LHC via the TT60/TI2 transfer line.

The LSS6 extraction channel requires minor modification to serve nuSTORM. These modifications would be based closely on the configuration of LSS4 which was designed specially to accept the high-brightness beam for the LHC and the high-intensity beam for CNGS. The LSS6 extraction channel was used in the past to serve the West Area Neutrino Facility. For nuSTORM will be directed from the TT60 transfer line into the BA7 area using a set of fast switching magnets. A new transfer line will then bring the beam to the nuSTORM target cavern. A schematic of the proposed configuration is shown in figure 25.

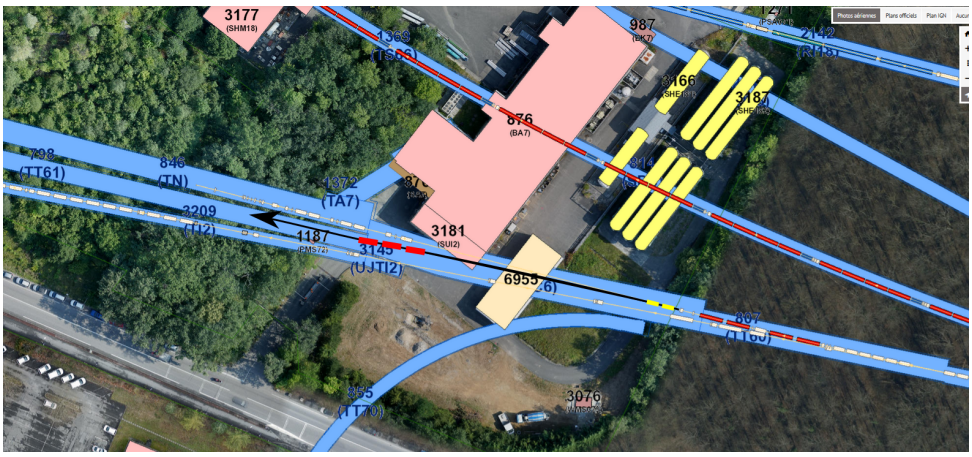

Figure 25: Beam lines from the SPS LSS6 extraction point, the nuSTORM line (black arrow) is shown branching off the HiRadMat line and bending horizontally and vertically into TT61.

5.4.1 Fast extraction from the SPS

Extraction of the CNGS-type beam at 100 GeV is limited in the horizontal plane to around 5σ by the septum protection TPSG and to about 4σ in the vertical plane by the extraction septum MSE. These apertures are considered reasonable. The pulse structure, two 10.5 μs-long pulses, however, poses an issue for the extraction-kicker system. The present system in LSS6 cannot reach the required rise-time of around 1 μs. Without an upgrade of the system, only one pulse per cycle can be extracted which will significantly reduce the number of protons on target (POT). An upgrade of the kicker system is technically feasible at moderate cost.

5.4.2 Beam transport onto target

Around 230 m downstream of the SPS extraction point, the TT60 line is split into the lines TI2 (LHC beam to P2) and HiRadMat (material test facility in the TN tunnel), see figure 25. It is proposed to provide beam to nuSTORM by constructing a new branch off the HiRadMat beam-line downstream of a main bend (MBB.660213) using C-shaped switching dipoles of the MBS type. Branching off the HiRadMat line makes use of large aperture QTL-type quadrupoles (80 mm diameter). After the switching section, the beam needs to be bent vertically to match the slope of the TT61 transfer tunnel using two MBB type dipoles; an additional MBB dipole is used to compensate for the switching angle in the horizontal plane.

After switching from the HiRadMat line, a 290 m section of beam-line is housed in existing tunnels. At the end of this section, a junction cavern must be constructed to allow the branch into the new tunnel. A beam line of length $\sim$ 585 m is required in the new cavern and new tunnel (see figure 26). Along this line there are two horizontal bending sections that require 5 and 10 MBB-type dipole magnets respectively and two vertical bending sections which require 6 and 3 MBB-type dipoles respectively. Since all bending sections bend in one plane only, a careful choice of magnet locations in the optics might allow for an achromatic design.

A FODO lattice with 30 m half-cell length is assumed. Large aperture QTL-type quadrupoles, which are usually used for SPS fixed-target beam-lines, have been considered. F 30 quadrupoles are required for the full 875 m beam line. Three additional quadrupoles are needed for the final focus, the same magnet type has sufficient aperture. Each quadrupole shall be equipped with a corrector magnet and, between the final focus and the target, a set of two correctors per plane is considered for orthogonal steering.

Beam instrumentation will consist of dual-plane beam-position monitors at each quadrupole, 4 screens in

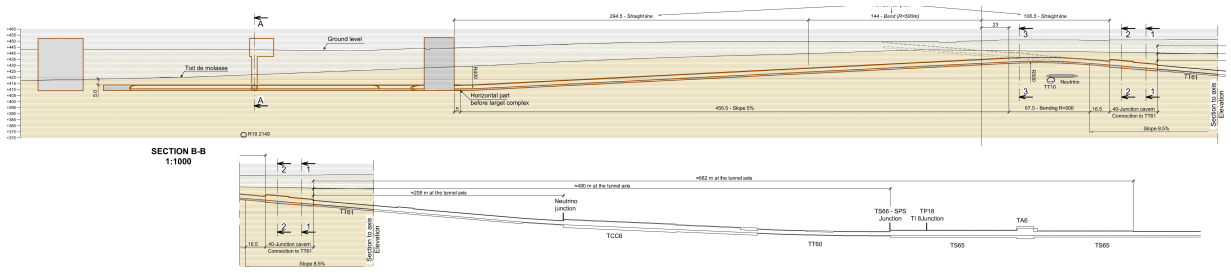

Figure 26: Elevation drawing of the nuSTORM beam line from SPS extraction on the right of the top figure to the target complex to the far left.

the switching and final-focus areas, 2 beam-current transformers, and 10 loss monitors along the line.

Two power supplies will be required for the FODO quadrupoles. An additional 8 supplies will be required for the initial matching and final-focus sections. The main dipoles will require several different power supplies, optimisation with strong correction magnets or trim supplies could be envisaged.

5.5 Experimental hall

The plans for the near-detector hall, the requirements for this detector facility, and the key considerations will be addressed briefly in this section. The possible future expansion of nuSTORM to include a far-detector hall is also outlined. Proposals for the experimental areas are necessarily at an outline stage and will need to be developed further as the project progresses. At this stage, the layout and concept is largely based on work carried out at FNAL.

5.5.1 Near Detector Facility

The near detector facility will be sited just beyond the production straight of the muon decay ring. The facility is aligned to allow installation of a detector in line with the production straight, with the rest of the building offset away from the ring to minimise radiation protection issues and to allow detectors to be mounted off the neutrino-beam axis. The building is currently designed on multiple levels combined into one facility (see figure 27):

- An experimental hall beneath ground, in plane with the muon decay ring to house the experimental area;
- A surface building to allow assembly, maintenance, services and handling for the detector and associated infrastructure; and
- A shaft connecting the two allowing access to the area below ground as required.

5.5.1.1 Experimental Hall

The space reserved for the experimental hall is sufficient to accommodate the nuSTORM near detector while retaining flexibility for other future experiments. The hall would be a radiation controlled area and would not be accessible during beam operation. The area will need suitable HVAC systems to accommodate the experimental needs. The experimental hall will be served by a 20 tonne overhead crane to allow movement of materials and detector components as well as handling of shielding blocks.

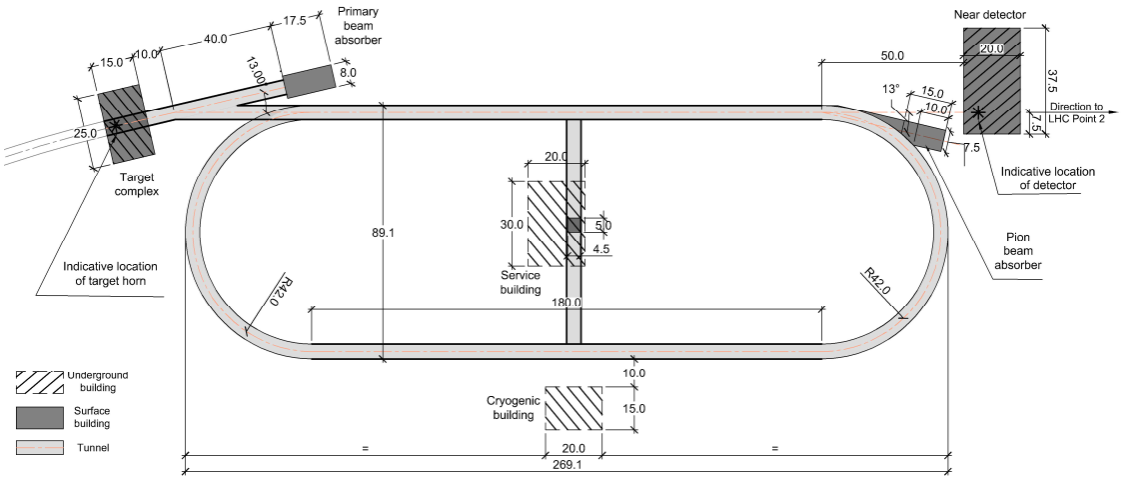

Figure 27: Plan view showing the location of the near detector hall in relation to the muon decay ring.

Experimental surface building

The surface building will house:

- Loading dock or access for HGVs to enable deliveries;
- An assembly area to construct and bring together detector components;
- Maintenance facilities to facilitate work on the detector;
- A control room to monitor and control the experiment (and potentially aspects of the decay ring);
- Storage for shielding blocks when not in use;
- Electrical, mechanical and HVAC services for the sub-surface area;
- IT hardware (although the majority is likely to be housed off-site); and
- Ancillary facilities such as toilets and meeting rooms.

The surface building will be served by a 20 tonne overhead crane to allow unloading and movement of materials as well as transport to the sub-surface experimental area. The crane will, in addition, allow handling of shielding blocks. The surface building will be classified as a controlled or supervised area for radiation protection purposes with access systems designed accordingly.

Experimental access shaft

The access shaft will provide direct vertical access between the surface building and experimental area. When not in use, approximately 1.8 m of precast concrete shielding blocks will be stacked within the shaft to provide the required level of shielding to allow use of the surface building during beam operation. The shaft will also provide access for service ducts and cabling between surface and the experimental area. A shielded personnel lift will be provided. The shaft will be strategically located above the detector location to allow direct positioning of large components. This will also facilitate maintenance of components likely to become more activated.

Miscellaneous and general

The civil engineering issues are dealt with in section 5.6. Fire detection equipment will be provided throughout along with access control systems. The facility in full, with particular focus on the underground experimental

area, will be designed with 'as low as reasonably achievable' (ALARA) principles in mind for management of radiation. The civil engineering in particular will prevent migration of water into or out of the facility. HVAC systems will contain and minimise activation of air within the facility. A more detailed strategy is presented in section 6.1.

5.5.2 Far detector facility

The far detector facility will be sited at or close to LHC Point 2 (see figure 24). This distance is suitable for the planned energy range in order to achieve the aims of the nuSTORM physics programme. At this stage the building has not be costed or designed in detail. The required facilities, services and form of construction would all be comparable to those of the near detector.

5.6 Civil engineering and infrastructure considerations

Substantial civil engineering (CE) works will be required for the nuSTORM facility to be realised. The results of a study carried out by CERN's SMB-SE Future Accelerator Studies (FAS) section to identify design constraints and considerations in order to produce an outline CE design along with the next steps for development of nuSTORM will be reported below.

5.6.1 Location

The proposed site for nuSTORM is located to the north of CERN's Meyrin site, with all required CE works within France as shown in figure 28. The site is located west-north-west of Geneva within the Lake Geneva depression between the Alps and the Jura mountain chains. The Geneva Plain in this area consists of Moraines overlying Molasse. The Moraines are glacial deposits comprising gravel, sands, silt and clay with some water bearing layers. The Molasse is a stratified series of marls, sandstones and formations of an intermediate composition, collectively termed the Molasse. This rock is generally considered good rock to tunnel within because it is relatively dry and stable without being excessively hard. There are some well documented issues however, with weaker marl strata between stronger layers causing issues as well as some faulting and fissures throughout.

The location has been determined primarily by the experimental physics requirements, but the site is also well suited from a CE perspective. Throughout the development of CERN, many tunnelling projects have been implemented in this area and so ground conditions are well understood with a plethora of ground investigation information available. The tunnelling required to enable nuSTORM can be carried out within the Molasse rock. Shafts constructed in this area would only need to advance through around 20 m of the weaker Moraines before entering the more competent Molasse.

At the proposed location, the existing land consists of green spaces including some agricultural land and a small area of woodland. Out of necessity, the majority of the overground works are located just north of CERN's Meyrin campus, at the west end of the site, just to the north-east of the Porte de France roundabout. The junction cavern and first part of the extraction tunnel are sited beneath the D984F and its junction with the C5 Route de l'Europe before continuing under agricultural land to the west. The site is bounded to the south by the D984F road and to the west by the D35 road.

The site is partially within existing CERN land, although a portion to the west is outside this. Initial discussions have been held with local authorities to reserve this land for possible future CERN use.

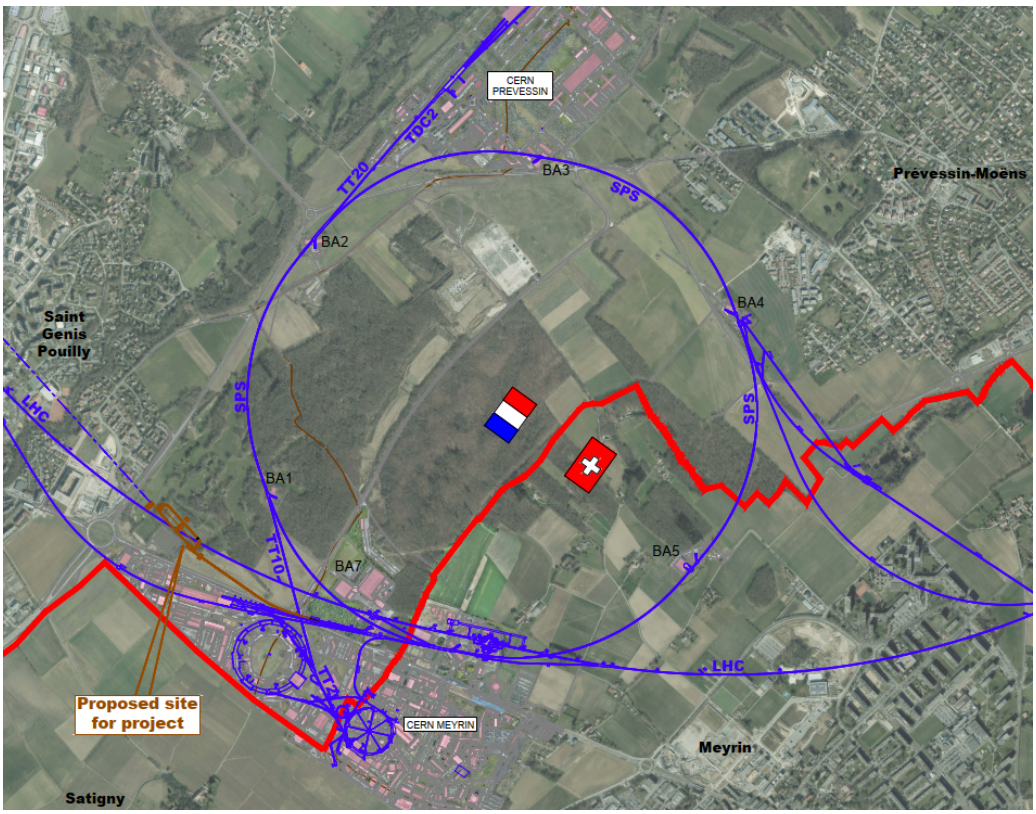

Figure 28: Plan showing proposed location of nuSTORM in relation to CERN and the Franco-Swiss border.

5.6.2 Proposed facilities

The major CE elements required to implement nuSTORM are:

- A 40 m long junction cavern to allow connection to the existing tunnel TT61;
- A 545 m long extraction tunnel;
- A target complex;
- A 625 m circumference muon decay ring;
- A near detector facility; and
- Support buildings and infrastructure.

The general arrangement is as shown in figure 24.

Junction cavern

The junction cavern, shown schematically in figures 29 and 30 measures 40 m in length, however this is split into two equal sections of 20 m. The two sections measure 7 m and 10 m in width and 3.9 m and 5.0 m in height respectively. The new Austrian tunnelling method would be used with the likely structural form consisting of rock bolts, a sprayed concrete temporary lining, drainage layer, a reinforced concrete cast in-situ permanent lining and mass concrete invert. Drainage will be required within the tunnel, with a sump and pumping arrangement required at the low point. The junction cavern has been sized to allow beam-line equipment to split and bend the beam away from its path in TT61 into a new extraction tunnel. This area is very congested with the existing neutrino tunnel TN and TI12 both close-by.

The location for the junction was chosen to retain certain minimum distances from existing tunnels to

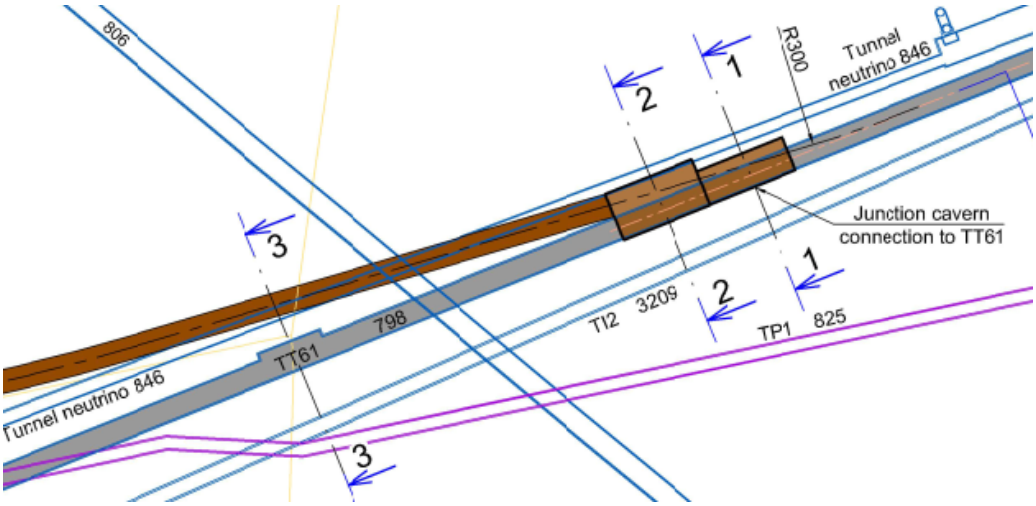

Figure 29: Plan view of required junction cavern connecting with the existing tunnel TT61.

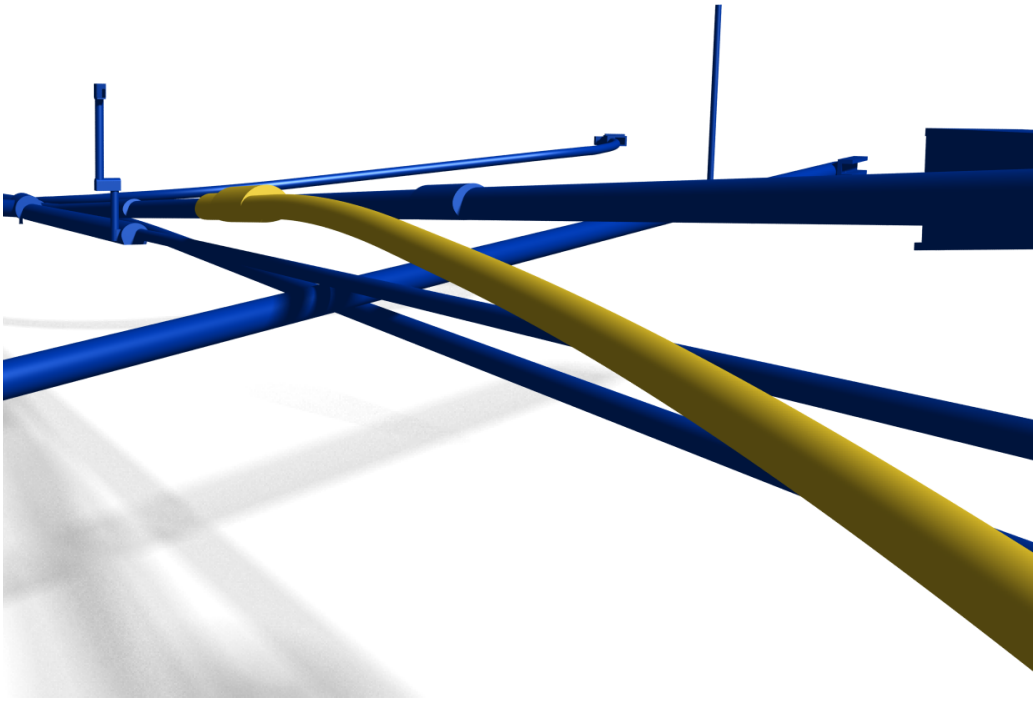

Figure 30: 3D view looking south-west taken from CE model of junction cavern and extraction tunnel showing nuSTORM proposed facilities in yellow and congested existing infrastructure in blue.

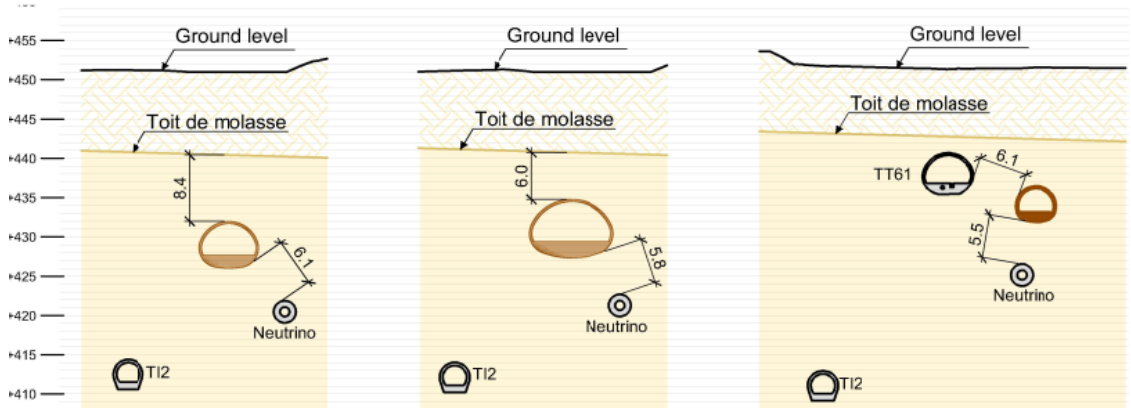

Figure 31: Sections through junction cavern as shown in figures 29 and 30 showing proximity of existing tunnels. Sections 1-1, 2-2 and 3-3 are shown from left to right.

minimise impact on their stability. The junction cavern works must also be carried out within the Molasse. In general the Molasse is weathered, more fractured and less structurally competent as it approaches the rockhead or *toit de Molasse*. To facilitate the complex junction cavern works, the design has aimed to avoid going within 5 m of the rockhead, reducing the chances of encountering very poor quality rock.

The junction cavern is split into two separate sections to strike a balance between reducing the size (and cost), while allowing a degree of consistency in cross section: allowing the practical construction of the required cavern (see figure 31). As shown, a typical mined section is envisaged with a span suitable to ensure stability.

Extraction tunnel

The extraction tunnel measures 545 m in length between the junction cavern and the target complex. This would be built using the same form of construction as the junction cavern albeit with a constant cross section of 4.5 m wide by 3 m high as shown in figure 32. The proposed tunnel cross section is estimated based on similar mined tunnel profiles at CERN but will need to be designed in detail following ground investigation. The proposed cross-section is considered reasonable to base preliminary design and cost estimates on.

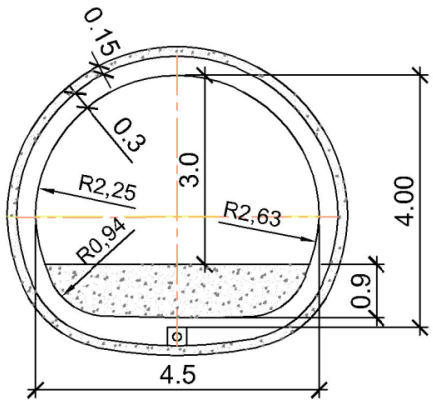

Figure 32: Typical cross-section of extraction tunnel N.B. rock bolts omitted.

The geometry of the extraction tunnel has been developed in line with beam transfer constraints regarding minimum bending radii, the requirement to stay within the Molasse and CERN transportation maximum

gradients to ensure future installation and maintenance can be carried out both safely and cost effectively (see figure 33). In terms of bending radii, limits of 300 m when bending in one plane or 430 m when bending in two planes simultaneously have been respected. The length of bending sections have been minimised where practical, to avoid the need for unnecessary magnets. Where the extraction tunnel approaches the target complex, it returns to horizontal in order to facilitate construction of the muon decay ring and to avoid a future far detector site being at considerable depth when the inclination is projected at distance.

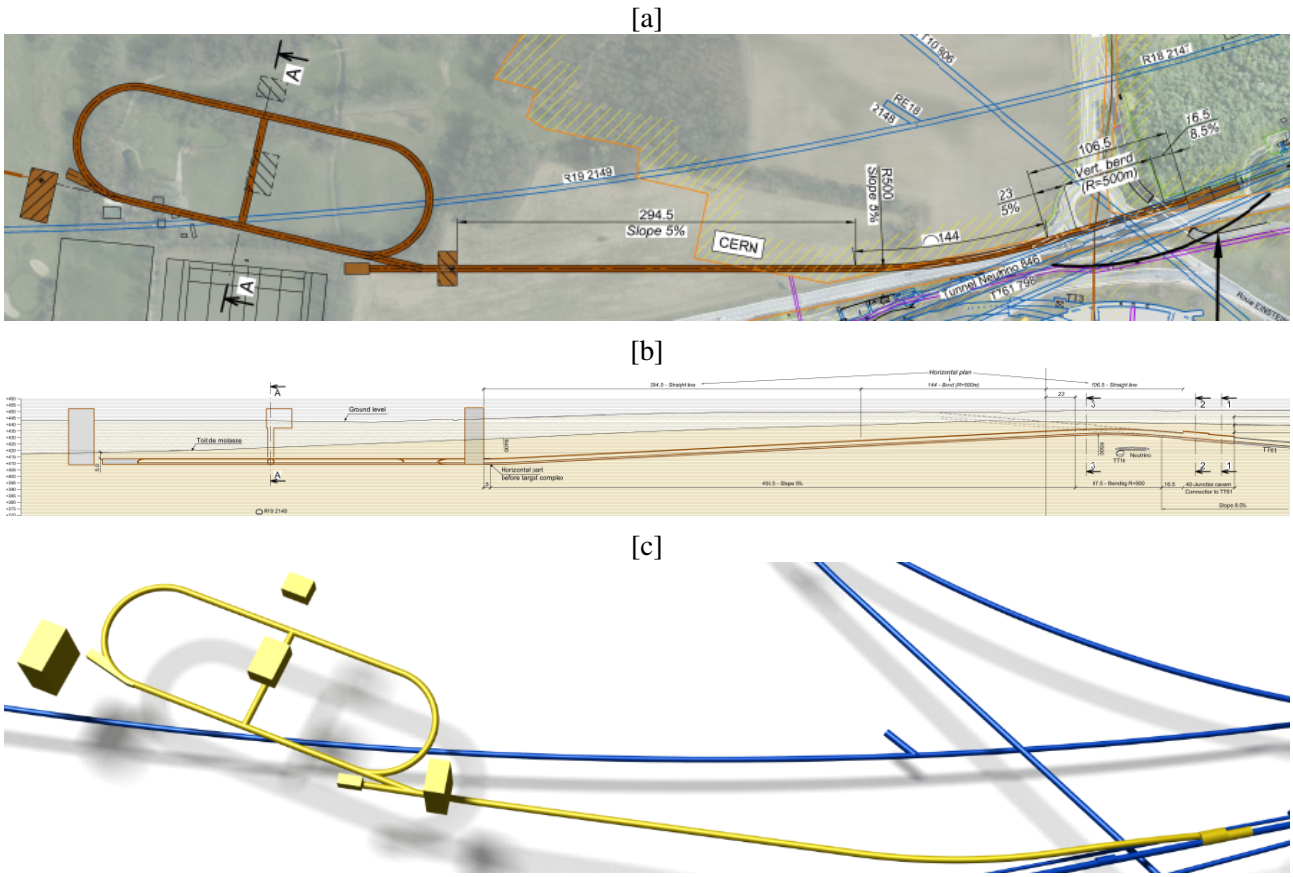

Figure 33: Plan view showing general arrangement (a), long section of extraction tunnel (b) and 3D view of proposed facilities in yellow (c), all between the extraction point and Muon decay ring.

Target complex

The target complex measures 15 m by 25 m in plan with a 9 m height above the surface, extending below ground to the level of the beam-line via a shaft. At this stage in development, a suitable space reservation has been allowed for the target complex with input from CERN's target and target complex team. Further design development will be required at a later stage.

The complex would be constructed with diaphragm walls. This would allow construction at depth, while avoiding significant volumes of earthworks above. Diaphragm walls have a significant benefit in terms of water tightness, helping to minimise water ingress and egress to and from the target complex. This would assist in minimising any activation of water in close proximity to the complex. The technique can be used successfully up to 100 m depth so is well suited to the situation. The target complex would be part overground, part underground, constructed within a diaphragm wall box which would also allow the use of this point as a

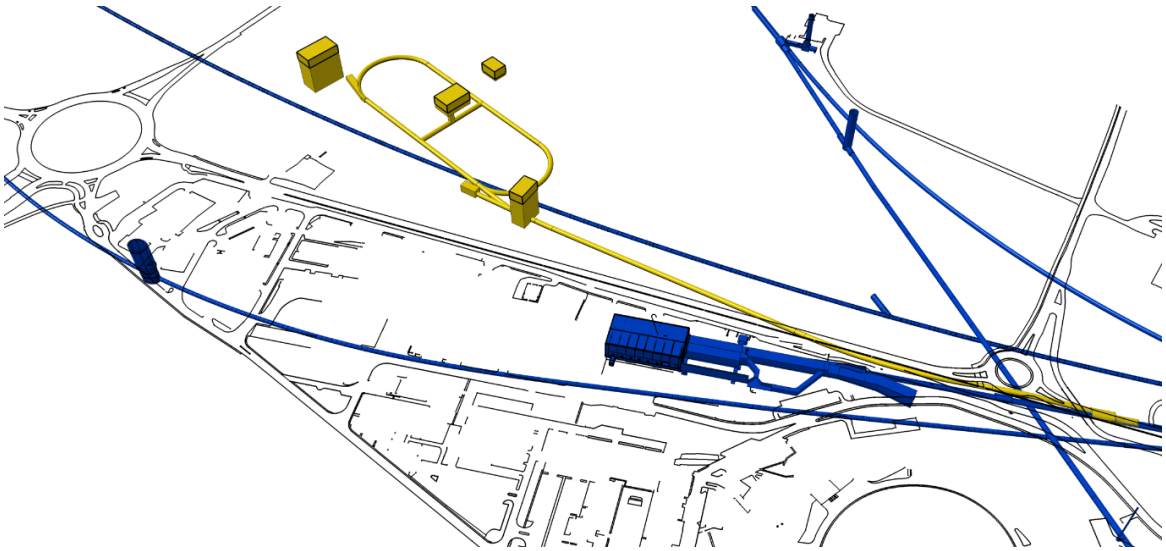

Figure 34: 3D view showing underground (yellow) and overground nuSTORM (black outlined yellow) facilities in context of CERN existing site and infrastructure (blue).

shaft during construction from which tunnelling would be carried out.

Above ground, the target complex would be constructed as a conventional steel portal frame building with cladding for insulation and water tightness.

Muon Decay Ring and associated infrastructure

Following the target complex, the tunnel splits to a muon decay ring at a 13° 'kink' and a primary beam absorber in line with the extraction tunnel (see figure 34). The dimensions of the muon decay ring are as shown in figure 35. The cross section will be the same as the extraction tunnel. The geometry of the ring has been determined by experimental physics factors to ensure the ring radii can accommodate bending magnets for the energy levels proposed. The length of straight sections is determined to allow sufficient decays to produce a volume of data to achieve the objectives of nuSTORM.

The muon decay ring is to be horizontal with the end of the ring 5 m below the *toit de Molasse* to increase the chances of tunnelling in competent rock. Although the muon decay ring crosses the line of the Large Hadron Collider (LHC), there is nearly 35 m vertical clearance. There is not expected to be any effect on the LHC during works or operation.

Additional support infrastructure, including a primary beam absorber, service building, cryogenic building, pion beam absorber and near detector facility, will be located close to the muon decay ring. Both the primary and pion beam absorbers would be accommodated within small caverns/alcoves with the possibility to place shielding at the entrance from the tunnel as required for radiation protection purposes.

The service building would provide an access from ground level to beam-level both for personnel and equipment, with a shaft 29 metre deep from ground level envisaged (see figure 36). A surface building to house necessary infrastructure and utilities for the ring has been included, sized based on other similar projects. This would consist of a steel portal-frame building above ground with a basement structure below. The muon decay ring requires super-cooled magnets, therefore allowance is made for a cryogenic service building and supply.

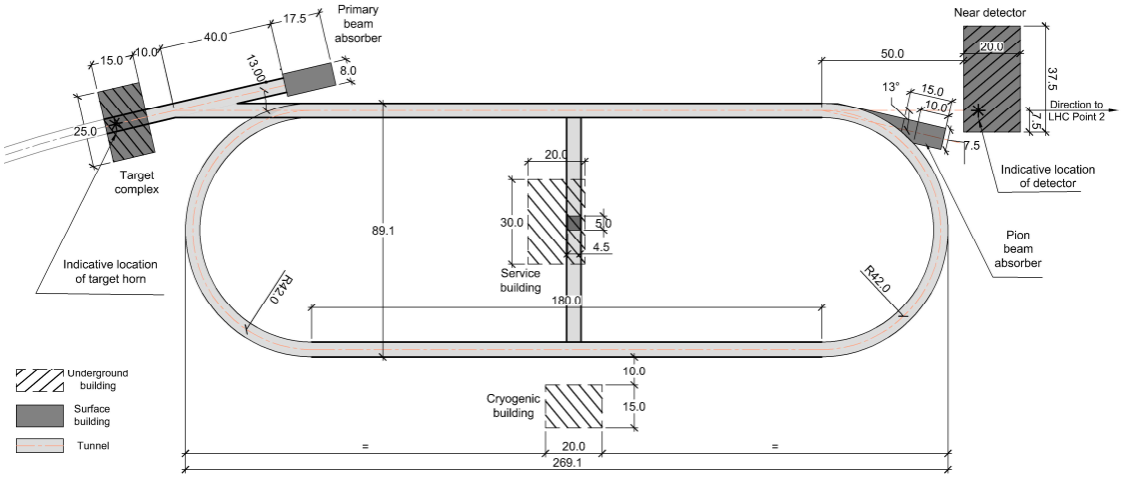

Figure 35: Plan view showing Muon decay ring dimensions and arrangement of associated infrastructure.

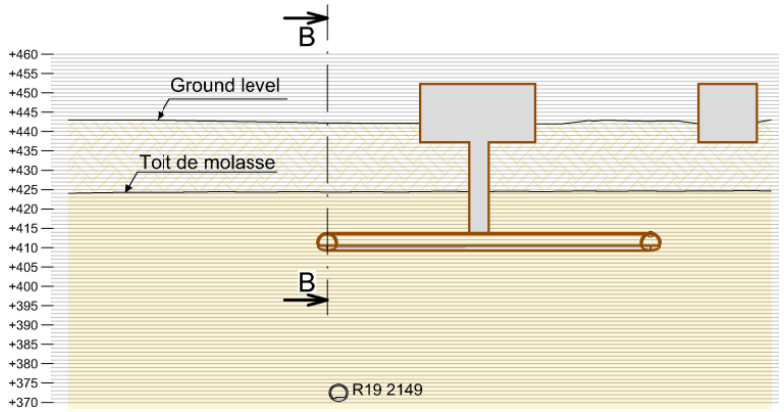

Figure 36: Section through muon decay ring at location of service building and shaft showing ground levels and cryogenic building adjacent.

Near detector facility

The near detector facility will be of a similar structural form to the target complex, with diaphragm walls used to provide a large 'box'. This will house the detector hall (below ground) and detector assembly/ support building (at the surface). Again, a shaft for personnel and equipment access will be provided. Although the building is separated from the muon decay ring at this point, in practice it may be joined, since the shaft would be suitable to launch tunnelling operations for the ring. Again, above ground, the building will be constructed from a clad steel frame.

Future far detector facility

The back straight of the muon decay ring has been aligned with an area at Point 2 on the Large Hadron Collider where CERN own land of sufficient size, in case it is beneficial in the future to construct a far detector building. At this stage, the far detector is excluded from the design and costing beyond the provision of the siting option. There remain a number of opportunities to optimise the design at future stages as requirements are developed.

5.6.3 Construction methods

An estimated construction programme has been developed as part of the cost estimate and in order to consider the timescales necessary to deliver the CE works. The first site operations would be shaft construction using diaphragm walls to provide one or more launch points for tunnelling operations. Diaphragm walls (see figure 37) are now a relatively commonly used technique in CE. The technique has recently been successfully used at CERN in broadly similar ground conditions as part of the CERN Neutrino Platform (CENF) project (see figure 38).

The ground conditions present at this location favour the use of the new Austrian tunnelling method as detailed above. The spacing and length of rock bolts and the thickness of concrete linings can be adjusted accordingly based on the rock quality encountered.

Following completion of the shafts, tunnelling equipment would be lowered into place by crane. Due to the variable tunnel cross-sections and the overall length of tunnelling required, it is assumed that roadheaders would be used to advance excavation. These have the benefit of being far less specialised and expensive than tunnel boring machines and are able to adapt to suit the changing tunnel profile (see figure 39).

The underground works would continue in parallel to the surface works constructing and fitting out buildings. The last element of underground work would be the connection with TT61 and the junction cavern. Building construction would be optimised to allow fit-out of the most complex buildings and installation of experimental hardware as soon as possible.

The connection below ground with TT61 is likely to be the most challenging aspect of the works, due to constraints associated with work next to an activated existing tunnel as well as the inherent difficulties of connecting to existing infrastructure. The works sequence for the junction cavern will need to be carefully planned and monitored before, during and after works.

There will be a substantial amount of spoil produced which, it is assumed, can be permanently stockpiled on site. The proposed location has few constraints in terms of space. There is an ample sufficiency of agricultural land which could be used to stockpile material. There would, in addition, be options to use the material to provide screening from the adjacent roads to limit any visual impact, if required.

The civil engineering works should not pose feasibility issues since generally the works will be implemented by standard techniques. More investigative work will, however, be required to develop the design and assess this in full.

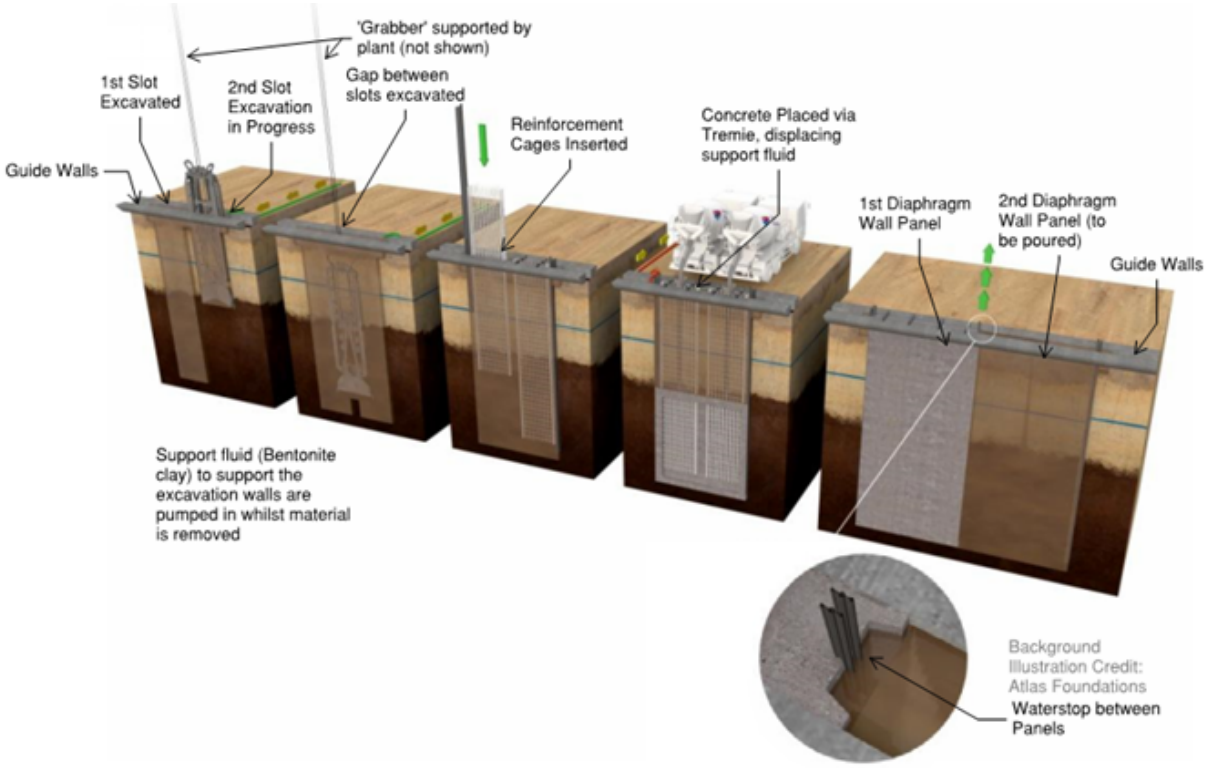

Figure 37: Illustration of the diaphragm walling sequence of works.

5.6.4 Recommendations for work at the next stage of project development

In order for the project to progress, a number of additional studies will be required to allow a detailed design to be completed:

- A detailed ground investigation will be required to confirm or disprove existing assumptions and refine the accuracy close to the proposed alignment;
- A detailed integration study will be required for the project in full with input from transport, radiation protection, electrical engineering, cooling, cryogenics and ventilation teams a priority;
- Further study will be required to assess service supplies required following integration studies. The need for additional technical galleries will need to be considered;
- Thought will be required to avoid or minimise the impact on adjacent beam-line operations and experiments during construction work. Vibration could be an issue for work close to TT61 in particular and mitigation measures may be required for work carried out during 'beam-on'. Tunnel monitoring is also likely to be required during works;
- A survey and study of existing drainage systems should be made to assess condition and capacity in order to design connections; and
- A condition survey of TT61 should be carried out to plan and design the best sequence for connection of the junction cavern.

Figure 38: Photographs taken during (left) and after (right) diaphragm walling works at CENF.

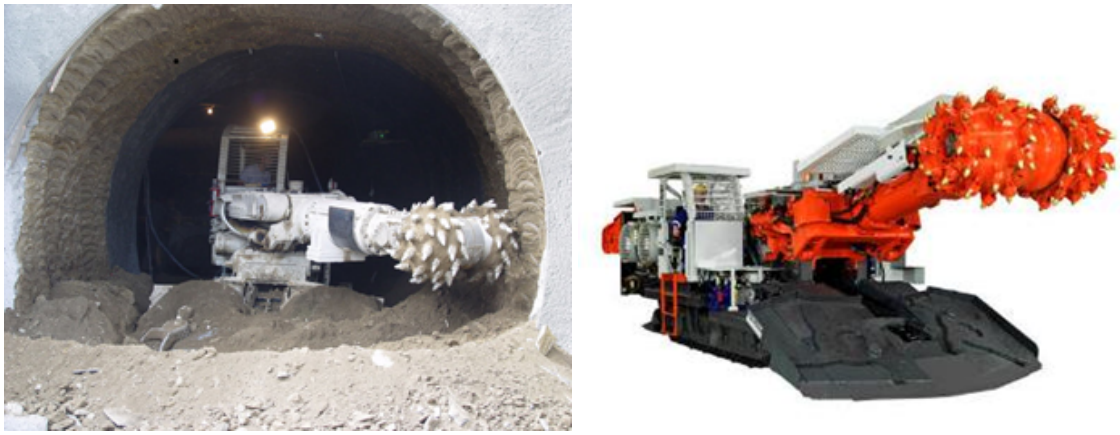

Figure 39: Examples of roadheaders used for tunnel excavation.

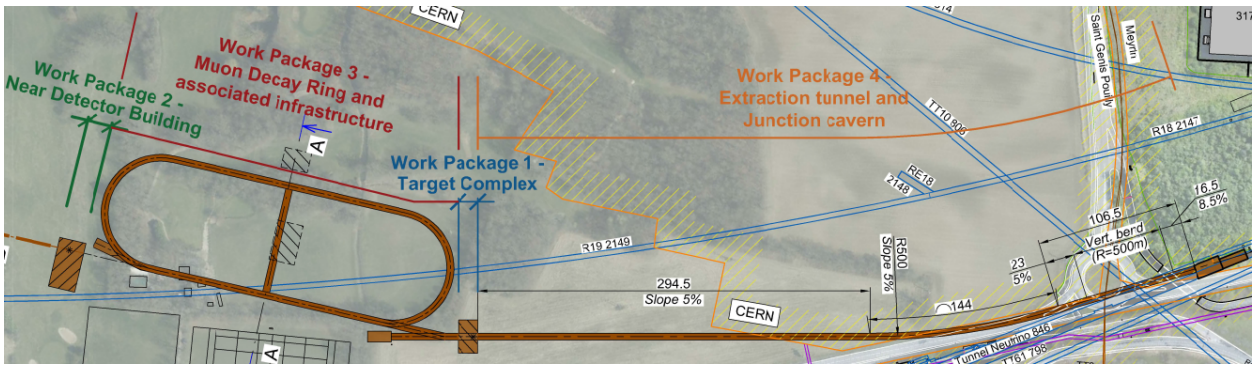

Figure 40: Plan showing proposed split and phasing of work packages during CE works.

5.6.5 Cost estimate for civil engineering works

Basis of estimate

The cost estimate for the nuSTORM project has been based on the layouts presented in this chapter. The estimate includes all aspects of construction, detailed engineering design work and construction management except where stated otherwise. Many of the rates used to formulate this estimate have been based on real construction costs from the large hadron collider experience (1998-2005), from consultant, ILF's future circular collider cost studies [56] and following recent tendering for similar projects at CERN such as CENF and HiLumi.

The civil engineering activities have been split into four different packages as shown in figure 40. The provisional cost for the main tasks identified and included within each package is shown in table 6.

Table 6: Summary cost estimates for the CE work packages

Work package	Cost [kCHF]
Work Package 1	6.2
Work Package 2	11.1
Work Package 3	17.8
Work Package 4	11.2
Miscellaneous CE	0.9
Site investigation	0.5
nuSTORM total	47.7

The accuracy of the estimate is considered Class 4 - Study or Feasibility which could be 15-30 % lower or 20-50 % higher (in line with AACE international's best practice recommendations [57] as has been used for previous CERN projects). The study is at an early feasibility stage so until the project requirements are further developed, it is suggested that the maximum range be adopted i.e. −30 % to +50 % for CE costs.

Costing assumptions and exclusions

The cost estimate is based on the following assumptions:

- Costs have been based on retaining spoil on CERN land with no tipping and disposal costs. If this were to change, the cost increase would be significant;
- The proposed drainage can be connected into existing drainage without significant capacity enhancement of the existing;
- Build up of hardstanding areas and access road can be carried out using site won material with only 1.5 metre depth road construction;
- Radiation protection requirements during junction cavern construction/demolition works do not increase the overall cost of these works by more than 10 %;
- The construction works programme will be as stated in 42. This programme is outline and will need to be reviewed to optimise activities to allow multiple work packages to progress in parallel;
- Ground and ground water conditions do not vary significantly from those previously found in the area;
- Assumptions have been made on the required depth of diaphragm walling and on the required tunnel cross-section, however the cost is very sensitive to changes in these items due to the large proportion of related total scheme costs (approx. 55 %);
- Allowances have been made for temporary propping of excavations during diaphragm wall construction, however this will depend on ground conditions and are subject to change;
- Tunnel mining has been based on one third poor rock to two thirds good rock;
- No land purchase costs are included within the estimate;
- No costs of replacing facilities on existing land has been made; and
- The cost estimate doesn't include CERN staff costs in the lead up to project implementation.

All temporary facilities needed for the civil engineering works have been included in the cost estimate, but nothing for any temporary areas/buildings needed for machine or detector assembly/installation.

For clarity, the overall cost estimate does not include:

- SMB-SE Resources;
- Spoil removal off site. It is assumed to be stockpiled on CERN land close to the site;
- Instrumentation for tunnel monitoring;
- Special foundation support for facilities (e.g. Detector, etc);
- Shielding precast concrete blocks;
- Infrastructure and services costs e.g. heating, ventilation, cooling, electricity, gas etc.; and
- Land purchase and re-provision of existing facilities.

Spend profile

The annual cost forecast is indicated in Figure 41. The cost per year has been split between the 'civil engineering works' related to the construction phase and initial site investigation and the 'expert assistance' that covers the entire civil engineering project development process.

5.6.6 Schedule and Resource Considerations

A preliminary schedule has been studied for the construction of the nuSTORM facilities using the knowledge acquired from the construction of previous similar schemes at CERN. This timeline is shown in Figure 42. Some further investigation work as detailed in Section 5.6.4 will need to be carried out before detailed civil engineering design can begin with specialist external consultancies. Once these designs are complete, tendering for the civil construction contracts can start. In parallel, an environmental impact study must be prepared and approved by the local authorities, prior to the timely submission of the building permit application for the

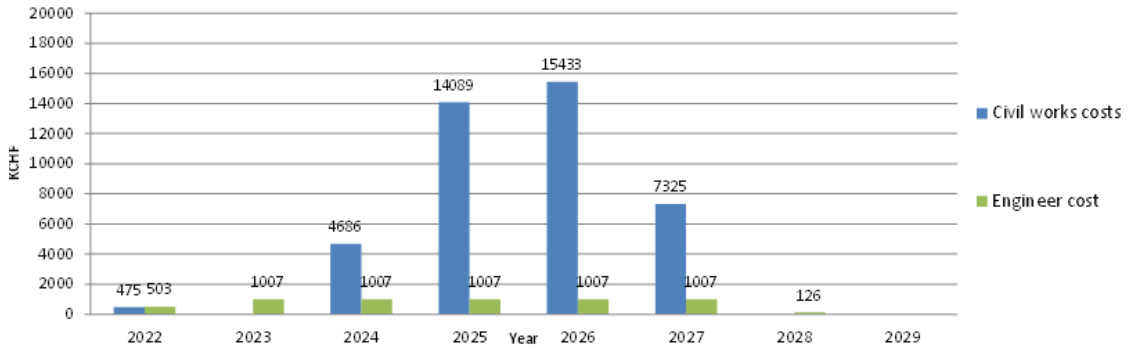

Figure 41: Indicative annual spend profile for CE works based on Figure 42

project, to allow construction works to commence. The CE works are split into four main packages and a miscellaneous costs section, as indicated within the cost evaluation.

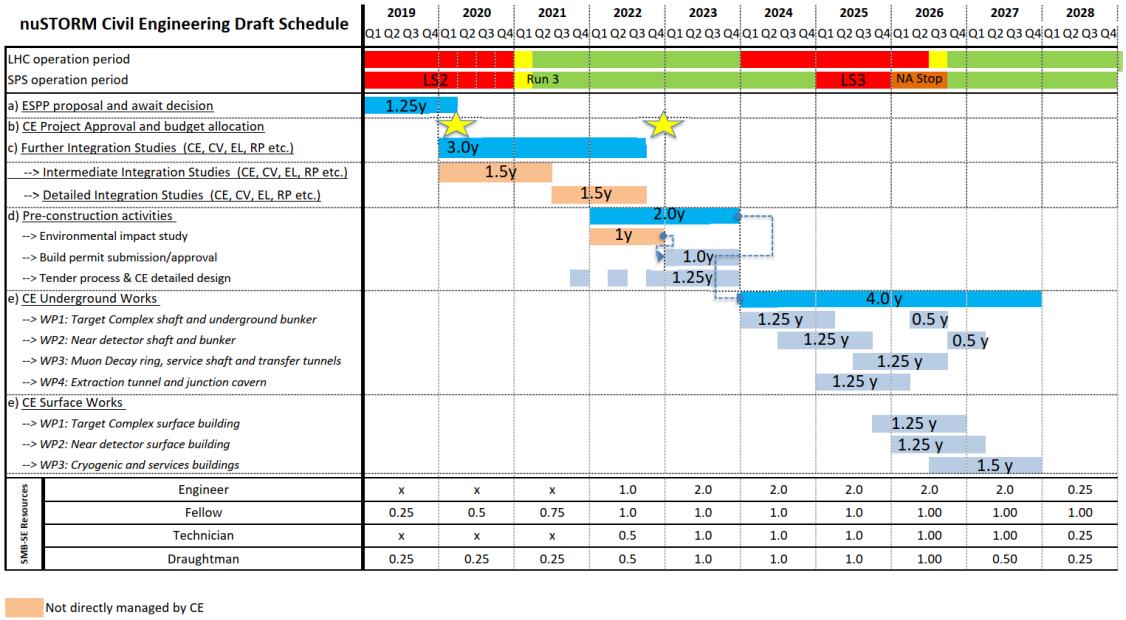

Figure 42: Indicative draft schedule for CE implementation.

6 Radiation protection and safety

It is essential to consider safety and environmental protection as an integral part of the comprehensive design of a facility such as nuSTORM. A project approach in which decisions are made consciously to eliminate or significantly reduce potential hazards, in a 'cost-effective', pragmatic manner from the very beginning will be established. The safety considerations presented in this section will be divided into radiation protection and overarching safety considerations.

6.1 Radiation protection and radiation safety

As nuSTORM requires a primary proton-beam power of the order of 200 kW, radiation protection considerations strongly determine the design of the facility. A few general radiation protection guidelines for the design of such a high powered facility are specified in section 6.1.1. The radiological and environmental assessments carried out for the design of the CENF target facility [58,59] were used for a preliminary radiological evaluation of nuSTORM. The latter is described in section 6.1.2.

6.1.1 General radiation protection guidelines

CERN's radiation protection regulations require the exposure of persons to radiation and the radiological impact on the environment to be as low as reasonably achievable (the ALARA principle) [60]. To allow for such optimization numerous radiation protection guidelines should be followed from the design phase of a facility onwards. A few of these general guidelines are listed below. They should particularly be taken into account for the areas in which high radiation levels will be produced. For nuSTORM these are expected to be the target complex, the primary beam absorber, and the pion beam absorber.

Key issues that must be addressed include:

Prompt and residual radiation

- The design of the entire facility must respect not only the legal dose limits but also satisfy the optimization principle (ALARA) with respect to individual and collective doses for workers and the public. The design goals for individual and collective doses are valid for commissioning, normal beam operation, maintenance and accidents.
- The activation properties of the materials used for the construction of the facility must be considered during the design process as they may have a direct impact on later handling (maintenance and repair) and waste disposal. For this the ActiWiz material catalog should be consulted [61].
- Only equipment absolutely necessary should be installed in areas of high radiation levels. The higher the activation the more reliable should equipment be.
- Depending on residual dose levels and tasks, manual interventions should partially or completely be replaced by remote maintenance/repair. Any component should be optimized to lower maintenance time and repair needs.

Air activation

- Air volumes should be minimized in areas of high levels of prompt radiation or even better be replaced by a helium or vacuum environment.
- Air volumes in which considerable air activation is expected should be separated from adjacent areas and the outside. Therefore, both static (e.g. sealing of air volumes) and dynamic (e.g. leak extraction) air confinement should be employed.
- A ventilation system should guarantee a pressure cascade from low to high contaminated areas.

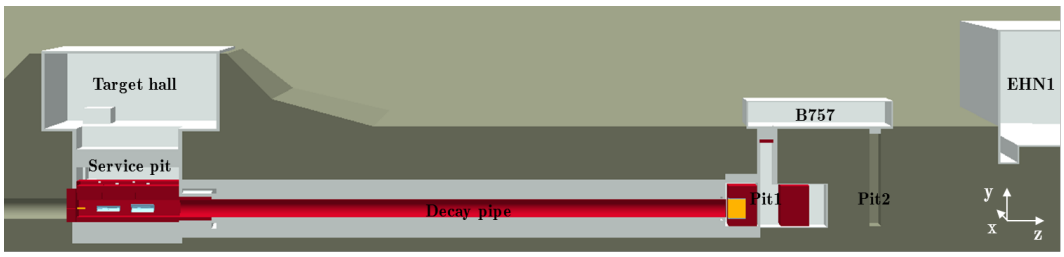

Figure 43: Side view of the CENF facility and the following experimental hall EHN1 as implemented in FLUKA. Iron is displayed in red, concrete in grey, aluminium in light blue, graphite in yellow and moraine in khaki.

- In the target area a "closed" ventilation circuit with high-efficiency particle and aerosol (HEPA(filters should be used. The area should be flushed before access. Also the air exhaust should be equipped with HEPA filters and the airborne radioactivity released into the environment have to be monitored.

Water and soil activation

- Water cooling circuits for highly radioactive elements like the target and the dump should be closed and separated from others.
- Water sumps should be avoided in areas with high tritium concentration.
- Activation and/or contamination of ground water and earth should be avoided.
- The facility should not be built in a "wet" environment. A hydrological study of the envisaged site should therefore be performed.
- Soil samples should be taken and analysed for their chemical and radiological composition.

Radioactive waste

- The design must consider minimization, decommissioning and dismantling of radioactive waste.

6.1.2 Preliminary RP evaluation

A preliminary RP evaluation of the proposed nuSTORM facility was performed on the basis of the extensive radiological assessment of the CENF target facility. The latter includes detailed studies on expected prompt and residual dose rates on the various accessible areas of CENF as well as the levels of the stray radiation in the surrounding experimental and public areas. Furthermore, it comprises the evaluation of the risk due to activated air and helium and the consequence of its release into the environment. Also studies on soil activation and radioactive waste zoning were conducted. All studies were based on simulations using the FLUKA Monte Carlo particle transport code [62, 63]. Figure 43 illustrates the proposed CENF facility as implemented in FLUKA.

In order to translate the given CENF studies to nuSTORM, the parameters mainly effecting the RP studies of both facilities are compared in Table 7. As can be seen, most of the parameters are the same for both facilities with a few differences where the nuSTORM parameters are less penalizing for radiological considerations.

Prompt and residual radiation

Just as for CENF, nuSTORM is designed under the condition that there is no access to its underground infrastructure during beam operation. Considerable shielding is nevertheless required to reduce the prompt radiation

Table 7: Comparison of the CENF and nuSTORM main parameters relevant for RP.

Parameter	**CENF**	**nuSTORM**
Beam momentum [GeV/c]	100	100
Beam intensity/spill	$4.5 \cdot 10^{13}$	$4 \cdot 10^{13}$
SPS cycle length [s]	3.6	3.6
POT per year	$4.5 \cdot 10^{19}$	$4 \cdot 10^{19}$
Total POT (5 years)	$2 \cdot 10^{20}$	$2 \cdot 10^{20}$
Target depth [m]	15	30
Min. distance to CERN facilities [m]	25	87
Min. distance to public area [m]	$\sim$70	$\sim$70

in the above-ground areas, which are accessible during beam operation. The shielding should also reduce the residual activation of the surrounding infrastructure. The main shielding elements for the CENF target cavern were therefore modeled with iron (160 cm sides, 80 cm bottom, 240 cm top) and concrete (200–300 cm sides, 260 cm bottom, 315 cm top). The resulting prompt ambient dose equivalent rates allowed for the above-ground target hall to be classified as Supervised Radiation Area with low occupancy ($<$15 μSv/h). The first beam dump was designed with a graphite core ($320 \cdot 320 \cdot 300\,\mathrm{cm}^3$) surrounded by cast iron ($600 \cdot 690 \cdot 500\,\mathrm{cm}^3$) and the second beam dump with cast iron ($600 \cdot 690 \cdot 500\,\mathrm{cm}^3$). The resulting dose rates allowed for an area classification of permanent Supervised Radiation Area ($<$3 μSv/h) in the above-ground area. The influence of the prompt radiation from the CENF facility on the closest experimental area EHN1 was estimated to be negligible. Furthermore, the prompt dose rates at the CERN fence were evaluated to be smaller than 5 μSv/y. Thus, with an equivalent shielding setup for nuSTORM, the expected prompt dose rates in the accessible surrounding areas should be similar or better, since the nuSTORM target depth is by a factor of 2 deeper. Detailed FLUKA simulations would at a later stage of the project allow the shielding thicknesses to be optimised.

The expected residual dose rates for the CENF facility were the highest in the central regions of the target area and the dump reaching up to O(200) mSv/h after 1 day of cooling. The dose rates on contact for the target were at the order of 1 Sv/h and 0.2 Sv/h after 1 day of cooling for the target and the proximity shielding, respectively. Therefore, remote handling and dedicated storage areas for the removable most activated elements were foreseen. For nuSTORM a remote handling and storage concept for the hottest elements such as the target, horn and proximity shielding must therefore designed. Furthermore, the demineralization cartridges and HEPA filters of the water cooling and ventilation circuits should be sufficiently shielded (e.g. with 80 cm concrete) to reduce the residual dose rates originating from these units.

One main difference of nuSTORM with respect to CENF is its pion-transport channel to the decay ring as well as the decay ring itself. The activation levels in the decay ring might be a crucial factor for the design of the pion transfer line. The experience from the Antiproton Decelerator (AD) has shown that double spectrometers arranged in a "dog-leg" structure located between the p-bar production target and the AD ring result in a significant reduction in the momentum spread of the beam resulting in significantly lower beam loss and activation levels in the ring. In order to quantify the effect of a dog-leg in comparison to a single dipole for the nuSTORM pion transfer line, further simulations would have to be performed. However, from an ALARA point of view, one can already say that the dog-leg option would be clearly favorable from an RP point of view.

Air and helium activation

For CENF, the air volumes in the high-radiation areas of the facility were minimized in order to reduce the production and releases of airborne radioactivity. In the most critical region, that is the central region of the

target area and the decay pipe, the air was further replaced by a helium environment. The central region of the target area was therefore embedded into a helium vessel. Compartments like the service pit (located around the He vessel) and the first beam dump, in which considerable air activation was expected, were further separated from accessible areas of the facility to avoid unjustified exposure to personnel. In addition, a ventilation system was foreseen to ensure a pressure cascade from low to high contaminated areas. The remaining production of radionuclides in air and helium and the consequent effective dose rates to workers and the reference group were evaluated with FLUKA. A total activity of $1.4 \cdot 10^9$ Bq (60 CA[1], $1.2 \cdot 10^9$ Bq short-lived[2]) and $5.0 \cdot 10^9$ Bq (1100 CA, $4.3 \cdot 10^9$ Bq short-lived) were estimated for the service pit and the first beam dump air regions after one operational year and no cooling time. The significant contribution of short-lived radionuclides demonstrates that delaying the release of activated air into the environment significantly reduces the effective dose rates delivered to members of the public. The leakage and extraction rates of the activated air were therefore foreseen to be kept as low as reasonably possible with a maximum delay time before being released into the environment.

For the helium compartments the production of radionuclides and the resulting activities arising from pure helium were derived and compared to the corresponding values in case of an air filling. This allowed the significant reduction in impact resulting from the use of helium to be demonstrated and the identification of acceptable level of air contamination in the helium-filled regions. A total activity of $5.3 \cdot 10^9$ Bq ($1.2 \cdot 10^2$ CA) and $5.7 \cdot 10^9$ Bq ($4.3 \cdot 10^1$ CA) were determined in case of a pure helium filling for the He-vessel and the decay pipe, respectively. With air this resulted in $3.9 \cdot 10^{11}$ Bq ($2.5 \cdot 10^4$ CA) and $6.9 \cdot 10^{11}$ Bq ($1.5 \cdot 10^4$ CA), respectively. As a consequence, the air contamination in the He-filled volumes shall not exceed 0.1% volumic of air in helium. The impact of the releases to the environment and the resulting effective dose to members of the public are furthermore discussed in section 6.1.2.

For nuSTORM, the main air activation is expected in the areas of the target, the primary beam absorber, and depending on the losses in the pion transfer tunnel, also in the latter. It is likely that the absorber could be similar to that designed for CENF in a completely separated volume such that the release of activated air into other areas would be negligible. However, in the target area this would not be feasible as the area has to be accessible for remote maintenance and repair works. Here, it would most probably be necessary to include the most central region inside of a helium vessel as the environmental impact would otherwise not fulfill the dose objective (see Section 6.1.2). At a later stage of the project, the air activation in the transfer tunnel and the ring should also be evaluated.

Soil activation

The evaluation of induced radioactivity in the soil is essential for the environmental impact studies of a facility. A prerequisite for a realistic estimation of radionuclide production is a knowledge of the soil composition. For CENF, soil samples were therefore taken from 15 m deep drillings at the target station, the decay pipe and the hadron absorber. The soil samples were analysed for their elemental composition and water content. The results are presented in [65]. The soil composition was then used to determine the production of the soluble radionuclides ^{3}H and ^{22}Na as they are likely to pass through the karstic system and therefore critical for the protection of groundwater resources. Based on the given results, the location of a geo-membrane [66] was defined, which encompassed all zones where the derived earth activation limits of 10 Bq/g for ^{3}H and 2 Bq/g for ^{22}Na were exceeded.

Depending on the final shielding setup for nuSTORM, slight activation of soil above the given limits might also be expected. These regions could be surrounded by a geo-membrane, which would also prevent infiltration

[1] Swiss guidance value for chronic occupational exposure to airborne activity. Exposure to an airborne activity concentration CA for 40 hours per week and 50 weeks per year yields a committed effective dose of 20 mSv [64].

[2] The most relevant short-lived isotopes include C-11, N-13, O-14, O-15 and Ar-41.

of water into the facility.

Environmental considerations

Table 7 shows that the main parameters pertinent to the environmental impact of nuSTORM and CENF are identical except for the target depth, which is less penalising for nuSTORM. The radiological impact study for CENF [59] showed that, after following certain design principles aimed at mitigation of the radiological environmental impact of accelerator facilities, the resulting effective dose to members of the public could be reduced well below the facility optimisation threshold of 10 μSv/y [60]. Namely [59]: $< 0.2\,\mu$Sv/y due to stray radiation, $< 0.2\,\mu$Sv/y due to releases of radioactive substances to the ambient air, and $< 1\ \mu$Sv/y due to evaporation of water contaminated with tritium. The earth around the CENF target station would fall into the category of non-radioactive solid material after a reasonable cooling time and it would not contaminate groundwater to a level of radiological concern. In addition, the depth of the target station and the water table observed in area foreseen for installation exclude contact of the activated soil with the aquifer. Despite the fact that the detailed design of the facility has not been performed, one can state, based on the study [59], and table 7, that the radiological environmental impact of nuSTORM will be manageable using the present state of technology and that engineering solutions by which impact can be minimised already exist. Finally, the release of airborne radioactive substances from CENF are critically dependent on the purity of He used in certain high activation zones. In the study [59], the maximum admixture of air in He of 0.1% was assumed and it seems that this solution could not be avoided in the nuSTORM target station if the impact should remain negligible.

6.1.3 Conclusions

The preliminary RP evaluation of the proposed nuSTORM facility showed the general feasibility of such a project in terms of exposure of persons to radiation and the radiological impact on the environment. At a later stage of the project, detailed studies allowing to further optimise the facility according to the ALARA principle should be envisaged. However already at the present state of technology, engineering solutions for the minimisation of the radiological impact are available.

6.2 Safety

6.2.1 Legal context of CERN

By virtue of its inter-governmental status, CERN is entitled to adopt its own internal organisational rules, which prevail over national laws to facilitate the execution of its mission. In the absence of specific CERN regulations, the laws and regulations of the Host States generally prevail. In response to its unique geographical situation (straddling the Swiss-French border without discontinuity) and its highly specific technical needs, the Organization stipulates its safety policy, in the frame of which it establishes and updates rules aimed at ensuring uniform safety conditions across its sites. CERN's safety rules apply to the Organization's activities, as well as to persons participating in CERN's activities or present on its site. When establishing its own safety rules, CERN takes into account the laws and regulations of the Host States, EU regulations and directives as well as international regulations, standards and directives and, as a general principle, CERN aligns with these as much as reasonably possible. Where such compliance is not possible or desirable due to technical or organisational constraints, such as for equipment and facilities not covered by normal standards, specific clearance from CERN's HSE unit based on a risk assessment and compensatory measures is required.

Table 8: Safety objectives for the nuSTORM project.

	A: Life Safety	**B: Environmental Protection**	**C: Property Protection**	**D: Continuity of Operation**
1	Safe evacuation of valid occupants	Limited release of pollutants to air	Continuity of essential services	Limit downtime
2	Safe evacuation or staging of injured occupants	Limited release of pollutants to water	Incident shall not cause further incidents	
3	Safe intervention of rescue teams		Limit property loss	

6.2.2 Occupational Health and Safety

CERN's Safety Policy, in order of priority, sets out to protect all persons affected by its activities, to limit the impact of the Organization's activities on the environment, and to protect its equipment and ensure continuity of operations. The agreed safety objectives are shown in table 8.

6.2.3 Fire safety

The goal of fire safety is to protect occupants, rescuers, the external population, the environment, the facility itself, and continuity of operation. To this end, all buildings, experimental facilities, equipment and experiments installed at CERN shall comply with CERN Safety Code E. In view of the special nature of the use of certain areas, in particular underground, with increased fire risk, the HSE Unit is to be considered the authority of approving and stipulating special provisions.

As the project moves to the Technical Design Report stage, finalising layouts and interconnecting ventilation systems, detailed fire risk assessments will have to be made for all areas of the nuSTORM complex. At this stage, a general fire safety strategy has been produced, based upon the location and current level of design, along with the latest fire safety strategies employed at CERN.

The most efficient protection strategy is one that uses multi-level 'safety barriers', with a bottom-up structure, to limit fires at the earliest stages with the lowest consequences, thus considerably limiting the probability and impact of the largest events.

In order to ensure that large adverse events are possible only in very unlikely cases of failure of many barriers, measures at every possible level of functional design need to be implemented:

- in the conception of every piece of equipment (e.g. materials used in electrical components, circuit breakers, etc.);
- in the grouping of equipment in racks or boxes (e.g. generous cooling of racks, use of fire-retardant cables, and fire detection with power cut-off within each rack, etc.);
- in the creation and organisation of internal rooms (e.g., fire detection, power cut-off and fire suppression inside a room with equipment);
- in the definition of fire compartments; and
- in the definition of firefighting measures.

The key fire safety strategy concepts can be split into compartmentalisation, fire detection, smoke extraction and fire suppression, as set out below.

Compartmentalisation

Compartmentalisation impedes the propagation of fire and potentially activated smoke through a facility, allowing occupants to escape to a comparatively safe area much more quickly than otherwise, as well as facilitating the effective fighting of the fire, and evacuation of victims by the Fire Brigade. In the North Area fire concept, the following requirements have been set:

- All ventilation doors must be fire doors EI90;
- Isolate communicating galleries with fire doors EI90;
- Isolate neighbouring surface facilities with fire doors EI120;
- Avoid compartments longer than 450 m; and
- Normally opened fire doors to be equipped with remote action release mechanism, monitoring position and self-action thermal fuse.

Fire Detection

An early fire detection system, integrated into the safety action system is a crucial component of fire strategy. Early detection is such that it allows evacuation (last occupant out) before untenable conditions are reached; the CERN HSE Fire Safety team shall be consulted for this design.

Smoke Extraction

Careful risk assessment of the effect of smoke in the event of a fire is required for all underground and surface areas, taking into account both the safe evacuation of occupants, and the effective intervention of the fire brigade to locate victims and prevent the further spread of a fire. A buildup of smoke can also result in lasting damage to the sensitive and valuable equipment present, an effect that can be limited through extraction.

An additional consideration for fires in accelerator tunnels is the danger of potentially activated smoke, and the need to handle this in a controlled manner to limit the release of polluting agents to the environment. A fire assessment methodology that entails the radiological hazard induced by a fire event is currently under development by the FIRIA Project led by HSE. Once the FIRIA Methodology is fully available in July 2021, it is recommended to consider carrying out a FIRIA exercise as part of the Technical Design Report phase. A description of the FIRIA project is available in [67].

Fire Suppression

The CERN Fire Brigade need adequate means of fighting a fire on arrival, including a surface hydrant network, which shall be foreseen as the project moves to the Technical Design Report stage, in tandem with the HSE Fire Safety specialists.

Access Safety

For underground access, it is required that:

- The lift and stairs are protected against fire are not connected to the general electrical circuit (i.e., can be used at any time); and

Figure 44: The CERN Fire Brigade ”PEFRA” vehicle.

- A safe area, with an overpressure relative to the surroundings is available at the base of the lift (or other vertical egress path). The size of this area shall be commensurate with the number of occupants, in addition to the time taken for evacuation, and shall be determined as the project moves to the Technical Design Report stage.

For the tunnels it is important that fire equipment and the Fire Brigade vehicle (for example, the ‘PEFRA’, shown in figure 44) can move freely in and out of the lift and pass through the tunnels without any problem, especially for a rescue operation.

6.2.4 Cryogenic systems

The use of superconducting technology requires specific considerations relating to the use of cryogenic fluids, including conformity of pressure equipment and considerations of a potential oxygen deficiency hazard. Cryogenic pressure equipment is covered within the CERN Safety rules by General Safety Instruction GSI-M-4 *Cryogenic Equipment*, which in general requires compliance with the applicable European pressure equipment directives. This also applies to component items such as the cold masses of superconducting magnets. The hazard category of the cryogenic pressure vessel and piping, and related conformity assessment procedures, will be determined based on the applicable directive, for each equipment item. The use of non-European industrially-recognised international standards for particular equipment items would be subject to further agreement but would nevertheless require full compliance with the Essential Safety Requirements of the applicable European directive.

Cryogenic pressure vessels are to be equipped with CE-marked pressure relief devices to ensure the safe release of the working fluid in case of overpressure. Piping sections that may become isolated with cryogenic liquid or cold gas are also to be equipped with CE-marked pressure relief devices to ensure the safe release of the working fluid in case of overpressure. Pressure relief devices are to be sized, installed, commissioned and periodically tested in accordance with the applicable international standards and CERN Safety rules. The governing case (e.g. loss of insulating vacuum) for the discharge capacity and sizing is to be duly determined and traceable. For cryogenic vessels, redundancy of pressure relief devices protecting the liquid container (the inner vessel in case of a vacuum insulated vessel) is to be evaluated based on a risk assessment and operational requirements.

The outer jacket of vacuum insulated cryogenic vessels is to be designed in a way to maintain the structural

stability in the event of a failure of the inner vessel. The outer jacket is to be equipped with either a pressure relief plate/plug or a rupture disc. The design of the plate/plug is to be such that it cannot harm personnel when ejected. The zones around relief points will be duly labelled and marked as 'no stay' zones, as per the current configuration around relief points in the Large Hadron Collider tunnels.

The different systems for protection against overpressure will be combined with fail-safe mode provisions in terms of the cryogenic process and with alarm and/or detection systems which will deploy emergency procedures whenever risks for safety of personnel have been identified in case of a discharge of cryogenic fluids. With further detailed design, a specific assessment of the risks of asphyxiation due to oxygen depletion will be made. The risk of exposure will be reduced to a minimum by applying the relevant control measures, commensurate with the risk assessment, in order of priority:

- General and/or local exhaust ventilation, and if not sufficient;
- Oxygen deficiency detection systems in any areas where asphyxiant gases can become trapped and which pose a risk to persons; and
- Adequate safety procedures in case the detection of oxygen deficiency is triggered.

6.2.5 Safety of Civil Structures

The installation of the nuSTORM complex will involve a significant amount of civil works, including tunnel modifications, numerous new buildings and a challenging target complex. At CERN, all structures are to be designed and manufactured according to the Eurocodes, especially accounting for the local seismic action. Due to the estimated levels of radiation foreseen across the facility, along with environmental considerations, the control of water ingress and egress is of particular interest.

Fire Resistance

New structures and infrastructure shall be designed and executed to guarantee a mechanical resistance for 120 minutes of exposure to the design fire. Eventual passive protection systems, e.g. intumescent paintings and plasters, will be foreseen only for those elements that are unable to respect such a requirement. The structural assessment will need to be carried out in accordance with EN 1991-1-2, EN 1992-1-2 and EN 1993-1-2.

6.2.6 Chemical Safety

The chemicals currently foreseen for the nuSTORM project represent standard risks seen in many other facilities at CERN. As these are subject to change as the project moves to the Technical Design Report stage, and as the exact quantities and storage conditions are not yet known, the installations will require proper risk assessment to CERN Safety Form C-0-0-1 when these details become fixed. As for all such facilities at CERN, activities involving chemical agents shall comply with the following CERN Safety rules:

- Safety Regulation on chemical agents (SR-C);
- General Safety Instruction (GSI-C-1) on prevention and protection measures; and
- General Safety Instruction (GSI-C-3) on monitoring of exposure to hazardous chemical agents in workplace atmospheres (where required).

Activities involving asphyxiant chemical agents shall comply with the following CERN Safety rules:

- Safety Regulation on chemical agents (SR-C); and
- General Safety Instruction (GSI-C-1) on prevention and protection measures.

Should any additional chemicals be proposed for use in the facility, the Chemical Specialists within the HSE group must be consulted.

6.2.7 Electrical Safety

The electrical infrastructure design for the nuSTORM facility is currently at a general level, but will incorporate subsystems that either produce, or use, high voltage or current, both of which represent electrical hazards to personnel. Dedicated electrical rooms will be used to contain all the electrical cabinets required for the power distribution. The hazards are expected to be standard for such an installation, and shall be mitigated through sound design practice and execution. The CERN Electrical Safety rules, alongside NF C 18-510, shall be followed throughout the design process; where exceptions are required, this shall be subject to an appropriate level of risk assessment to evaluate the residual risk, and determine the mitigation strategies required. NF C 18-510 compliant covers, interlocks preventing access to high voltage equipment, and restriction of access to the electrical rooms to those with the appropriate level of CERN electrical *habilitation* training shall be used to protect personnel from any electrical hazards present.

Electromagnets

For all electromagnets, appropriate grounding measures shall be implemented for the magnet yokes, and all live parts protected to a minimum of IPXXB for Low Voltage and IPXXC for High Voltage circuits or locked out for any intervention in their vicinity. Interventions may only be carried out by personnel with the necessary training, after following the work organisation procedures and authorisation of the facility coordinator (VICs, IMPACT etc.).

6.2.8 Mechanical safety

Pressure Equipment

All pressure equipment shall comply with the following CERN Safety rules:

- CERN Safety Regulation SR-M - Mechanical equipment; and
- CERN General Safety Instruction GSI-M-2 - Standard Pressure Equipment.

Moreover, there are specific sets of rules applicable only to certain types of standard pressure equipment. Those rules are defined in the following Specific Safety Instructions, of which the following may be applicable to the nuSTORM project:

- CERN Specific Safety Instruction on pressure vessels (SSI-M-2-1);
- CERN Specific Safety Instruction on safety accessories for standard pressure equipment (SSI-M-2-3);
- CERN Specific Safety Instruction on metallic pressurised piping (SSI-M-2-4);
- CERN Specific Safety Instruction on vacuum chambers and beam pipes (SSI-M-2-5); and
- CERN Specific Safety Instruction on transportable pressure equipment (SSI-M-2-6).

According to CERN Safety rules, pressure equipment shall meet the essential requirements set by the following applicable European Directives:

- Directive 2014/68/EU on pressure equipment - Pressure Equipment Directive (PED); and
- Directive 2010/35/EU on transportable pressure equipment– Transportable Pressure Equipment Directive (TPED).

Pressure equipment designed and manufactured according to harmonised European standards benefit from presumption of conformity with the essential requirements laid down

HVAC Equipment

Equipment purchased on the market (e.g.: Air Handling Units, chillers, boilers, fan coils) shall comply with the applicable European Directives and shall bear the CE marking.

Ductwork (supply or exhaust air) and piping systems incorporated in a permanent manner in a building, shall comply with the following European Regulations:

- European Regulation 305/2011 - Construction Products Regulation;
- EN 1505 - Ventilation for buildings. Sheet metal air ducts and fittings with rectangular cross-section;
- EN 1506 - Ventilation for buildings. Sheet metal air ducts and fittings with circular cross-section;
- EN 12097 - Ventilation for buildings. Requirements for ductwork components to facilitate maintenance of ductwork systems; and
- EN 13480 – Metallic Industrial piping.

These standards provide presumption of conformity to the Safety requirements regarding the design laid down in the applicable European Regulations. Electrical parts related to HVAC installations shall respect the general Safety requirements as indicated in Section 6.2.7.

Lifting and Handling Equipment

The nuSTORM facility is expected to use lifting equipment, including hoists, cranes and personnel lifts. All lifting and handing equipment installed at CERN shall comply with the CERN Safety rules:

- Safety Regulation on Mechanical Equipment (SR-M); and
- General Safety Instruction on Lifting Equipment and Accessories (GSI-M-1).

6.2.9 Protection of the environment

With regard to protection of the environment, CERN Safety Policy states that the Organization is committed to ensuring the best possible protection of the environment. This can be achieved by ensuring that the given regulations are followed for the different activities and experiments.

As the project moves to the Technical Design Report stage, a review with the Environmental Protection specialists within HSE shall be held to determine whether the relevant technical provisions of the following regulation shall apply for the nuSTORM project:

- *Arrêté du 29/05/00 relatif aux prescriptions générales applicables aux installations classées pour la protection de l'environnement soumises à déclaration sous la rubrique n° 2925*; and
- *Arrêté du 14/12/13 relatif aux prescriptions générales applicables aux installations relevant du régime de l'enregistrement au titre de la rubrique n° 2921 de la nomenclature des installations classées pour la protection de l'environnement*.

The technical environmental mitigation measures shall be determined more precisely once technical detail information are available such as the type and the quantity of chemicals or the solution chosen for the cooling.

6.2.10 Air

Atmospheric emissions shall be limited at the source and shall comply with the relevant technical provisions of the following regulations:

- *Arrété du 02 février 1998 relatif aux prélèvements et à la consommation d'eau ainsi qu'aux émissions de toute nature des installations classées pour la protection de l'environnement soumises à autorisation, Articles 26, 27, 28, 29, 30*.

The design of exhaust air discharge points shall comply with the requirements of the section 5.1.3 of the CERN Safety Guideline C-1-0-3 – Practical guide for users of Local exhaust ventilation (LEV) systems.

Whenever greenhouse gases are used, relevant technical provisions contained in the following regulations apply:

- Regulation (EU) No 517/2014 of the European Parliament and of the Council of 16 April 2014 on fluorinated greenhouse gases and repealing Regulation (EC) No 842/2006; and
- *Code de l'environnement Livre V: Titre II (Art. R521-54 to R521-68) and Titre IV (Art. R543-75 to R543-123)*.

All the appropriate preventive measures shall be taken against the release of greenhouse gases into the atmosphere. Working procedures shall be established and implemented for activities involving the use of those gases including the storage, handling, transport, recovery and disposal. Additionally such activities shall be performed by trained personnel. The emissions of fluorinated gases shall be registered during the entire life-cycle of the equipment or Experiment.

In accordance with the siting of the facility on French territory, the design, operation and maintenance of cooling tower water circuits shall comply with the relevant technical provisions of the following regulations and standards in order to limit the risk of legionella bacteria and its dispersion in the atmosphere:

- *NF E38-424 Aéroréfrigérants humides : terminologie et exigences de conception vis-à-vis du risque légionellose*;
- *Arrété du 14 décembre 2013 relatif aux prescriptions générales applicables aux installations relevant du régime de l'enregistrement au titre de la rubrique n° 2921 de la nomenclature des installations classées pour la protection de l'environnement*; and
- *Guide des bonnes pratiques Legionella et tours aéroréfrigérantes*.

6.2.11 Water

The nuSTORM project shall ensure the rational use of water. The discharge of effluent water into the CERN clean and sewage water networks shall comply with the relevant technical provisions contained in the following regulations:

- *Loi n° 2006-1772 du 30 décembre 2006 sur l'eau et les milieux aquatiques*; and
- *Arrété du 02 février 1998 relatif aux prélèvements et à la consommation d'eau ainsi qu'aux émissions de toute nature des installations classées pour la protection de l'environnement soumises à autorisation*.

The direct or indirect introduction of potentially polluting substances into water, including their infiltration into ground is prohibited. Applicable emission limit values for effluent water discharged in the Host States territory are defined in the following regulations:

- *Arrété du 02 février 1998 relatif aux prélèvements et à la consommation d'eau ainsi qu'aux émissions de toute nature des installations classées pour la protection de l'environnement soumises à autorisation Art. 31 and art.32*.

If cooling towers are installed, the cooling circuit shall be equipped with a recycling process, and the effluent resulting from the recycling process shall be discharged into the sanitary network.

Retention measures for water used to extinguish a fire are required for any CERN project in which large quantities of hazardous, or potentially polluting substances are used or stored. As the project moves to the Technical Design Report stage, through discussions with the Environmental Protection specialists from HSE, will determined whether the following guidance document shall be applied (in accordance with the French *Code de l'Environnement*:

- *Référentiel APSAD D9 : Dimensionnement des besoins en eau pour la défense contre d'incendie and Référentiel APSAD D9A : Dimensionnement des rétentions des eaux d'extinction available in the Centre National de Prévention et de Protection (CNNP) (http://www.cnpp.com/).*

6.2.12 Energy

The use of energy shall as efficient as possible. For the entire facility, adequate measures shall be taken to comply with the relevant technical provisions contained in the following regulations:

- *Loi n° 2010-788 du 12 juillet 2010 portant engagement national pour l'environnement (Grenelle II).*

In addition, construction of new buildings sited in France shall comply with the relevant technical provisions relating to thermal efficiency contained in the following regulation:

- *Décret n° 2012-1530 du 28 décembre 2012 relatif aux caractéristiques thermiques et à la performance énergétique des constructions de bâtiments*;
- *Arrété du 26 octobre 2010 relatif aux caractéristiques thermiques et aux exigences de performance énergétique des bâtiments nouveaux et des parties nouvelles de bâtiments and the French Réglementation Thermique 2012 (RT 2012)*; and
- *NF EN 15232 Performance énergétique des bâtiments - Impact de l'automatisation, de la régulation et de la gestion technique*.

6.2.13 Soil

The natural physical and chemical properties of the soil must be preserved. All the relevant technical provisions related to the usage and/or storage of substances hazardous to the environment shall be fulfilled to avoid any chemical damage to the soil. Furthermore, the excavated material shall be handled adequately and prevent further site contamination. All excavated material must be disposed of appropriately in accordance with the associated waste regulations.

6.2.14 Waste

The selection of construction materials, design and fabrication methods shall be such that the generation of waste is both minimised and limited at the source. Waste shall be handled from its collection to its recovery or disposal according to:

- *Code de l'environnement, Livre V: Titre IV-Déchets*; and
- *LOI n° 2009-967 du 3 août 2009 de programmation relative à la mise en œuvre du Grenelle de l'environnement (1), Art. 46*.

The traceability of the waste shall be guaranteed at any time.

6.2.15 Preservation of the natural environment

The nuSTORM project shall ensure the preservation of the natural environment (e.g. landscaping, fauna, floral reserve, etc.) according to the relevant technical provisions contained in the following regulations:

- *Code de l'environnement, Art. L411-1.*

Vegetal species listed in this regulation shall be protected, restored or adequately replaced (e.g. orchids). Whenever CERN natural areas are affected by a project, the Civil Engineering and Buildings (SMB-SE-CEB) section of the SMB Department shall be contacted for authorisation and definition of appropriate measures.

6.2.16 Noise

In order to ensure occupational health and safety to people exposed to noise, the nuSTORM project shall be compliant with the following rules and Regulations:

- CERN Safety Code A8 - Protection against noise;
- Directive 2003/10/EC of the European Parliament and of the Council of 6 February 2003 on the minimum health and safety requirements regarding the exposure of workers to the risks arising from physical agents (noise); and
- French Code du travail.

Emissions of environmental noise related to neighbourhoods shall respect the thresholds indicated in:

- *French Arrété du 23 janvier 1997 relatif à la limitation des bruits émis dans l'environnement par les installations classées pour la protection de l'environnement.*

6.3 Non-Ionising Radiation

The high magnetic fields from the proposed electromagnets in the current nuSTORM design represent a hazard similar to that found in many of the facilities at CERN, and shall be handled with standard mitigation strategies. The facility shall follow the Directive 2013/35/EU on the occupational exposure of workers, alongside CERN Safety Instruction IS 36 and its Amendment. Any activity inside the static magnetic field shall be subject to risk assessment and ALARA. Personnel shall be informed of the hazards and appropriately trained. Areas with magnetic flux densities exceeding 0.5 mT shall be delimited (use pacemaker warning signs), while areas with magnetic flux densities exceeding 10 mT shall be rendered inaccessible to the public.

7 Construction costs

A first-cut cost estimate has been performed as part of the preliminary study. Given resource constraints, it was necessary to rely on a number of sources including a well-developed study performed at FNAL in 2013 [2]. This study included a detailed cost breakdown. The cost estimate presented below has been derived using the following additional sources:

- The CE engineering cost breakdown was established in 2018 at CERN based on experience, depth, geology,required techniques, and enclosure-size estimates. Figure 45 shows a plan elevation of the nuSTORM facility at CERN with the various work packages defined for the CE cost breakdown indicated on the layout. The CE cost estimates are shown in table 9.
- The primary beam line estimate is based on experience at CERN. The teams are well-versed in equipping and pricing standard warm magnet beam line.
- The target, target hall, and proton absorber are based on a detailed study performed for CENF [68]. There is considerable expertise at CERN with neutrino target design, and the use of horn and reflectors.
- The muon decay ring estimate is taken from the FNAL study. Note that FNAL costing includes all manpower.
- The size of the experiment hall is that assumed in the FNAL study. The cost of the contents is based on the CENF estimate.

No contingency has been added. Tables 9 and 10 sumarise the civil-energeering cost estimate and the overall cost estimate respectively.

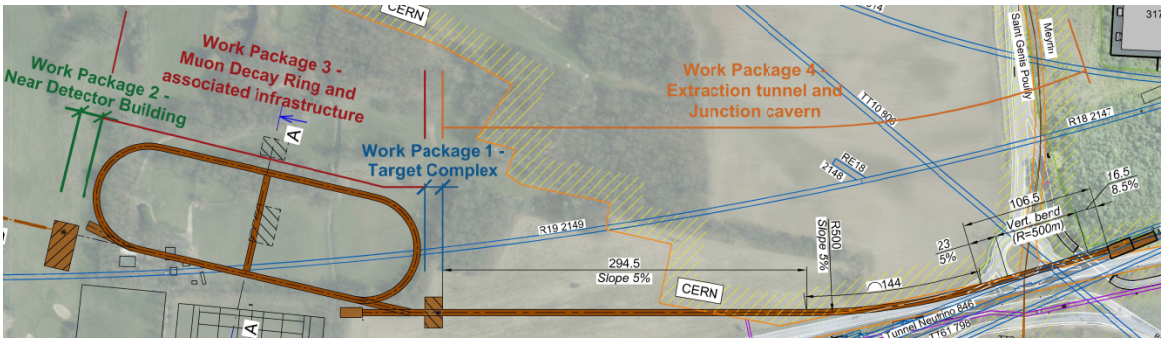

Figure 45: Civil Engineering work packages.

Table 9: Civil engineering cost estimate.

Year	**KCHF**	
CE for WP1:	6,189	Target complex works inc. access shaft to allow tunnelling launch
CE for WP2:	11,098	Near detector building works inc. access shaft to allow tunnelling launch
CE for WP3:	15,826	Muon decay ring tunnelling, assoc. transfer tunnels & infrastructure.
CE for WP4:	11,208	Extraction tunnel and junction cavern.
	460	Site investigation
TOTAL	44,781	

Table 10: Overall material cost estimate summary. *12% inflation since 2013 assumed.

Work package	MCHF	Source
Extraction and beam-line	21.0	CERN 2018
Target hall (target, horn, shielding, absorber etc.)	20.0*	CENF
Secondary beam line	9.0*	FNAL
Muon decay ring hardware	58.8*	FNAL
Muon decay ring utilities		
Detector Hall Infrastructure	2.4*	CENF
Civil engineering	44.8	CERN 2018
Total	156	

7.1 Project Costs FNAL

Detailed costing of the nuSTORM conventional facilities was performed by the Fermilab Facilities Engineering Services Section (FESS) and is reported on in the nuSTORM Project Definition Report (PDR) 6-13-1 [69]. The cost, summarised in table 11, included all manpower and are fully burdened (FY2013 dollars). The total base

Table 11: FNAL summary base cost with no contingency, 2013 prices. CF – conventional facilities, FNAL parlance for CE, and technical infrastructure (utilities) are included in the totals.

Work package	Base cost [M$]
Primary beam line	21.1
Target station	26.7
Capture & transport	10.8
Decay ring	89.3
Near detector hall	16.8
Site work	17.4
CF other	1.8
Total	183.9

cost quoted in the FNAL report was $206,130,755. This included the far detector hall and the magnetised-iron/scintillator neutrino detector, SuperBIND. The cost of the far-detector hall and SuperBIND have been removed from the totals in table 11.

8 Next steps

A meeting was held at CERN on the 21st and 22nd October 2019 [70] to discuss the next steps in the development of nuSTORM and the possible time-scales that might be involved. This section contains brief notes on the outcome of this meeting[3].

The implementation of nuSTORM at CERN was considered in the light of present commitments and likely future developments. These considerations indicated that implementation of nuSTORM might be possible from around 2030. Such an ambition is consistent with the following considerations:

- Upgrades to the injectors and LHC will follow the established Long Shutdown (LS)/Run timetable. The next LS for injectors is foreseen for 2025, in parallel with the execution of the main HL-LHC upgrades. The following LS foreseen for around 2030.
- If approval for the development of a CDR were to be granted, and resources assigned, a 3-year comprehensive Design Study would need to be carried out. An R&D period of around 3 years is likely to be required once the design-study phase is complete. The R&D phase would culminate in the publication of a TDR. Should the project then be approved, a period of component production and preparation for project execution would be required.

In consequence, a 10-year programme for the implementation of nuSTORM was felt to be a reasonable aspiration.

The case for nuSTORM was felt to be strong and to rest on the following three "pillars":

Neutrino Cross Sections:

The measurement of neutrino cross sections with precision at or below the 1% level was felt to be the "bread and butter" physics deliverable. While it was clear that the nuSTORM measurements would be independent, it was felt that the contribution to the oscillation programmes at DUNE and Hyper-K needed to be assessed critically based on quantitative estimates of the impact. The development of a credible nuSTORM neutrino detector, optimised for the cross section programme, will be required for quantitative estimates to be made. The possibility of using hydrogen as one of a number of targets should be considered.

Sterile neutrinos:

nuSTORM has a unique, and well documented, sensitivity to light sterile neutrinos. To match this it will be important to extend the new-physics case beyond sterile neutrinos. It was felt that broadening the physics case was important in order to convince the community of the opportunity that nuSTORM presents. Given the extremely well defined flux, it was felt that effects that cause distortions in the measured spectrum should be identified.

Muon-collider technology test-bed and demonstrator:

The case for nuSTORM as an essential "way point" on the path towards a muon collider was felt to be important, but not yet articulated strongly enough. The following arguments were identified as as being among those that should be developed:

- A series of demonstrators of increasing complexity will be needed to manage the risks that are implicit in the delivery of an energy-frontier muon collider. nuSTORM would be the first such demonstrator, delivering front-rank particle physics measurements and serving the muon-collider R&D programme.
- The implementation of nuSTORM will prove to be a catalyst for the development and demonstration of the technologies required to realise a muon collider. For example, an attractive option for nuSTORM and for the muon acceleration at a muon collider is provided by the FFA. The implementation of nuSTORM would allow this technology to be brought to maturity in the service of neutrino

[3] The notes in this section are based on an informal record provided by M. Lamont.

physics. FFA technology also has application elsewhere, for example in medical applications.

- nuSTORM has the potential to serve the exploration of ionization cooling in all six phase-space dimensions that is required to build on the MICE in-principle demonstration of the ionization-cooling technique [32].
- The staged exploitation of the infrastructure required for nuSTORM should be considered. One topic that could be investigated is the possible synergy with the ENUBET programme [71].

References

[1] **nuSTORM Collaboration** Collaboration, P. Kyberd *et al.*, "nuSTORM - Neutrinos from STORed Muons: Letter of Intent to the Fermilab Physics Advisory Committee," arXiv:1206.0294 [hep-ex].

[2] **nuSTORM** Collaboration, D. Adey *et al.*, "nuSTORM - Neutrinos from STORed Muons: Proposal to the Fermilab PAC," arXiv:1308.6822 [physics.acc-ph].

[3] K. R. Long, "Neutrinos from Stored Muons," *PoS* **NEUTEL2017** (2018) 049.

[4] **DUNE** Collaboration, B. Abi *et al.*, "The DUNE Far Detector Interim Design Report Volume 1: Physics, Technology and Strategies," arXiv:1807.10334 [physics.ins-det].

[5] **DUNE** Collaboration, R. Acciarri *et al.*, "Long-Baseline Neutrino Facility (LBNF) and Deep Underground Neutrino Experiment (DUNE)," arXiv:1601.05471 [physics.ins-det].

[6] **DUNE** Collaboration, R. Acciarri *et al.*, "Long-Baseline Neutrino Facility (LBNF) and Deep Underground Neutrino Experiment (DUNE)," arXiv:1512.06148 [physics.ins-det].

[7] **DUNE** Collaboration, J. Strait *et al.*, "Long-Baseline Neutrino Facility (LBNF) and Deep Underground Neutrino Experiment (DUNE)," arXiv:1601.05823 [physics.ins-det].

[8] **DUNE** Collaboration, R. Acciarri *et al.*, "Long-Baseline Neutrino Facility (LBNF) and Deep Underground Neutrino Experiment (DUNE)," arXiv:1601.02984 [physics.ins-det].

[9] **Hyper-Kamiokande Working Group** Collaboration, K. Abe *et al.*, "A Long Baseline Neutrino Oscillation Experiment Using J-PARC Neutrino Beam and Hyper-Kamiokande," arXiv:1412.4673 [physics.ins-det].
http://inspirehep.net/record/1334360/files/arXiv:1412.4673.pdf.

[10] **Hyper-Kamiokande Proto-Collaboration** Collaboration, K. Abe *et al.*, "Physics potential of a long-baseline neutrino oscillation experiment using a J-PARC neutrino beam and Hyper-Kamiokande," *PTEP* **2015** (2015) 053C02, arXiv:1502.05199 [hep-ex].

[11] **Hyper-Kamiokande** Collaboration, K. Abe *et al.*, "Hyper-Kamiokande Design Report,". http://www.hyperk.org/?p=215.

[12] **Hyper-Kamiokande proto-** Collaboration, K. Abe *et al.*, "Physics Potentials with the Second Hyper-Kamiokande Detector in Korea," arXiv:1611.06118 [hep-ex].

[13] B. Pontecorvo, "Inverse beta processes and nonconservation of lepton charge," *Sov. Phys. JETP* **7** (1958) 172–173.

[14] B. Pontecorvo, "Neutrino experiments and the question of leptonic-charge conservation," *Sov. Phys. JETP* **26** (1968) 984–988.

[15] Z. Maki, M. Nakagawa, and S. Sakata, "Remarks on the unified model of elementary particles," *Prog. Theor. Phys.* **28** (1962) 870–880.

[16] **Particle Data Group** Collaboration, C. Patrignani *et al.*, "Review of Particle Physics," *Chin. Phys.* **C40** no. 10, (2016) 100001.

[17] **DUNE** Collaboration, B. Abi *et al.*, "Long-baseline neutrino oscillation physics potential of the DUNE experiment," arXiv:2006.16043 [hep-ex].

[18] M. Scott, "Long baseline neutrino oscillation sensitivities with Hyper Kamiokande," 2020. Presented at the 40^{th} International Conference on High Energy Physics, ICHEP 2020, Prague, 20 July – 5 August.

[19] **T2K** Collaboration, K. Abe *et al.*, "Constraint on the matter–antimatter symmetry-violating phase in neutrino oscillations," *Nature* **580** no. 7803, (2020) 339–344, arXiv:1910.03887 [hep-ex]. [Erratum: Nature 583, E16 (2020)].

[20] M. Martini, M. Ericson, and G. Chanfray, "Energy reconstruction effects in neutrino oscillation experiments and implications for the analysis," *Phys. Rev.* **D87** no. 1, (2013) 013009, arXiv:1211.1523 [hep-ph].

[21] P. Coloma, P. Huber, C.-M. Jen, and C. Mariani, "Neutrino-nucleus interaction models and their impact on oscillation analyses," *Phys. Rev.* **D89** no. 7, (2014) 073015, arXiv:1311.4506 [hep-ph].

[22] P. Coloma and P. Huber, "Impact of nuclear effects on the extraction of neutrino oscillation parameters," *Phys. Rev. Lett.* **111** no. 22, (2013) 221802, arXiv:1307.1243 [hep-ph].

[23] U. Mosel, O. Lalakulich, and K. Gallmeister, "Energy reconstruction in the Long-Baseline Neutrino Experiment," *Phys. Rev. Lett.* **112** (2014) 151802, arXiv:1311.7288 [nucl-th].

[24] A. M. Ankowski, P. Coloma, P. Huber, C. Mariani, and E. Vagnoni, "Missing energy and the measurement of the CP-violating phase in neutrino oscillations," *Phys. Rev.* **D92** no. 9, (2015) 091301, arXiv:1507.08561 [hep-ph].

[25] A. M. Ankowski and C. Mariani, "Systematic uncertainties in long-baseline neutrino-oscillation experiments," *J. Phys.* **G44** no. 5, (2017) 054001, arXiv:1609.00258 [hep-ph].

[26] M. Ankowski, A., O. Benhar, P. Coloma, P. Huber, C. M. Jen, C. Mariani, D. Meloni, and E. Vagnoni, "Neutrino energy reconstruction in disappearance experiments with calorimetric and kinematic methods," *Nuovo Cim.* **C39** no. 1, (2016) 233.

[27] A. M. Ankowski, O. Benhar, C. Mariani, and E. Vagnoni, "Effect of the $2p2h$ cross-section uncertainties on an analysis of neutrino oscillations," *Phys. Rev.* **D93** no. 11, (2016) 113004, arXiv:1603.01072 [hep-ph].

[28] U. Mosel, "Neutrino Interactions with Nucleons and Nuclei: Importance for Long-Baseline Experiments," *Ann. Rev. Nucl. Part. Sci.* **66** (2016) 171–195, arXiv:1602.00696 [nucl-th].

[29] A. M. Ankowski, "Nuclear effects are relevant to the calorimetric reconstruction of neutrino energy," arXiv:1704.07835 [hep-ph].

[30] **nuSTORM** Collaboration, D. Adey *et al.*, "Light sterile neutrino sensitivity at the nuSTORM facility," *Phys. Rev.* **D89** no. 7, (2014) 071301, arXiv:1402.5250 [hep-ex].

[31] The MICE collaboration, "INTERNATIONAL MUON IONIZATION COOLING EXPERIMENT." http://mice.iit.edu.

[32] **MICE** Collaboration, M. Bogomilov *et al.*, "Demonstration of cooling by the Muon Ionization Cooling Experiment," *Nature* **578** no. 7793, (2020) 53–59. https://doi.org/10.1038/s41586-020-1958-9.

[33] D. Adey, S. Agarwalla, C. Ankenbrandt, R. Asfandiyarov, J. Back, *et al.*, "Neutrinos from Stored Muons nuSTORM: Expression of Interest," arXiv:1305.1419 [physics.acc-ph].

[34] S. Mishra, R. Petti, and C. Rosenfeld, "A High Resolution Neutrino Experiment in a Magnetic Field for Project-X at Fermilab," *PoS* **NUFACT08** (2008) 069, arXiv:0812.4527 [hep-ex].

[35] J. Kopp, P. A. N. Machado, M. Maltoni, and T. Schwetz, "Sterile Neutrino Oscillations: The Global Picture," *JHEP* **1305** (2013) 050, arXiv:1303.3011 [hep-ph].

[36] C. Andreopoulos *et al.*, "The GENIE Neutrino Monte Carlo Generator," *Nucl. Instrum. Meth. A* **614** (2010) 87–104, arXiv:0905.2517 [hep-ph].

[37] **Geant4** Collaboration, J. Apostolakis and D. H. Wright, "An overview of the GEANT4 toolkit," *AIP Conf. Proc.* **896** (2007) 1–10.

[38] A. Cervera-Villanueva, J. J. Gomez-Cadenas, and J. A. Hernando, "'RecPack' a reconstruction toolkit," *Nucl. Instrum. Meth.* **A534** (2004) 180–183.

[39] A. Hoecker, J. Stelzer, F. Tegenfeldt, H. Voss, K. Voss, *et al.*, "TMVA - Toolkit for Multivariate Data Analysis," *PoS* **ACAT** (2007) 040, arXiv:physics/0703039.

[40] R. Brun and F. Rademakers, "ROOT: An object oriented data analysis framework," *Nucl. Instrum. Meth.* **A389** (1997) 81–86.

[41] C. Tunnell, *Sensitivity to electronvolt-scale sterile neutrinos at a 3.8-GeV/c muon decay ring*. PhD thesis, University of Oxford, 2013.

[42] P. Huber, M. Lindner, and W. Winter, "Simulation of long-baseline neutrino oscillation experiments with GLoBES," *Comput. Phys. Commun.* **167** (2005) 195, hep-ph/0407333. http://www.mpi-hd.mpg.de/~globes.

[43] C. Tunnell, "Sterile Neutrino Sensitivity with Wrong-Sign Muon Appearance at nuSTORM," arXiv:1205.6338 [hep-ph].

[44] **MINOS** Collaboration, P. Adamson *et al.*, "New constraints on muon-neutrino to electron-neutrino transitions in MINOS," *Phys. Rev. D* **82** (2010) 051102, arXiv:1006.0996 [hep-ex].

[45] M. Antonello *et al.*, "Search for anomalies in the ν_e appearance from a ν_μ beam," *Eur.Phys.J.* **C73** (2013) 2345, arXiv:1307.4699 [hep-ex].

[46] C. Hagmann, D. Lange, J. Verbeke, and D. Wright, "Cosmic-ray shower library (cry)," Tech. Rep. UCRL-TM-229453, Lawrence Livermore National Laboratory, 2013. http://nuclear.llnl.gov/simulation/main.html.

[47] A. Laing and F. J. P. Soler, "Flux measurement at a neutrino factory near detector for neutrino oscillations," *AIP Conf.Proc.* **981** (2008) 166–168.

[48] **IDS-NF Collaboration** Collaboration, S. Choubey *et al.*, "International Design Study for the Neutrino Factory, Interim Design Report," arXiv:1112.2853 [hep-ex].

[49] W. Winter, "Optimization of a Very Low Energy Neutrino Factory for the Disappearance Into Sterile Neutrinos," *Phys.Rev.* **D85** (2012) 113005, arXiv:1204.2671 [hep-ph].

[50] S.-P. Hallsjö, *Charge Current Quasi-elastic Muon Neutrino Interactions in the Baby MIND Detector,*. PhD thesis, University of Glasgow, 2018.

[51] N. Charitonidis, M. Brugger, I. Efthymiopoulos, L. Gatignon, Y. Karyotakis, P. Sala, E. Nowak, and I. Ortega-Ruiz, "The beam lines design for the CERN neutrino platform in the CERN north area and an outlook on their expected performance," *J. Phys. Conf. Ser.* **874** no. 1, (2017) 012056.

[52] J. Alabau-Gonsalvo, A. Alekou, F. Antoniou, W. Bartmann, M. Benedikt, D. Berthoux, B. Biskup, A. Blondel, L. Bottura, M. Calviani, N. Charitonidis, J.-M. Cravero, A. Curioni, C. Densham, I. Efthymiopoulos, L. Faisandel, B. Ferral, M. Fitton, R. Garodby, and P. Vojtyla, "Laguna-lbno design study: Long-baseline neutrino beam facility from cern to a far detector site at 2300 km distance, conceptual design report,".

[53] A. Liu, A. Bross, and D. Neuffer, "A FODO racetrack ring for nuSTORM: design and optimization," *JINST* **12** no. 07, (2017) P07018, arXiv:1704.00798 [physics.acc-ph].

[54] J.-B. Lagrange, R. Appleby, J. Garland, J. Pasternak, and S. Tygier, "Racetrack FFAG muon decay ring for nuSTORM with triplet focusing," *Journal of Instrumentation* **13** no. 09, (Sep, 2018) P09013–P09013. https://doi.org/10.1088%2F1748-0221%2F13%2F09%2Fp09013.

[55] The LIU project team, "The LIU project." https://espace.cern.ch/liu-project/default.aspx.

[56] ILF, "Fcc cost and schedule study," 2017. https://edms.cern.ch/document/2050504/1.

[57] P. Christensen, L. R. Dysert, J. Bates, D. Burton, R. Creese, and J. Hollmann, "Cost estimate classification system-as applied in engineering, procurement, and construction for the process industries," *AACE, Inc* **2011** (2005) .

[58] C. Strabel, H. Vincke and K. Zabrzycki, "*Radiation protection studies for the CERN Neutrino Facility (CENF)*," Tech. Rep. EDMS 1427729, CERN (2017), CERN, 2017.

[59] P. Vojtyla, C. Strabel and H. Vincke, "*Radiation protection studies for the CERN Neutrino Facility (CENF)*," Tech. Rep. EDMS 1427092, CERN (2015), CERN, 2015.

[60] CERN, "*Safety Code F - Radiation Protection*," Tech. Rep. EDMS 335729, CERN (2006), CERN, 2006.

[61] R. Froeschl et al., "*Radiological Hazard classification of materia in CERN's accelerators*," Tech. Rep. EDMS 1184236, CERN (2012), CERN, 2012.

[62] A. Fassò, A. Ferrari, J. Ranft and P.R. Sala, "*FLUKA: a multi-particle transport code*," Tech. Rep. CERN-2005-10 (2005), INFN/TC-05/11, SLAC-R-773, CERN, 2005.

[63] T.T. Böhlen, F. Cerutti, M.P.W. Chin, A. Fassò, A. Ferrari, P.G. Ortega, A. Mairani, P.R. Sala, G. Smirnov and V. Vlachoudis, "*The FLUKA Code: Developments and Challenges for High Energy and Medical Applications*," Tech. Rep. Nuclear Data Sheets 120, 211-214 (2014), 2014.

[64] Office federal de la santé publique (OFSP), "*Ordonnance sur la radioprotection (ORaP)*," Tech. Rep. 2018, 2018.

[65] C. Strabel, H. Vincke, "*Soil sample analysis at the CERN Neutrino Facility (CENF)*," Tech. Rep. EDMS 1427736, CERN (2015), CERN, 2015.

[66] M. Calviani, "*CENF target facility civil engineering specifications*," Tech. Rep. EDMS 1416787, CERN (2014), CERN, 2014.

[67] **FIRIA** Collaboration, "FIRIA project: addressing fire safety at CERN." `https://home.cern/news/news/cern/firia-project-addressing-fire-safety-cern`.

[68] Vojtyla, P. and Strabel, C. and Vincke, H., "CENF radiological environmental consideration," 2018. EDMS 1427092.

[69] A. D. Bross, "nuSTORM Costing document,".

[70] **nuSTORM** Collaboration, "nuSTORM–the next steps, CERN, 21-22 October 2019." `https://indico.cern.ch/event/837890/`.

[71] **ENUBET** Collaboration, E. Parozzi *et al.*, "The ENUBET ERC project for an instrumented decay tunnel for future neutrino beams," *Nucl. Instrum. Meth. A* **958** (2020) 162162.

The nuSTORM collaboration

Canada
S. Bhadra, S. Menary
Department of Physics and Astronomy, York University, 4700 Keele Street, Toronto, Ontario, M3J 1P3, Canada

M. Hartz†
TRIUMF, 4004 Wesbrook Mall, Vancouver, BC V6T 2A3, Canada
† *Also at Kavli Institute for the Physics and Mathematics of the Universe, The University of Tokyo Kashiwa Campus, 5-1-5 Kashiwanoha, Kashiwa, Chiba 277-8583, Japan*

China
J. Tang
Institute of High Energy Physics, Chinese Academy of Sciences, Beijing, China

Germany
U. Mosel
Justus Liebig Universität,m, Ludwigstraße 23, 35390 Gießen, Germany

M.V. Garzelli
II. Institut für Theoretische Physik, Universität Hamburg, Luruper Chaussee 149, 22761 Hamburg, Germany

W. Winter
Deutsches Elektronen-Synchrotron (DESY), Platanenallee 6, 15738 Zeuthen, Germany

India
S. Goswami, K. Chakraborty
Physical Research Laboratory, Ahmedabad 380009, India

S.K. Agarwalla
Institute of Physics, Sachivalaya Marg, Sainik School Post, Bhubaneswar 751005, Orissa, India

Italy
E. Santopinto
INFN Sezione di Genova, Via Dodecaneso, 33-16146, Genova, Italy

M. Bonesini
Sezione INFN Milano Bicocca, Dipartimento di Fisica G. Occhialini, Milano, Italy

L. Stanco
INFN, Sezione di Padova, 35131 Padova, Italy

D. Orestano, L. Tortora
INFN Sezione di Roma Tre and Dipartimento di Matematica e Fisica, Università Roma Tre, Roma, Italy

Japan
Y. Mori
Kyoto University Institute for Integrated Radiation and Nuclear Science (KURNS), 2, Asashiro-Nishi, Kumatori-cho, Sennan-gun, Osaka 590-0494, Japan

Y. Kuno, A. Sato
Osaka University, Graduate School, School of Science, 1-1 Machikaneyama-cho, Toyonaka, Osaka 560-0043, Japan

South Korea
M. Chung
UNIST, Ulsan, Korea

The Netherlands
F. Filthaut†
Nikhef, Amsterdam, The Netherlands
† *Also at Radboud University, Nijmegen, The Netherlands*

Poland
J.T. Sobczyk
Institute of Theoretical Physics, University of Wroclaw, pl. M. Borna 9,50-204, Wroclaw, Poland

Spain
J.J. Gomez-Cadenas
Donostia International Physics Center (DIPC), Paseo Manuel de Lardizabal 4, 20018 Donostia-San Sebastián, Gipuzkoa, Spain

J.A. Hernando Morata
Universidade de Santiago de Compostela (USC), Departamento de Fisica de Particulas, E-15706 Santiago de Compostela, Spain

L. Alvarez Ruso, A. Cervera, A. Donini, P. Hernandez, J. Lopez Pavon†, J. Martín-Albo, O. Mena, P. Novella, M. Sorel
Instituto de Fisica Corpuscular (IFIC), Centro Mixto CSIC-UVEG, Edificio Institutos Investigación, Paterna, Apartado 22085, 46071 Valencia, Spain
† *Theoretical Physics Department, CERN, 1211 Geneva 23, Switzerland*

Sweden
R. Ruber
Department of Physics and Astronomy, Uppsala University, Ångströmlaboratoriet, Lägerhyddsvägen 1, Box 516, 751 20 Uppsala, Sweden

Switzerland
C.C. Ahdida, W. Bartmann, J. Bauche, M. Calviani, N. Charitonidis, J. Gall, B. Goddard, C. Hessler, J. Kopp†, M. Lamont, J.A. Osborne, E. Radicioni, A. de Roeck, F.M. Velotti
CERN,CH-1211, Geneva 23, Switzerland
† *Also at PRISMA Cluster of Excellence, Johannes Gutenberg University, Mainz, Germany*

A. Blondel, E.N. Messomo, F. Sanchez Nieto
University de Geneve, 24, Quai Ernest-Ansermet, 1211 Geneva 4, Suisse

United Kingdom
M.A. Uchida
Cavendish Laboratory (HEP), JJ Thomson Avenue, Cambridge, CB3 0HE, UK

S. Easo, R.E. Edgecock, J.B. Lagrange, W. Murray, C. Rogers
STFC Rutherford Appleton Laboratory, Chilton, Didcot, Oxfordshire, OX11 0QX, UK

J.J. Back, G. Barker, S.B. Boyd, P.F. Harrison
Department of Physics, University of Warwick, Coventry, CV4 7AL, UK

S. Pascoli
Institute for Particle Physics Phenomenology, Department of Physics, University of Durham, Science Laboratories, South Rd, Durham, DH1 3LE, UK

S.-P. Hallsjö, F.J.P. Soler
School of Physics and Astronomy, Kelvin Building, University of Glasgow, Glasgow G12 8QQ, Scotland, UK

H.M. O'Keeffe, L. Kormos, J. Nowak, P. Ratoff
Physics Department, Lancaster University, Lancaster, LA1 4YB, UK

C. Andreopoulos†, N. McCauley, C. Touramanis
Department of Physics, Oliver Lodge Laboratory, University of Liverpool, Liverpool, L69 7ZE, UK
† *Also at STFC, Rutherford Appleton Laboratory, Harwell Campus, Chilton, Didcot, OX11 0QX, UK*

D. Colling, P. Dornan, P. Dunne, P. Franchini, P.M. Jonsson, P.B. Jurj, A. Kurup, P. Litchfield, K. Long†, T. Nonnenmacher, J. Pasternak†, M. Scott, J.K. Sedgbeer, W. Shorrock, M.O. Wascko
Physics Department, Blackett Laboratory, Imperial College London, Exhibition Road, London, SW7 2AZ, UK
† *Also at STFC, Rutherford Appleton Laboratory, Harwell Campus, Chilton, Didcot, OX11 0QX, UK*

F. di Lodovico, T. Katori
King's College London, Strand, London WC2R 2LS, UK

A. Bevan, L. Cremonesi, P. Hobson
Queen Mary University of London, Mile End Road, London E1 4NS, UK

R. Nichol
Department of Physics and Astronomy, University College London, Gower Street, London, WC1E 6BT, UK

R. Appleby, S. Tygier
The University of Manchester, 7.09, Schuster Laboratory, Manchester, M13 9PL, UK and the Cockcroft Institute, Daresbury Laboratory, WA4 4AD, UK

X. Lu, D. Wark, A. Weber†
Particle Physics Department, The Denys Wilkinson Building, Keble Road, Oxford, OX1 3RH, UK
† *Also at STFC, Rutherford Appleton Laboratory, Harwell Campus, Chilton, Didcot, OX11 0QX, UK*

P.J. Smith
University of Sheffield, Dept. of Physics and Astronomy, Hicks Bldg., Sheffield S3 7RH, UK

P. Kyberd, D.R. Smith
College of Engineering, Design and Physical Sciences, Brunel University London, Uxbridge, Middlesex, UB8 3PH, UK

United States of America
S.J. Brice, A.D. Bross, S. Chattopadhay†, S. Feher, L. Fields, P. Hanlet, N. Mokhov, J.G. Morfín, D. Neuffer, J. Paley, S. Parke, Z. Pavlovic, M. Popovic, P. Rubinov, V. Shiltzev
Fermilab, P.O. Box 500, Batavia, IL 60510-5011, USA
† *Northern Illinois University, 1425 W. Lincoln Hwy., DeKalb, IL 60115-2828, USA*

P. Huber, C. Mariani, J.M. Link
Virginia Polytechnic Inst. and State Univ., Physics Dept., Blacksburg, VA 24061-0435

B. Freemire, A. Liu
Euclid Techlabs, LLC, 365 Remington Blvd, Bolingbrook, IL, 60440, USA

D.M. Kaplan, P. Snopok
Illinois Institute of Technology, Chicago, IL, USA

S.R. Mishra
Department of Physics and Astronomy, University of South Carolina, Columbia SC 29208, USA

K. Mahn
High Energy Physics, Biomedical-Physical Sciences Bldg., Michigan State University, 220 Trowbridge Rd, East Lansing, MI 48824, USA

A. de Gouvêa
Northwestern University, Dept. of Physics and Astronomy, 2145 Sheridan Road, Evanston, Illinois 60208-3112 USA

V. Pandey
Department of Physics, University of Florida, Gainesville, FL 32611, USA

Y. Onel, D. Winn
Department of Physics and Astronomy, The University of Iowa, 203 Van Allen Hall, Iowa City, Iowa 52242-1479, USA

H.A. Tanaka
SLAC National Accelerator Laboratory, 2575 Sand Hill Rd, Menlo Park, CA 94025, USA

M. Hostert
School of Physics and Astronomy, University of Minnesota, Minneapolis, MN 55455, USA

S.A. Bogacz
Thomas Jefferson National Accelerator Facility, 12000 Jefferson Avenue, Newport News, VA 23606, USA

L. Cremaldi, D. Summers
University of Mississippi, Oxford, MS, USA

K.T. McDonald
Princeton University, Princeton, NJ, 08544, USA

G. Hanson
Department of Physics and Astronomy, University of California, Riverside, CA 92521, US

M. Palmer
Brookhaven National Laboratory, P.O. Box 5000, Upton, NY 11973 USA

M. Liu
Purdue University, 610 Purdue Mall, West Lafayette, IN, 47907, 765-494-4600, USA